Johannes Gutenberg Universität Mainz
Department Chemie - Standort TRIGA

New Ways for a Faster Alpha Spectrometry

Dissertation
zur Erlangung des Grades
"Doktor der Naturwissenschaften"
im Promotionsfach Chemie
am Fachbereich Chemie, Pharmazie, Geographie
und Geowissenschaften
der Johannes Gutenberg Universität Mainz

Dominik Krupp

geb. in Jülich

Advisor: Prof. Dr. U. W. Scherer
Co-advisor: Prof. Dr. Ch. E. Düllmann

The date of the oral exam will be determined in the second week of October 2021.

(Signature) *(Signature)*

. . . . . Prof. Dr. U. W. Scherer

. . . . . Prof. Dr. Ch. E. Düllmann

Mainz, 2021

Declaration of academic integrity

With this statement I declare that I have completed the PhD thesis entitled with “New ways for a faster alpha spectrometry” self-directed. The thoughts taken directly or indirectly from external sources as well as other resources are properly marked as such. I have not or had not submitted the work now submitted as a dissertation as an examination paper for a state or other scientific examination. I did not submit the present work or parts of it as a dissertation to another faculty or department.

Hiermit versichere ich, dass ich die vorliegende Dissertation mit dem Titel ”New ways for a faster alpha spectrometry” selbständig angefertigt habe. Die direkt oder indirekt aus externen Quellen entnommenen Gedanken sowie andere Hilfsmittel und Materialien sind ordnungsgemäß als solche gekennzeichnet. Ich habe oder hatte die jetzt als Dissertation vorgelegte Arbeit nicht als Prüfungsarbeit für eine staatliche oder andere wissenschaftliche Prüfung eingereicht. Ich habe oder hatte weder die jetzt als Dissertation vorgelegte Arbeit noch Teile davon bei einer anderen Fakultät beziehungsweise einem anderen Fachbereich als Dissertation eingereicht.

Heidelberg, 01.10.2021

Abstract

Alpha spectrometry is a key technology in many radioanalytical fields for nuclide- and activity determination. Due to the very short range of α radiation in condensed matter, great care must be taken during sample preparation to avoid self-absorption of the α radiation by the measurement sample itself. However, extensive sample preparation and production efforts in conventional α spectrometric analysis are accepted, since it is often the only way to obtain information about the radionuclide(s) in question. In no other discipline is the problem of complex sample preparation as clear as in the investigation of the heaviest known elements, the transactinides (atomic number $Z \geq 104$), often also referred to as "superheavy elements" (SHE). Since these elements are only produced at accelerators with production rates of single atoms per hour or day, all steps from production to the actual chemical experiment to the detection of the characteristic α radiation must be kept as efficient as possible. A key aspect of making SHE studies efficient is the time that elapses from nuclide production until the start of the measurement to identify its nuclear decay. With the aid of automated systems, the chemical properties of the first three SHEs, namely rutherfordium, dubnium and seaborgium, could be studied in liquid phase chemistry experiments. Subsequent SHE could only be studied in the gas phase. In order to be able to investigate the chemical properties of the transseaborgium elements in the aqueous phase, new technologies for a more efficient investigation of the SHE in the aqueous phase were developed within this work. One approach was to combine various individual steps in a previous experimental setup into a single step. Here, the primary focus was on the chemical separation of a sample, followed by sample preparation and measurement with a silicon detector. These steps can be combined if the detector surface is simultaneously a stationary phase with functional groups that selectively accumulate radionuclides from the aqueous solution on the detector surface according to their chemical properties. If this extractive layer is thin enough, the emitted α radiation of the radionuclides can be measured without significant loss of kinetic energy. In the case of accelerator based experiments, the transport of produced radionuclides, the transfer of the SHE into the liquid phase and the separation of by-products of the fusion reaction are additional complex challenges with great optimization potential. To this end, a system was developed to stop recoil nuclei directly in an aqueous phase after they have passed through a physical pre-separator and are then transported along the shortest possible path to the chemical experiment, such as a Si-detector, coated with extractive functional groups. In order to be able to test such systems without access to particle accelerators, a system was also developed to continuously elute from a generator system ^{211}Bi as an α-emitter with a 2 min half-life in a liquid phase. To better classify these new techniques for a fast α-spectrometry, the following sections give a short theoretical overview related to α-emitting radionuclides. In doing so, an overview of the origin of α-emitting radionuclides, the theory of this type of radiation, the currently most common measurement methods and the technical developments in the field of fast analysis of α-emitters will be given.

Zusammenfassung

Die Alphaspektrometrie ist in vielen Bereichen der Radioanalytik eine Schlüsseltechnologie zur Nuklid- und Aktivitätsbestimmung. Aufgrund der sehr kurzen Reichweite der α-Strahlung in kondensierter Materie muss die Probenvorbereitung und Herstellung mit großer Sorgfalt durchgeführt werden, um eine Selbstabsorption der α-Strahlung durch die Messprobe selbst zu vermeiden. Daher wird bei der konventionellen α-Spektrometrie ein hoher Aufwand bei der Probenvorbereitung und -herstellung in Kauf genommen, da dies oft die einzige Möglichkeit ist, Informationen über das betreffende Radionuklid zu erhalten. In keiner anderen Disziplin ist das Problem der aufwendigen Probenvorbereitung so deutlich wie bei der Untersuchung der schwersten bekannten Elementen, den Transactiniden (Ordnungszahl $Z \geq 104$), die oft auch als "superschwere Elemente" (engl. *superheavy elements* SHE) bezeichnet werden. Da diese Elemente nur an Beschleunigern mit Produktionsraten von einzelnen Atomen pro Stunde oder Tag hergestellt werden, müssen alle Schritte von der Produktion über das eigentliche chemische Experiment bis hin zum Nachweis der charakteristischen α-Strahlung so effizient wie möglich gehalten werden. Ein wesentlicher Aspekt, um eine SHE Experiment effizient zu gestalten, ist die Zeit, die von der SHE Produktion bis zur Detektion der Kernstrahlung benötigt wird, so gering wie möglich zu gestalten. Mit Hilfe von automatisierten Systemen konnten die chemischen Eigenschaften der ersten drei SHEs, nämlich Rutherfordium, Dubnium und Seaborgium, in Experimenten der Flüssigphasenchemie untersucht werden. Alle nachfolgenden SHE konnten nur in der Gasphase untersucht werden. Um die chemischen Eigenschaften der Transseaborgium-Elemente in der wässrigen Phase untersuchen zu können, wurden neue Methoden zur effizienteren Untersuchung der SHE in der wässrigen Phase im Rahmen dieser Arbeit entwickelt. Ein Ansatz war die verschiedene Einzelschritte eines Experiments zu einem einzigen Schritt zusammenzufassen. Hier lag der primäre Fokus auf der chemische Trennung einer Probe, gefolgt von der Probenpräparation und der Messung mit einem Siliziumdetektor (Si-detektor). Diese Schritte können kombiniert werden, wenn die Detektoroberfläche gleichzeitig eine stationäre Phase mit funktionellen Gruppen ist, die selektiv Radionuklide aus der wässrigen Lösung entsprechend ihrer chemischen Eigenschaften an der Detektoroberfläche anreichern. Ist diese extraktive Schicht dünn genug, kann die emittierte α-Strahlung der Radionuklide ohne nennenswerten Verlust an kinetischer Energie gemessen werden. Im Falle von beschleunigerbasierten Experimenten sind der Transport der produzierten Radionuklide, die Überführung der SHE in die flüssige Phase und die Abtrennung von Nebenprodukten der Fusionsreaktion weitere komplexe Herausforderungen mit großem Optimierungspotenzial. Zu diesem Zweck wurde ein System entwickelt, um Rückstoßkerne direkt in einer wässrigen Phase zu stoppen, nachdem sie einen physikalischen Vorsepartor durchlaufen haben. Die wässrige Phase, in der sich dann die SHE befinden, kann dann auf kürzesten Weg zum chemischen Experiment, wie z.B. einem Si-Detektor, der mit extraktiven funktionellen Gruppen beschichtet werden, transportiert werden. Um solche Systeme ohne Zugang zu Teilchenbeschleunigern testen zu können, wurde auch ein Generatorsystem entwickelt, mit dem ^{211}Bi

als α-Strahler mit einer Halbwertszeit von 2 min in einer flüssigen Phase kontinuierlich aus einem Generatorsystem eluiert werden kann. Um diese neuen Techniken für eine schnelle α-Spektrometrie besser einordnen zu können, wird im folgenden Abschnitt ein kurzer theoretischer Überblick über α-emittierende Radionuklide gegeben. Dabei wird ein Überblick über die Herkunft der α-emittierenden Radionuklide, die Theorie dieser Strahlungsart, die derzeit gängigsten Messmethoden und die technischen Entwicklungen auf dem Gebiet der schnellen Analyse von α-Strahlern dargelegt.

List of Abbreviations

AASIFIT	-	Advanced Alpha-Spectrometric Simulation and Fitting
ADB18C6	-	4'-Aminodibenzo-18-crown-6 ether
AIDA	-	Automated Ion-exchange separation apparatus coupled with the Detection system for α-spectroscopy
ARCA	-	Automated Rapid Chemistry Apparatus
BG	-	Background
BGS	-	Berkeley Gas-filled Separator
CIX	-	Cation exchanger
CN	-	Compound Nucleus
COMPCAT	-	Cryo-Online Multidetector for Physics And Chemistry of Transactinides
DI	-	Deionized
CVD	-	Chemical Vapor Deposition
DABCO	-	Diazabicyclo [2.2.2] octane
EVR	-	Evaporation Residue Nucleus
FWHM	-	Full Width at Half Maximum
HMF	-	Heavy-Mass peak Fragments
ICPTES	-	3-Isocyanatopropyltriethoxysilane
LMF	-	Light-Mass peak Fragments
LSC	-	Liquid Scintillation Counter / Liquid Scintillation Counting
MCA	-	Multi Channel Analyser
MDA	-	Minimum Detectable Activity
MDG	-	Membrane Degasser
MPTHS	-	(3-Mercaptopropyl)trihydroxysilan
MPTMS	-	(3-Mercaptopropyl)trimethoxysilane
MRT	-	Mean Residence Time
PHA	-	Pulse Height Analysis
PMT	-	Photo Multiplier Tube
PPO	-	2,5-Diphenyloxazole
PSD	-	Pulse Shape Discrimination
PTFE	-	Polytetrafluoroethylene
PVBC	-	Polyvinyl benzyl chloride
ROI	-	Regions Of Interest
RC	-	Recoil Chamber
RTC	-	Recoil Transfer Chamber

SAM	-	Self Assembled Monolayers
SF	-	Spontaneous Fission
SHE	-	Super Heavy Element
Si detector	-	Silicon semiconductor detector
SISAK	-	Short-lived Isotopes Studied by the AKUFVE-technique
SRIM	-	Stopping and Range of Ions in Matter
TASCA	-	TransActinide Separator and Chemistry Apparatus
TEA	-	Triethylamine
THF	-	Tetrahydrofuran
TRIM	-	Transport of Ions in Matter
TTA	-	Thenoyltrifluoroacetone
UV	-	Ultraviolet
VLTC	-	Vacuum to Liquid Transfer Chamber

Publications

This thesis is based on three publications, which are listed below. The author is the main author of these publications.

[1] D. Krupp and U. W. Scherer, "Prototype development of ion exchanging alpha detectors," *Nuclear Instruments and Methods in Physics Research Section A: Accelerators, Spectrometers, Detectors and Associated Equipment*, vol. 897, pp. 120–128, 2018.

[2] D. Krupp, et al., "Development of a fast characterization setup for radionuclide generators demonstrated by a ^{227}Ac-based generator," *Radiochimica Acta*, vol. 109, no. 3, pp. 205–214, 2021.

[3] D. Krupp, et al., "Speeding up liquid-phase heavy element chemistry: development of a vacuum to liquid transfer chamber (VLTC)," *Nuclear Instruments and Methods in Physics Research Section A: Accelerators, Spectrometers, Detectors and Associated Equipment*, vol. 1011, pp. 165486, 2021. (online)

Contents

Chapter 1

Introduction

The radioactive decay, as a spontaneous nuclear reaction, was discovered by Antoine Henri Becquerel in 1896 while handling a uranium mineral [1]. Natural uranium is a α-emitter [2]. Alpha-decay is the emission of a $^{4}_{2}He^{2+}$ - ion from a radioactive nuclide and is one of the dominant decay modes of elements heavier than lead (Z > 92). The kinetic energy of α-radiation varies from about 3 - 12 MeV. However, due to the mass and the charge state of the $^{4}_{2}He^{2+}$ - ion, α-particles have only a very short range of typically a few µm in practically any condensed matter. The short range of the α-particles represents a particular challenge for the (energy-resolved) measurement, since the radiation can easily be shielded by the sample itself (self-absorption). The energy resolved measurement of this radiation was made possible in 1940 by gas-filled grid detectors. For some 60 years, it is now possible to perform α-spectrometry with semiconductors [1]. For a measurement with high spectral resolution, the samples which potentially contain α-emitters must often be elaborately chemically pretreated and, in a subsequent step, deposited in extremely thin layers on surfaces in order to prevent self-absorption. The samples are then measured in evacuated chambers using a silicon semiconductor (Si detector). Alternatively, the samples are measured with so-called liquid scintillation counters (LSC). However, with these measurement techniques, care must be taken to ensure that the samples are suitable for measurement. Whether the sample preparation was successful is usually only revealed by the measurement itself. These different circumstances are accepted, as the spectrometric measurement of α-radiation is often the only way to get information about the α-emitting radionuclide and its activity. The possible sources for α-emitting radionuclides are very diverse and vary in the sample and measurement requirements: from naturally occurring radionuclides ^{232}Th, ^{235}U and ^{238}U (and their progeny) [3] to industrial sources, like those used in the decommissioning of nuclear facilities [4] [5] to medical fields, e.g. for cancer therapy [6] [7] [8]. In addition to the mentioned applications of α-spectrometry in the sense of radiation protection or medical treatment, this technique is also an essential component of fundamental research when it comes to the discovery of new elements and the investigation of their chemical properties [9] [10]. These transactinide elements are also referred to as super heavy elements (SHE with Z $\geq$ 104).

The difference in the investigation of SHE compared to the other examples mentioned are the extreme conditions under which the measurement must be carried out. SHE have not yet been found in nature and are only available through fusion reactions at particle accelerators. These heavy elements are typically produced at rates of single atoms per hour or atoms per day. Production via irradiation of radioactive targets with heavy ions often also results in addition in the production of by-products with significantly

higher production rates, which must be reliably separated from the SHE in question. After the successful separation of the SHEs, in a physical preseparator or according to their chemical behavior, these must also be deposited on surfaces in extremely thin samples before these substrates can then be measured using Si detectors to obtain spectrometric information. Compared to conventional applications of α-spectrometry, these investigations of SHE are further complicated by the fact that the currently producible isotopes of the heaviest elements typically have half-lives of only a few minutes to fractions of a second. Despite these limitations, it was possible to extend the periodic table to element 118 [11], with an ongoing search for element 119 and beyond [12]. However, due to technical limitations, it was only possible for elements up to seaborgium to investigate chemical properties in the liquid phase by fast automated chemistry apparatus and LSC or silicon detectors. Elements beyond Sg could only be investigated in the gas phase [13].
However, there is great potential in the individual steps to improve the overall process of α-spectrometry from sample preparation to the subsequent measurement, in conventional applications, as well as in fundamental research. Based on the new techniques developed in this work, experiments on transseaborgium chemistry in the aqueous phase could be made possible in the future. Therefore, in the following chapters, first the theoretical basics and the current state of the art for the measurement of α-radiation will be described briefly. Subsequently, the new ways for a more efficient α-spectrometry, which have been developed within this thesis, will be explained.

1.1 Origin of α-emitting radionuclides

Alpha emitters can be found in nature as well as produced artificially by neutron capture or the irradiation of atoms with charged particles (protons or heavy nuclei). Therefore, the sources for α-emitters can be divided into two categories [14]:

1) Primordial radionuclides: radionuclides with long half-lives (in the order $\leq 10^9$ y), which have been present since the formation of the earth and their progeny.
2) Anthropogenic radionuclides: artificially produced radionuclides, e.g., by irradiating nuclides with neutrons, protons or heavier nuclei.

In this section, these categories are described briefly.

1.1.1 Primordial radionuclides and their progenies

Primordial radionuclides were already present when earth was formed. These radionuclides have half-lives in the order of at least several million years and were produced e.g. by cosmic processes, like supernovae or the merging of neutron stars and their corresponding ejections of matter. The primordial α-emitter with the smallest mass number is ^{144}Nd [2]. However, ^{144}Nd is an exception in this region of the nuclide chart. The α-decay becomes one of the major decay modes beyond lead (Z = 82). Therefrom, nearly all elements up to uranium (Z = 92) can be found in large quantities on earth [15]. Especially the long-lived isotopes of uranium, ^{238}U ($t_{1/2} = 4.5 \cdot 10^9 y$), ^{235}U ($t_{1/2} = 7.0 \cdot 10^8 y$) and the long-lived isotope of the thorium (Z = 90), ^{232}Th ($t_{1/2} = 1.4 \cdot 10^{10} y$) and their progeny are the major sources of terrestrial radiation, as the decay chains run over ten or more decay steps.

As one can see from figure 1.1, the major decay mode in all of these decay chains is the α-decay. In

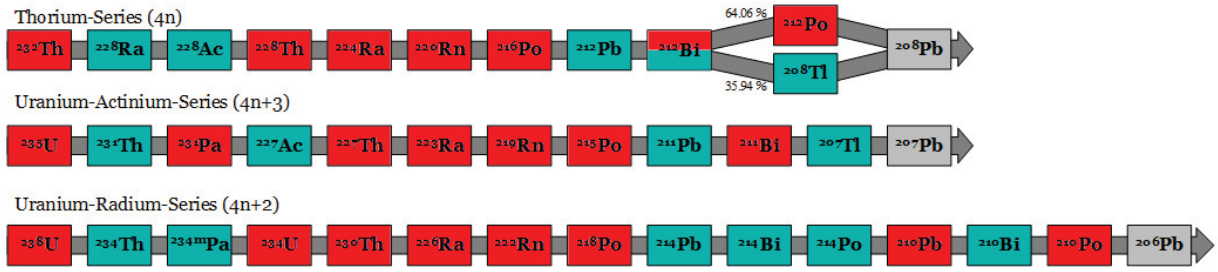

Figure 1.1: *Decay chains of the primordial radionuclides ^{232}Th, ^{235}U and ^{238}U. Alpha-decays are highlighted in red, β-decays are highlighted in green.*

addition to the three decay series still existing today, there was also a fourth decay series starting from ^{237}Np. However, the half-life of ^{237}Np ($t_{1/2} = 2.1 \cdot 10^6 y$) is too short to find the chain in geological formations today [16]. From this decay series only the very long-lived ^{209}Bi ($t_{1/2} = 2.0 \cdot 10^{19} y$) is left. The activity concentration of a certain nuclide in a decay chain depends on the activity of the corresponding parent nuclide. In a system from which no decay products are separated radiochemically, a decay equilibrium is established between the decay of the progeny and the production by the decay of the parent nuclides. The general solution of the successive radioactive decays was presented by Bateman in 1908 [17]. For a decay equilibrium to occur between a parent nuclide and a daughter in a decay chain of any length, the progeny must have a shorter half-life than the parent. If the half-life of the progeny is similar to or longer than that of the mother, no equilibrium is formed. The conditions can be generalized as follows [17]:

$$A_1 \xrightarrow{\lambda_1} A_2 \xrightarrow{\lambda_2} \ldots \quad |\lambda_1 < \lambda_2 \tag{1.1}$$

According to Bateman's equation for an isolated mother nuclide with an activity A_1, the activity of the shorter-lived daughter A_2 builds up over time t according to the following equation:

$$A_2(t) = \frac{\lambda_2}{\lambda_2 - \lambda_1} \cdot A_1^0 \cdot (e^{-\lambda_1 \cdot t} - e^{-\lambda_2 \cdot t}) \tag{1.2}$$

Two cases can be derived from this:

1) If the half-life of the parent nuclide is longer than that of the progeny, a transient equilibrium is established. In equilibrium, the activity of the daughter exceeds the activity of the parent nuclide.
2) If the half-life of the parent nuclide is significantly greater than that of the daughter, a secular equilibrium is established. The progeny decays with the same activity as the parent, in equilibrium.

1.1.2 Anthropogenic radionuclides

Since the decay series, starting from neptunium (Z = 93) has already largely decayed, uranium (Z = 92) is the heaviest element that can be found on earth in large amounts. Plutonium has been discovered in extremely small amounts in uranium ores, and the isotope ^{244}Pu was reported in 1971 by D.C. Hoffman et al. in bastnäsite [18] and recently by A. Wallner et al. [19] in deep-sea crust samples. In order to gain access to heavier elements (or heavier isotopes of naturally occurring radionuclides), they have to be produced artificially. In general, this means conduction nuclear reactions by the irradiation of enriched

isotopes with neutrons, protons or heavier nuclei. The activity of a radionuclide produced by irradiation (with neutrons or charged particles) is calculated by the activation equation [6]:

$$A(t_{irr}) = N \cdot \phi \cdot \sigma \cdot (1 - e^{\lambda \cdot t}) = \frac{m}{M} \cdot N_A \cdot H \cdot \phi \cdot \sigma \cdot (1 - e^{-\frac{ln(2) \cdot t_{irr}}{t_{1/2}}}) \tag{1.3}$$

where A is the activity of the produced radionuclide, $t_{1/2}$ the half-life, N the number of target atoms, ϕ is the particle flux, σ is the cross section and the $(1 - e)$-term describes the saturation of the produced activity with the decay constant of the produced radionuclide λ over the irradiation time t_{irr}.

Neutron irradiations are one way to produce transuranium elements, from neptunium (Z = 93) up to fermium (Z = 100), by successive neutron capture reactions in high flux reactors, followed by β^- decays [20]. The neutron irradiation of ^{238}U, followed by subsequent β^- decays results in ^{239}Pu, followed by further (n,γ) reactions. ^{243}Pu decays under the emission of a β^--particle into ^{243}Am. Further stages of neutron captures and β^- decays result in ^{255}Fm, which concludes this production line through further (n,γ) reactions as ^{257}Fm. As this way of production requires several stages with decreasing amount of target atoms, elements up to californium (Z = 98) can be produced in gram amounts. Einsteinium (Z = 99) is still available in microgram amounts and fermium only in picograms [21].

Fermium isotopes decay either by spontaneous fission or α-decay, therefore it is not possible to produce elements with a higher atomic number by neutron capture followed by β^- decay. The only way to create transfermium elements is to bombard heavy element targets (up to the actinides) with suitable atomic nuclei [22]. Through accelerator based fusion reactions, the heavier elements of the actinide series mendelevium, nobelium and lawrencium (Z = 101 - 103) and even the transactinides have been produced. As mentioned above, elements with Z $\leq$ 98 are available as target material [23]. As the protons of the projectile nucleus and the target nucleus are repelled from each other by Coulomb forces, the projectile requires a certain threshold energy to overcome the Coulomb barrier to induce a nuclear reaction. If the kinetic energy of the projectile is too low to overcome the Coulomb barrier, the projectile is scattered away from the target nucleus and no reaction occurs. With sufficient kinetic energy, the projectile overcomes the Coulomb barrier and comes into the reach of the attractive nuclear force. However, besides the desired complete fusion resulting in production of a super heavy element, there are competing reactions [24]: according to one systematics of nuclear reactions, reactions are distinguished by central or peripheral collisions: in a decentral encounter, a large number of nucleons and energy are exchanged before two fragments separate. This mechanism is called quasifission. In case of a central impact the projectile may fuse with the target nucleus to form a compound nucleus (CN) having a long lifetime compared to that of the binuclear system found in quasifission processes. A fraction of the kinetic energy which was required to overcome the repulsive forces between the nucleus and the projectile will heat the CN. This excess energy can cause fission of the nucleus, so this competitive reaction is called fusion fission. If the CN is able to release its excess energy by evaporation of neutrons instead of a fission reaction, the super heavy element survives as an evaporation residue (EVR). An overview over the different stages in nuclear fusion reaction is shown in figure 1.2.

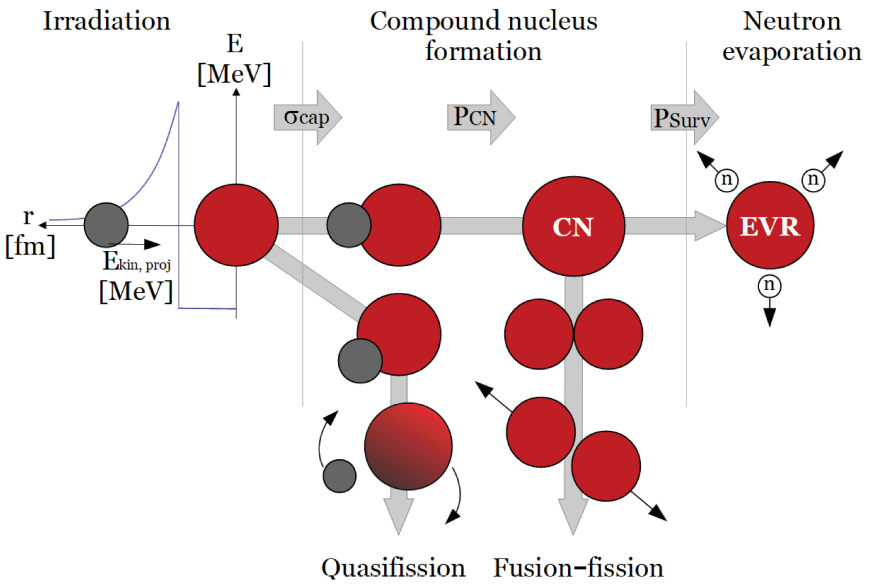

Figure 1.2: *Nuclear reaction mechanisms of a fusion process. Projectiles (grey circle) are accelerated to a threshold energy to overcome the Coulomb barrier (blue line) between target nucleus (red circle) and projectile. In a central collision, the projectile and target nuclei can merge, forming a compound nucleus (CN). By evaporation of neutrons, CN can release excess energy to remain as an evaporation residue (EVR) after the fusion reaction. In addition to the desired production of EVR, quasifission and fusion-fission can occur, resulting in the generation of sideproducts instead of SHE. Based on figure shown in [25].*

The cross section for EVR production is the product of the cross section for the target capturing a projectile (σ_{cap}), weighted by the probability to form a compound nucleus (P_{CN}), instead of undergoing quasifission and also weighted by the chance to deexite, and therefore "survive" (P_{Surv}), instead of undergoing fusion fission. The EVR production cross section (σ_{EVR}) can therefore be described as follows [24]:

$$\sigma_{EVR} = \sigma_{cap} \cdot P_{CN} \cdot P_{Surv} \tag{1.4}$$

As shown the reaction cross section depends not only on the capture of the projectile but also on the survival probability of the generated CN. Since the excitation energy in the CN is higher than the threshold for a fission reaction, the survival probability of the CN (P_{Surv}) depends on a neutron is evaporated (Γ_n) instead of inducing fission (Γ_f). If the energy level is still higher than the fission barrier $P_<$ further neutrons may be evaporated in competition with fission [24].

$$P_{Surv} = \frac{\Gamma_n}{\Gamma_n + \Gamma_f} \cdot P_< \tag{1.5}$$

Besides of the above described reaction scheme fusion reactions leading to elements with high atomic number can be divided into two subcategories [10] [26] [27]: "cold fusion" and "hot fusion". It refers in a fuzzy way to the nuclear excitation energy of the CN. This goes along with the combination of target and projectile. Fusion reactions with medium-heavy projectiles (A ~ 48-70 u), and double magic ^{208}Pb or ^{209}Bi targets show low excitation energies of 10-15 MeV (if the beam energy has the same value as the height of the Coulomb barrier) and, hence, are referred to as cold fusion reactions [10]. One example is the production of ^{265}Hs by bombarding a ^{208}Pb target with ^{58}Fe projectiles. One disadvantage, however, is the production mainly of neutron-deficient nuclei with comparatively short half-lives. In order to gain

access to more neutron-rich isotopes of a SHE, reactions known as hot fusion are carried out [10]: Here actinide targets, typically in a range from ^{238}U up to ^{254}Es, are irradiated with light projectiles (A ~ 18-26 u). The CN mostly have excitation energies of more than 40 MeV. As a result of the higher excitation energies, more neutrons need to be evaporated than in a cold fusion. For example, if ^{248}Cm is bombarded with ^{26}Mg, the heavier hassium isotopes ^{269}Hs (5n reaction) and ^{270}Hs (4n reaction) can be produced. However, in both cold and hot fusion reactions, the reaction cross sections σ_{EVR} decrease sharply with increasing atomic number (see figure 1.3). This is explained for the cold fusion reactions mainly by the increasing fusion hindrance due to the increasing nuclear charge numbers. In the case of hot fusion, the high probability of the competing fission reaction (as discussed in context with equation 1.5) is the main reason for the decreasing cross sections [10]. There is a category in between: "warm fusion" ractions where double magic ^{48}Ca is used as projectile described in more detail below.

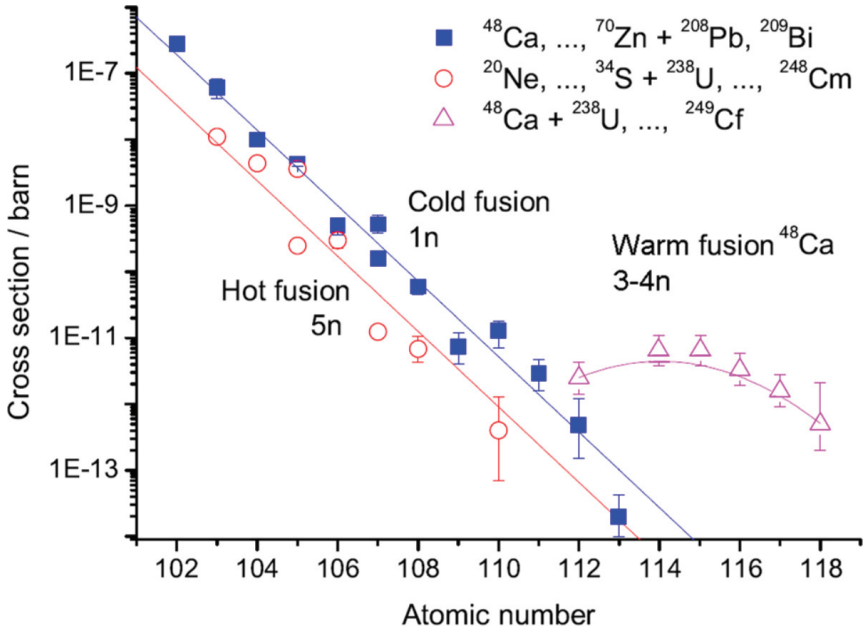

Figure 1.3: *Experimental cross sections for the production of elements in a Z range from 102 - 118 in cold fusion(■), hot fusion(○) and warm fusion(△). Reprinted from [27] with permission of ACS publication.*

Due to the drop in production cross sections, at typical beam intensities of 10^{13} heavy ions per second [28] and a limit on target thicknesses, production rates of single atoms per hour can be expected for Rf and Db according to equation 1.3. For heavier elements such as Hs, it is then only single atoms per day [27]. Since the production rate is directly proportional to the cross section, the expected rate for the elements after Hs would quickly drop to atoms per week. However, by using ^{48}Ca-ions as projectiles, it is possible to keep the production cross section in the picobarn range, where the unexpectedly large production rates are explained by the nuclear shell model [11]. According to this, there are closed shells in the atomic nucleus, similar to the Bohr model for electron shells. Nuclei with completely full shells are particularly strongly bound [29]. The comparably high nuclear stability was observed for nuclei with proton and/or neutron numbers of 2, 8, 20, 28, 50, 82 or 126 (for neutrons). Reactions with $^{48}_{20}$Ca-ions produce CN with excitation energies around 30 MeV. However the competition between the fission probability and the neutron evaporation probability is more beneficial, than in hot fusion, making it more likely that the CN will deexcite into a stable EVR by evaporation of neutrons. Since Ca reactions can produce comparatively more neutron-rich nuclei (than hot fusion ones), but the intermediately produced CN have a higher survival probability (than

in cold fusion), Ca-induced reactions are often referred to as "warm fusion" reactions [27]. With the help of these nuclear reactions it was possible to produce all elements up to element 118 - oganesson [26]. Due to the comparably high reaction cross sections of Ca-reactions, heavy nuclei with $Z \geq 114$ are preferably produced in warm fusion reactions, since hot fusion reactions would have smaller surviving probabilities, leading to lower production cross sections. Due to the comparatively high production cross sections of warm fusion reactions one can produce a heavier element first, which subsequently decays via α-decay into the nuclide of interest [26]. This is called indirect production. An overview of the various nuclear reactions used to produce different isotopes of the SHE is shown in figure 1.4.

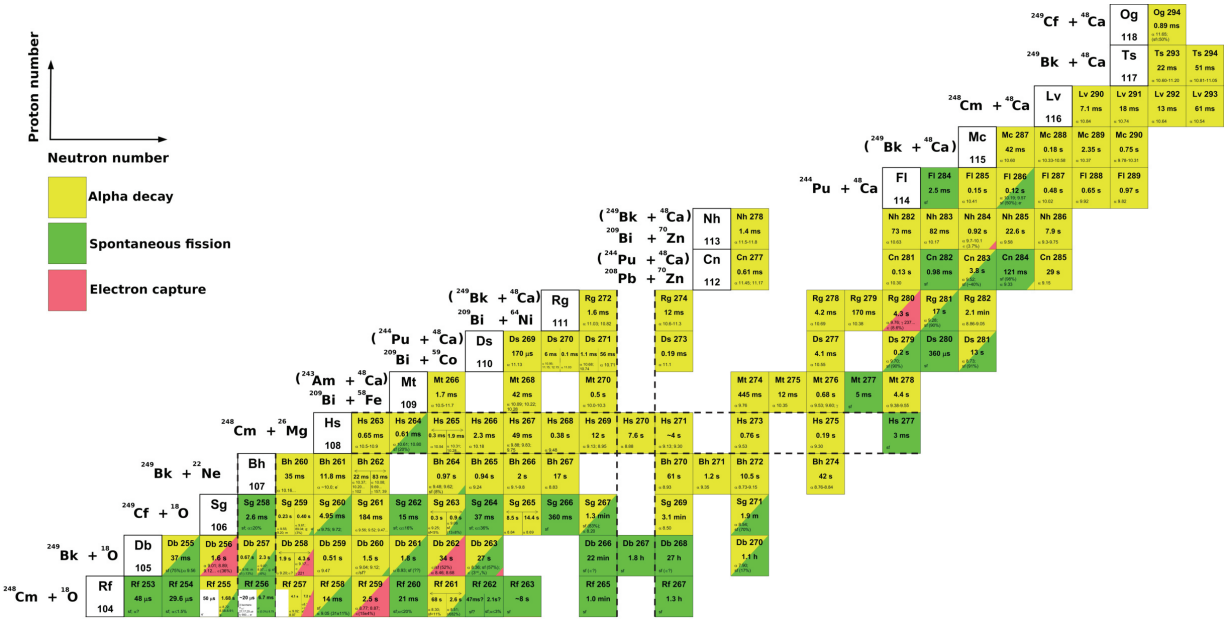

Figure 1.4: *SHE nuclei and production reactions. Neutron deficient isotopes up to elements $Z = 113$ are produced in cold fusion reactions, the others in Ca based warm fusion reactions. Each colored box contains the proton and mass number, as well as the half-life. The coloring indicates the major decay mode: yellow) α-decay, green) spontaneous fission, pink) electron capture. The reactions in brackets represent indirect reactions via heavier nuclei. Reactions were taken from [30] and [22].*

In addition to the already known elements, the next element 119 is currently being searched for [12]. A further goal of current research is the search for heavier isotopes of the already known elements, since a further shell closure is expected for neutron rich isotopes, which should result in comparatively long half-lives [30]. This area in the nuclide map is called the island of stability [31]. However, even with nuclear reactions with high production cross sections and particle accelerators with strong beam currents, the SHE are produced as single atoms per hour or day. In addition, the mean lifetimes of these individual atoms typically range from a few minutes to fractions of a second. This makes the study of SHE a major challenge, as the technologies have to be designed to be as efficient as possible in order to perform a chemical experiment and the subsequent energy resolved measurement. This needs to be done many times in succession with consistent reproducibility in order to obtain a statistically meaningful result on the investigated property of the SHE at the end.

1.1.3 Radionuclide generators

Only a few facilities in the world are capable of producing elements in the SHE-region. Since experimentation time in such facilities is limited, a large number of preliminary tests of new devices must be carried out without an accelerator facility. Radionuclide generators offer the possibility of providing short-lived radionuclides even without an accelerator or neutron source. This allows a large number of experimental parameters to be tested "offline". In general, a radionuclide generator consists of at least two radionuclides, of different elements, which are in decay equilibrium [32]. Well known examples of generator pairs are ^{99}Mo ($t_{1/2}$ = 66 h) / ^{99m}Tc ($t_{1/2}$ = 6 h) [33] or ^{68}Ge ($t_{1/2}$ = 271 d) / ^{68}Ga ($t_{1/2}$ = 68 min) [34] generators, which are primarily used for diagnostic or therapeutic medicine. However, these equilibria can also be described for longer decay chains, like the decay chains of the primordial nuclides ^{232}Th and $^{235/238}$U (see section 1.1.1). Since the mother and daughter nuclide are chemically different from each other, the mother can be fixed on a stationary phase (e.g. an ion exchange column) to produce the shorter-lived daughter nuclide by its decay. Using a suitable eluent, the daughter nuclide is selectively eluted, while the parent nuclide remains fixed on the stationary phase. How well an ion is retained at a stationary phase can be expressed, e.g., by the distribution coefficient D [35] (here shown for a cation (X^+) and a cation exchanger ($Resin - SO_3H$)):

$$D = \frac{[Resin - SO_3^- X^+]}{[X^+]} \tag{1.6}$$

The distribution coefficient depends on the stationary phase, the respective ion and the eluent. In addition to the diagnostic/peutic aspect in radiopharmacy, such generator systems also allow the production of homologous elements of SHE, e.g. Pb for Fl (Z = 114) and Bi for Mc (Z = 115) in no carrier added state [36]. This fact makes it possible to produce short-lived radionuclides for chemical experiments of SHE homologs without the need for an accelerator. An example of this is shown in [37]: ^{228}Th is fixed on a cation exchange column. Over successive decays, ^{212}Pb is formed, which in turn decays into ^{212}Bi. In the ^{228}Th decay chain example, using hydrochloric acid solutions of different concentrations, it is possible to selectively elute first only ^{212}Bi and then ^{212}Pb from the cation exchange column (see figure 1.5).

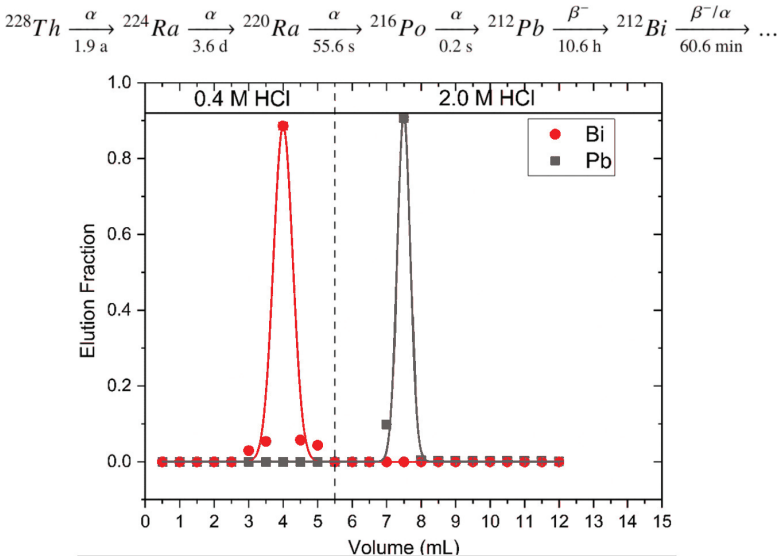

Figure 1.5: *Selective elution of ^{212}Bi in 0.4 M HCl and ^{212}Pb from a ^{228}Th decay chain. Graphic was taken from [37]. Reprinted with permission of Springer Nature.*

The half-life of the eluted nuclide determines the time intervals at which the generator can be eluted again. According to equation 1.2, as long as ^{228}Th, ^{224}Ra and ^{212}Pb remain on the column, 99.9 % of the equilibrium ^{228}Th activity is reproduced as ^{212}Bi activity within 606 min ($10 \cdot t_{1/2}$ (^{212}Bi)).

1.2 Theory of α-decay

The term "α-radiation" was first mentioned in 1899 by Ernest Rutherford, who distinguished between α- and β-decay by the different ranges in matter and their behavior in an electromagnetic field [38]. Later on, it was proven that the α-particle is a $^4_2He^{2+}$ - ion, which is mainly emitted by elements heavier than lead. The generalized equation for the α-decay can be written as [14]:

$$^A_ZX \rightarrow ^{A-4}_{Z-2}Y^{2-} + ^4_2He^{2+} + Q \tag{1.7}$$

where the parent nuclide X decays spontaneously into its progeny Y under the emission of an α-particle ($^4_2He^{2+}$). The sum of the masses of the decay products is smaller than the masses of the parent nuclide. The mass difference is converted into decay energy Q due to the mass defect and Einsteins general relativity equation [39]:

$$E = \Delta M \cdot c^2 = Q = (M_X - M_Y - M_\alpha) \cdot c^2 \tag{1.8}$$

The decay energy is distributed between the kinetic energy of the α-particle E_α and the recoil of the daughter nuclide E_{recoil}. In some cases, the daughter nuclide is in an excited state after decay, which subsequently deexcites by other nuclear processes E_{NP} (e.g. by γ - ray emission):

$$Q = E_\alpha + E_{recoil} + E_{NP} \tag{1.9}$$

The kinetic energy of the recoil nucleus and the alpha particle Q_{alpha} can therefore be calculated from the decay energy Q minus the energy of the excited state:

$$Q - E_{NP} = Q_\alpha = E_\alpha + E_{recoil} \tag{1.10}$$

Due to conservation of momentum, both decay products are emitted in opposite directions. In the center of the mass frame, the decay energy is distributed between the decay products according to:

$$E_{Recoil} = E_\alpha \cdot \frac{M_\alpha}{M_{recoil}} \tag{1.11}$$

If the parent nuclide is in motion $\vec{E}_{kin,X}$, this must also be taken into account in the calculation of the kinetic energy of the alpha particle $\vec{E}_{\alpha,total}$.

$$\vec{E}_{\alpha,total} = \vec{E}_\alpha + \vec{E}_{kin,X} \tag{1.12}$$

As shown by equation 1.7 - 1.11, the fraction of decay energy, which is converted into the kinetic energy of the α-particle is discrete. These distinct energies vary between 1.90 MeV (^{144}Nd) and 11.70 MeV (^{294}Og) [2]. However, typically α-energies range between 4 - 10 MeV [39]. In contrast to the narrow energy range, the half-life of α-emitters range around 30 orders of magnitude [2]. In 1911, Hans Geiger and John M. Nuttall discovered the inverse correlation between the half-life of an α-emitter and the kinetic energy of the emitted α-particles (represented by their range in air), in the natural decay series [40]. Based on their observation, Geiger and Nuttall formulated the empirical formula:

$$log\left(\frac{ln(2)}{t_{1/2}}\right) = a \cdot log(R) + b \tag{1.13}$$

where the half-life $t_{1/2}$ is correlated with the range R. The coefficients a and b represent parameters for the best curve fit of the individual decay chain. The Geiger-Nuttall law and modifications of this formula later on were able to describe phenomenologically the inverse relation between the energy of α-particles and the half-life of the α-emitting radionuclide. However, there was still no proper theory why a nucleus is able to emit $^4_2He^{2+}$ ions at all.

The protons and neutrons in a nucleus are attracted by the strong nuclear force. The range of the strong nuclear force is in the order of femtometers. Contrary to the attractive nuclear force, the protons in the nucleus are repelled by the Coulomb force. This electromagnetic force has an infinite range, where the repulsive Coulomb potential decreases with the radius, by the factor r^{-1}. This repulsive force acts in both directions: it repels incoming $^4_2He^{2+}$-ions from entering the nucleus and the strong nuclear force prevents $^4_2He^{2+}$-ions from leaving the nucleus. Typical heights of such Coulomb barriers are 25 - 30 MeV [41]. Hence, according to classical physics, there is no explanation why α-particles with energies of 4 - 10 MeV are observed. The explanation for the emission of α-particles, having insufficient kinetic energies to overcome the Coulomb barrier was given by George Gamow in 1928. In his work, he combined quantum mechanics with the theory of α-decay [42]. The principle is shown in figure 1.6.

Based on these combined theories, the α-particles, described by a wave motion, don't require the energy to overcome the Coulomb-barrier, but can tunnel through the potential wall. The probability of tunneling depends on the area under the potential curve, which has to be passed by the α-particle. In other words, the tunneling probability increases with the energy of the α-particle in a given nucleus. So Gamow's theory was also in agreement with the Geiger-Nuttall law, as it states that high energetic α-particles have a higher probability to be emitted and therefore the corresponding radionuclide has a shorter half-life. By irradiating 392 MeV protons onto tin targets, it was also experimentally shown that α-nuclei form in the neutron-rich surface of the target nucleus, as these α-nuclei could be knocked out of the Sn-nucleus by the proton bombardment [44]. Experimental observations like these further supports Gamow's theory.

After the emission of an α-particle, the range of the $^4_2He^{2+}$-ion depends on its kinetic energy and the material through which it passes. In order to quantify the absorption potential of a substance for α-particles, the stopping power S is used. It is defined as the fraction of its kinetic energy dE lost per distance dx traveled by the particle in the medium [39].

$$S(E) = -\frac{dE}{dx} \tag{1.14}$$

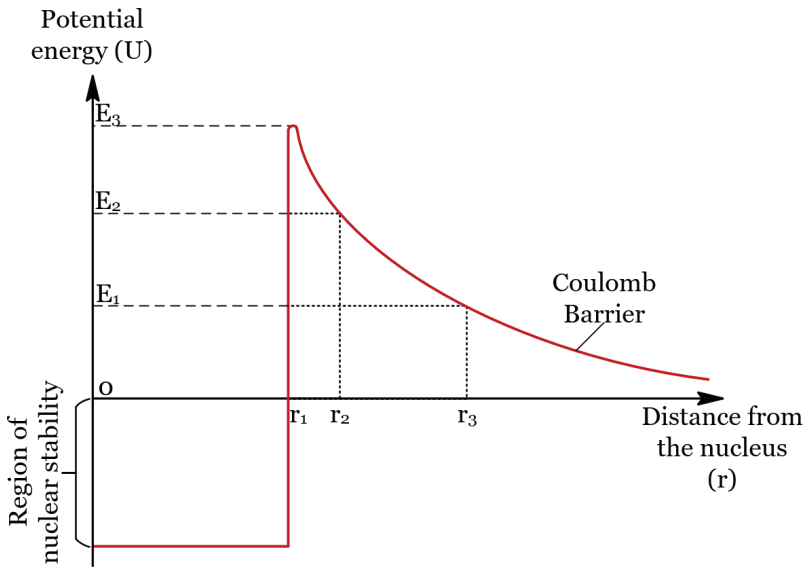

Figure 1.6: *Nuclear potential energy and coulomb barrier in a nucleus scheme. Alpha particles with an energy E in the region of nuclear stability cannot escape the nucleus. Alpha particles with an energy E* $\geq E_3$ *would overcome the Coulomb barrier and escape. Alpha particles with energies* E_1 *or* E_2 *have to tunnel through the region between* r_1 *and* r_3*, respectively between region* r_1 *and* r_2 *in order to escape. (The graphic was adapted from [43]).*

There are different mechanisms of how the emitted ions transfer their energy to the surrounding material. Through Coulomb attraction, the ion interact with the electrons of the surrounding material, causing ionization in the materials. If the energy transferred from the ion to the electrons of a material is too low for ionization, excitation is caused by transferring an electron into an excited state, resulting in subsequent deexcitation of this electron by the emission a photon. As the ions (A_{ion} = 4 u) are much heavier than the electrons ($A_e = 5 \cdot 10^{-4}$ u), the ion path is nearly unaffected. A less common interaction is the deflection of an ion due to direct collision with the Coulomb barrier of a nucleus, having a chance of one in several thousand collisions [39]. So, the total stopping power S_{total} consists of the electronic stopping power $S_{electronic}$, as energy loss due to inelastic collisions between the α-particle and the electrons of the substance and the nuclear stopping power $S_{nuclear}$ of direct interaction with the nucleus. For ${}^4_2He^{2+}$-ions, the electronic stopping power has the the higher probability and therefore the main contribution to the total stopping power.

$$S_{total} = S_{nuclear} + S_{electronic} \approx S_{electronic} \tag{1.15}$$

The kinetic energy of a charged particle is typically several orders of magnitude higher than the ionization energy in a material. For example, the ionization energy of air is around 35 eV, where as α-particles have kinetic energies in the order of 4 - 10 MeV. Even a "low energy" α-particle of 4 MeV creates up to $1.1 \cdot 10^5$ ion pairs before it is stopped.

The range R of an ion with its initial kinetic energy E_0 can be calculated from the stopping power of the material $S(E)$ according to equation 1.16.

$$R = \int_0^{E_0} \frac{dE}{S(E)} \tag{1.16}$$

A common program for stopping power calculations is the program package SRIM (Stopping and Range of Ions in Matter) [45]. For more complex ion transport calculations (and the corresponding total stopping power calculations), the Monte Carlo based simulation programs TRIM (TRansport of Ions in Matter) and, especially for α-particles, AASIFIT (Advanced Alpha-Spectrometric Simulation and Fitting) [46] are widely used.

1.3 Detection principles for α-emitting radionuclides

Alpha spectrometry yields line spectra, which serve as a fingerprint information for the α-emitting radionuclides and can be used for nuclide- and activity determination. To enable energy-resolved measurements of α-radiation, the kinetic energy of the α-particle must be converted into an electrical signal. The intensity of the electrical signal must be proportional to the kinetic energy of the α-particle. Regardless of the type of detector, this electrical signal is triggered by interaction processes of the α-particles with a detector material. The first detectors for energy-resolved α-measurement were so-called gridded ionization chambers [1]. Here, the α-particle interacts with gas molecules, generating cations and electrons. The cations are drawn to the cathode and discharged. However, unlike gas-filled detectors that cannot measure energy-resolved (such as the Geiger-Müller counting tubes), the electrons do not travel directly to the anode, but first pass through a grid. The drift of the electrons between the grid and the anode generates the electrical signal that is used for the energy-resolved measurement [47]. However, the energy-resolved measurement with gas-filled detectors has now been largely replaced by other forms of detection [39]: currently, the most widely used method for the high-resolution measurement of α-radiation is the measurement of a sample made as thin as possible (ideally without self-absorption) with a silicon semiconductor detector in a vacuum chamber. Alternatively, special liquid scintillation measuring systems, often referred to as liquid scintillation counters (LSC), are used, especially for quantitative α-measurements and increasingly also for spectrometric measurements. Here, the α-emitting radionuclides are mixed with a cocktail consisting of a solvent and a scintillator.

In order to achieve highly resolved α-spectra, two main aspects need to be considered: the type of detection system and the sample preparation. Especially the sample preparation is different for industrial applications and for fundamental research experiments. In this section, semiconductor detectors and LSC, as the most common detection systems for energy resolved α-spectrometry, including widely used techniques for sample preparations in commercial applications, are described. Subsequently, an overview of sample preparation and detection purposes, with focus on SHE-research applications is given.

1.3.1 Silicon-semiconductor-detectors (Si detectors)

One of the most used solid state detector types for high resolution α-spectrometry is the silicon semiconductor detector (Si-detector), a technology, which has been available since the late 1960s [1]. The electrical properties of a Si detector can be described with the band model [48]: According to the band model, electrons in a crystal are either tightly bound in the valence band or mobile in the conduction band. There is an energy gap between the valence and conduction band. Only electrons with a sufficiently high energy can be transferred from the valence band to the conduction band. The gap width can then be used to distinguish between non-conductors (large gap), conductors (overlapping valence and conductor band) and semiconductors (small gap). Silicon is a semiconductor, however, at room temperature, silicon has practically no electrons in the conduction band. Only at higher temperatures some electrons have enough energy to move from the valence band to the conduction band. In order to use silicon as an α-detector, differently doped silicon layers are typically combined [14]: in this doping process, individual atoms in the silicon lattice are replaced by elements of group 13 or 15. Doping with arsenic (group 15), for example, results in excess electrons at these points in the silicon lattice (n-doping). These electrons are bound more weakly and therefore have higher mobility in the silicon. Doping with e.g. boron (group 13) creates an electron deficient "hole" (p-doping). A so-called depletion layer is formed between the p- and n-layers. Unlike the p- or n-doped layer, there is no electron or hole excess in this thin intermediate layer, since electrons and holes cancel each other out here (see figure 1.7).

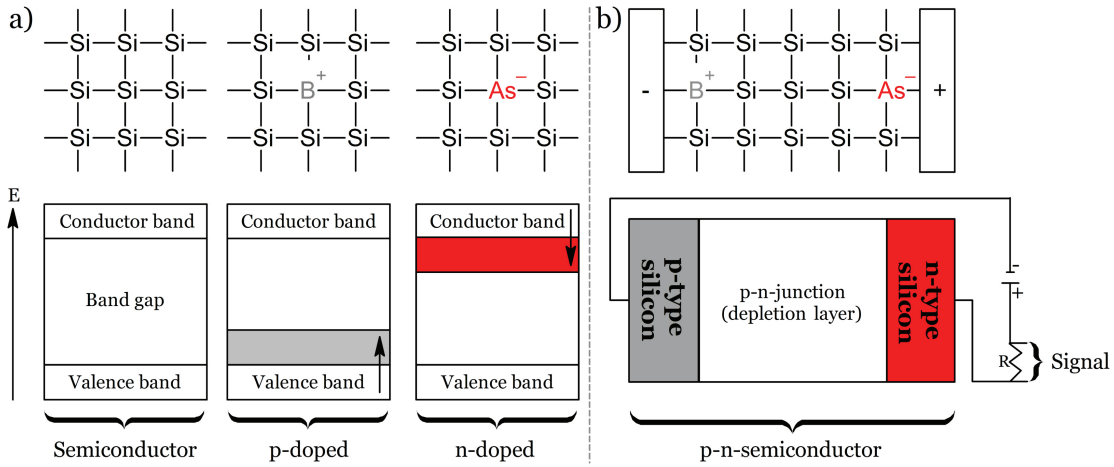

Figure 1.7: *a) Schematic representation of pure and doped silicon with effects of doping according to the band theory. b) Combination of p- and n-doped silicon with applied plus and minus poles in a "reversed bias" configuiration.*

By using a DC voltage, the negative pole is applied to the p-doped side and the positive pole to the n-doped side, which allows the Si detector to operate in a "reversed bias" configuration [39], unlike ordinary diodes. Due to this arrangement, the detector blocks the current flow and acts as a resistor in the circuit (the current, which flows through the circuit is minimal). At the same time, depending on the applied voltage, the depletion layer is increased. Only when radiation is incident on the detector electron/hole pairs are generated in the depletion layer, which are then attracted to the respective pole. Thereby 3 eV energy is required to generate a electron/hole pair [47]. This results in very small currents (µA), which are then amplified proportionally as an analog signal by the connected hardware and digitized with the aid of pulse height analysis (PHA). Since the number of generated primary electron/hole pairs is proportional to the

energy of the α-particle, an energy-resolved spectrum of the measured α-particles can be displayed as a histogram after digitization. Since the leakage currents are very low, due to the bias configuration stronger signals are only generated by the interaction of α-radiation. Hence, Si-based detectors have a low intrinsic background (10^{-5} – 10^{-6} cps) [39]. Due to the short range of α-radiation in matter (see section 1.2), 200 µm of silicon is sufficient to completely stop α-particles with a kinetic energy of 10 MeV [49]. Due to the thin design, Si detectors only have a weak response to γ- and β-radiation. Each α-particle that enters the detector material is therefore measured with an intrinsic efficiency of ≈ 100 %. The overall efficiency of the measurement thus depends only on the relative position of the sample to the detector (geometric efficiency) and on possible absorbers between source and detector. In order to achieve the highest possible overall efficiency (with good spectral resolution) of the measurement, samples are manufactured in special processes (see following section). An ideal sample should be applied homogeneously to a substrate and should not exhibit any self-absorption. To prevent air from being between the sample and the detector and stopping α-particles, the sample is usually placed in an evacuated chamber at a short distance from the detector. A schematic overview of essential components in the Si detector based α-detection is shown in figure 1.8.

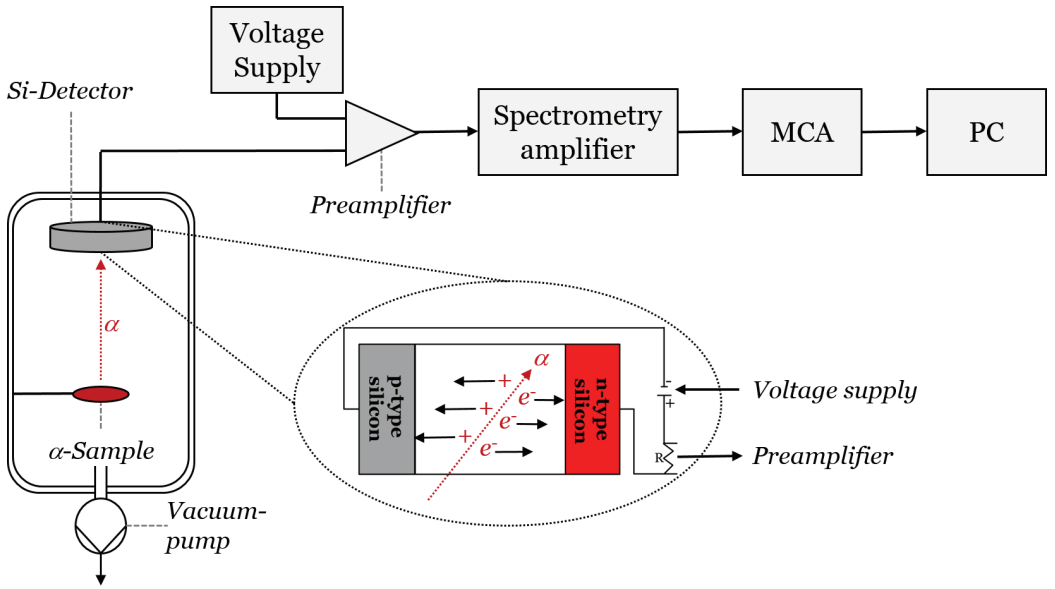

Figure 1.8: *Schematic overview of Si detector based spectrometry. A sample, deposited on a surface, is placed in a vacuum chamber, in front of a Si detector. The bias voltage is applied to increase the thickness of the depletion layer in the Si detector. Through interactions of α-particles with the silicon, the kinetic energy of the α-radiation is converted into electron-hole pairs in the Si detector. When the electrons generated in this way (a few µA) pass through a resistor, a voltage signal can be generated which is then amplified and converted into an energy-resolved spectrum in a multi channel analyzer (MCA).*

Due to their size and two positive charges, α-particles are stopped within a few µm in literally any material (see chapter 1.2). This circumstance usually requires special effort in the sample preparation and the production of a measurable sample, since too thick samples but also inactive contaminations on the sample would already lead to absorption of the α-particles. To overcome the problem of self-absorption, various methods have been developed to produce homogeneously deposited samples that are as thin as possible. The general procedure of an α-sample analysis can be divided into seven points [39]:

1) Raw sample collection and preconcentration
2) Addition of a tracer
3) Sample dissolution
4) Chemical separation
5) Deposition of the α-emitting radionuclide (ideally thin and homogeneous)
6) Energy resolved measurement
7) Calculation of tracer recovery and sample activity

Depending on whether the sample is solid, liquid or gaseous, the sample must first be enriched before a sufficient amount of α-emitter is available for a sample. An example are uranium measurements in drinking water [50], where several liters of water samples are evaporated to dryness before further processing. In the case of e.g. soil samples, they are first dried and ground. Organic components are then pyrolyzed in a furnace at elevated temperatures (around 500 - 600 °C) [51]. As the subsequent steps usually involve yield losses, a known quantity of a tracer is added in order to calculate the original activity in the sample at the end of analysis. Typically (but not exclusively), the tracers are isotopes of the radionuclides to be analyzed. Examples are ^{232}U tracer for $^{238/235}$U analysis [50] or ^{242}Pu tracer for ^{239}Pu analysis [51]. The concentrated solid residue is then dissolved in a solution suitable for subsequent chemical separation, in the simplest case with dilute acids (e.g. nitric acid). In the case of geological samples or metals, more aggressive media such as mixtures of concentrated hydrochloric acid and nitric acid [51] up to aqua regia (conc. HCl, conc. HNO_3 v/v 3:1) with HF added can also be used to dissolve the sample completely. The dissolving process can also be supported by heating (e.g. in microwave oven). In addition to the radionuclide in question, many (stable) elements are still present in the sample after dissolution, which must first be separated to ensure successful preparation of a sample. Techniques like ion exchange chromatography [52] [53], micro precipitation [54] [55] and liquid-liquid [56] or solid-liquid [57] extraction are mainly used for preconcentration of the radionuclide in question, while separating potential impurities. In many cases, the micro precipitation can also be used to prepare the final sample. After successful separation, several options are available to produce thin homogeneous layers of the α-emitting radionuclide. Direct evaporation on a stainless steel plate can be sufficient in many cases, since after successful chemical separation the radionuclide is concentrated in a small volume [58] [59]. This technique is still used today to prepare actinides homogeneously on surfaces with precision stepper motors and micro pipettes [60]. Nevertheless, care must be taken during the evaporation process to ensure that no increased material accumulation forms at the edges of the dropped-on sample during the drying process. Otherwise, increased self-absorption of the α-radiation may occur in these areas. Therefore, surfactants are often added to the evaporation process to reduce the surface tension of the droplet. In addition to micro precipitation and direct evaporation, electrodeposition from the aqueous phase [61] [62] [63] or molecular plating from the organic phase [64] [65] are standard methods for the production of α-samples. The general structure is similar for electrodeposition and molecular plating:

A solution suitable for the electrodeposition application in question is filled into a container made of electrically non-conductive material such as PTFE. A cathode made of conductive material is located at the bottom of the container (e.g. stainless steel) and an anode (e.g. platinum) is attached to the opposite side. By applying a DC voltage, the metal ions in the solution are reduced and plated on the cathode surface, over several hours. The dried samples can then be measured in a vacuum chamber by a Si detector (see

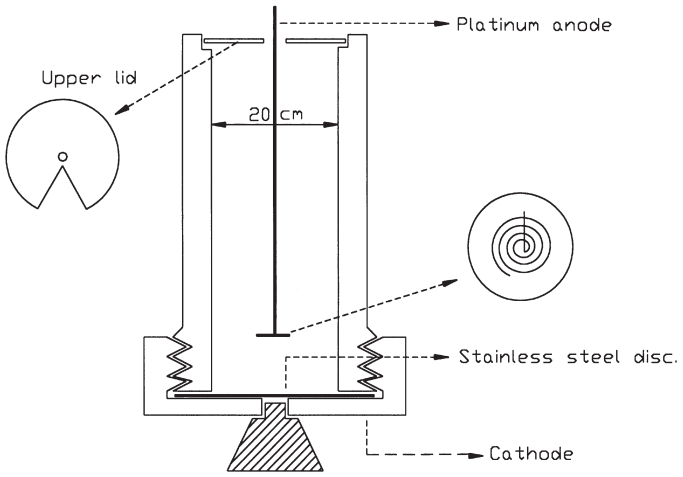

Figure 1.9: *Electroplating cell for α-sample preparation. A dissolved sample of α-emitting radionuclides (not shown in the figure) is filled into the cylinder. By applying a voltage between the platinum anode (oxidative reaction) and the metal substrate cathode (reduction), a deposition of the radionuclide on the substrate takes place. Adapted from [63]. Reprinted with the permission of Elsevier.*

section 1.3.1). Depending on the overall efficiency of the measurement setup and the required statistical accuracy, samples are measured for several hours to days. A typical α-spectrum of a $^{238/234}$U sample is shown in figure 1.10. The sample was prepared from a [$^{238/234}$U]uranyl acetate stock solution according to the ISO 13166 [50] specification and measured for 6 h.

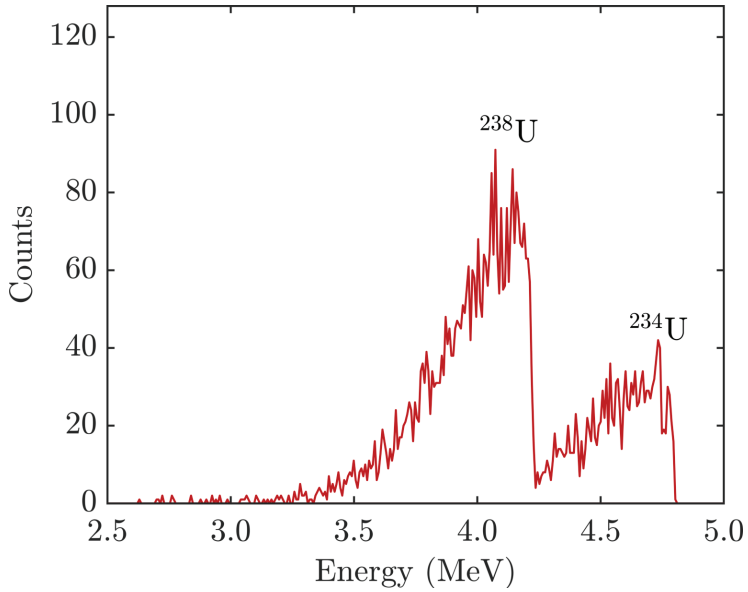

Figure 1.10: *$^{238/234}$U spectrum, acquired for 6 h. The measurement was performed in an ORTEC α-chamber, equipped with an ORTEC ULTRA^{TM} Si detector (active window 25 mm^2).*

An ideal sample yields peaks with a symmetric Gaussian shape. However, due to self-absorption effects in the deposited sample and collisions of the α-particles with the remaining gas particles in the vacuum chamber, the measured peaks often have a tail towards lower energies. In spectra with several α-emitters, the peaks may therefore have to be deconvolved. The measured count rates can be used to calculate the activity of the α-emitter in the original sample either by using a reference source measured in the same geometry or by using the known tracer activity.

1.3.2 Liquid Scintillation Counting (LSC)

In liquid scintillation counting (LSC), α- or β- emitting radionuclides are mixed homogeneously with a so called scintillation cocktail [39] [66]. This cocktail consists of scintillator molecules (light emitting molecules), dissolved in an organic solvent, like benzene, toluene or xylene. Depending on whether the radionuclide to be measured is present in an aqueous matrix, additional substance classes such as short-chain alcohols or dioxanes are added to the cocktail to enable mixing of the aqueous sample matrix with the organic phase. Due to the short range of β- and α- radiation compared to γ- radiation, it is very likely that the full kinetic energy of these particles is deposited in the cocktail. Along their trajectories, different interactions with the cocktail take place. Since the scintillator molecules are present only in low concentrations in the cocktail, it is likely that these interactions take place primarily with the solvent molecules [39]. In addition to ionization, radical formation and molecule fragmentation, molecular excitations also take place. If one compares theoretically a β- and an α- particle of the same energy, the range of the β-particles in the cocktail is greater than that of the α-particles. At the same time, the excitation of the molecules along the trajectories is lower in energy for β-particles than for α- particles. When this excitation energy is then transferred from a solvent to a scintillator, like 2,5-diphenyloxazole (PPO), this excited scintillator can deexcite to the ground state by e.g. emission of photons. Mainly due to the higher linear energy transfer and the stronger excitation of single molecules, the photon yield of α-particles is on average ten times lower than that of β-particles with the same kinetic energy. At the same time, the scintillator molecules take longer to return from the higher energy level to the ground state ($t_\alpha \sim$ 200 - 300 ns, $t_\beta \sim$ 1-2 ns) [67].

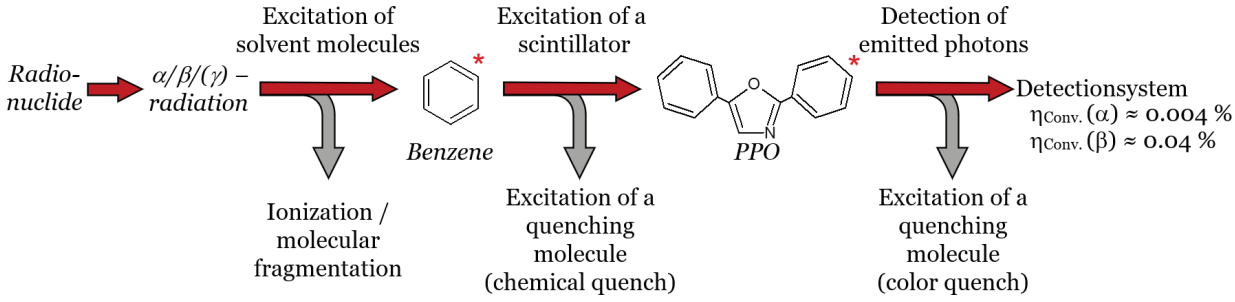

Figure 1.11: *Schematic overview of LSC based spectrometry: α- or β- particles transfer their kinetic energy as excitation energy to solvent- and scintillator molecules. Scintillators deexcite by photon emission, which are processed by electrical components. In each process step, competitive reactions can occur that can lower the photon yield (quench). Due to the varying degree of molecular excitation and the possible quenching reactions, approx. 0.04 % of the kinetic β-energy is converted into photons in a low quenched sample. For α-particles, only 0.004 % of the energy is used for photon generation, as described in [67].*

The emitted photons can then be detected by a photomultiplier tube. However, this process of energy transfer can also be disrupted [68], e.g., if the excitation energy is transferred from a solvent molecule to a molecule, like nitrobenzene, which deexcites primarily by molecule vibration and not through photon emission. Such a process is called chemical quenching. In addition to chemical quenching, other effects such as color quenching can also lead to an interruption of the chain of events [69]. In the case of color quenching, a substance is present in the cocktail that absorbs the photons emitted by the scintillator. Similar to the chemical quench, the absorbed energy is no longer emitted as photons during the deexcitation [70]. The schematic sequence of conversion of a primary radiation event into photons is shown in figure 1.11.

The photons are converted to analog signals by a photo multiplier tube (PMT). This analog signal is amplified and shaped for subsequent analog to digital conversion in a multi channel analyzer (MCA). As described above, in order to differentiate between α- and β-pulses, the time information of the individual pulses is sampled, too. The photon pulses related to α-decays are longer than those of β-decays. In case of a suitable scintillation cocktail, the difference in the pulse decays can be differentiated by an α/β-discrimination in two plateaus [39]. As schematic overview of the essential electronic steps in the α/β-LSC technique is shown in figure 1.12.

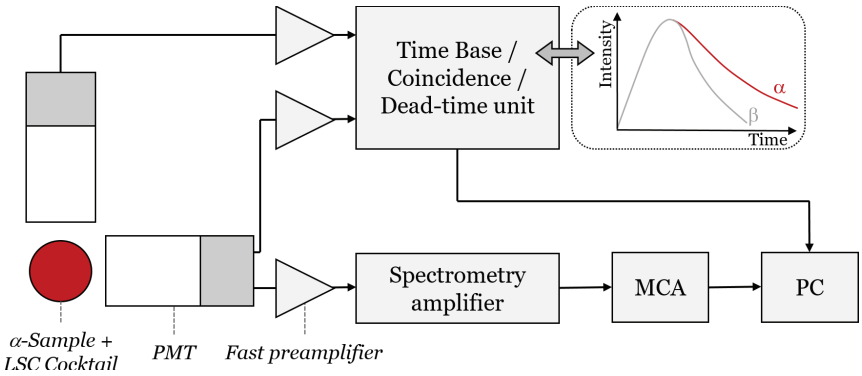

Figure 1.12: *Schematic overview of the electronic signal processing steps in the α/β-LSC technique. For better readability, only the essential components for the production of a α/β-separated spectrum are shown. A sample (top view) emits photons after α-and β-decays. These are converted into electrical signals in photo multiplier tubes (PMT). These signals are amplified and digitized. In addition, the length of the photon pulse is recorded in a time base in order to subsequently perform an α/β-separation.*

When measuring a sample in which α- and β-emitting radionuclides are present in the cocktail, a sum spectrum (events from α-decays and events from β-decays) is first constructed in an MCA. The separation is then performed via a manually set discriminator threshold, which separates the pulse height spectrum according to the time information of the individual impulses as shown in figure 1.13. Here $^{238/234}$U was measured in equilibrium with the ^{238}U β^--emitting progeny ^{234}Th ($t_{1/2}$ = 24.1 d) and ^{234m}Pa ($t_{1/2}$ = 1.2 min).

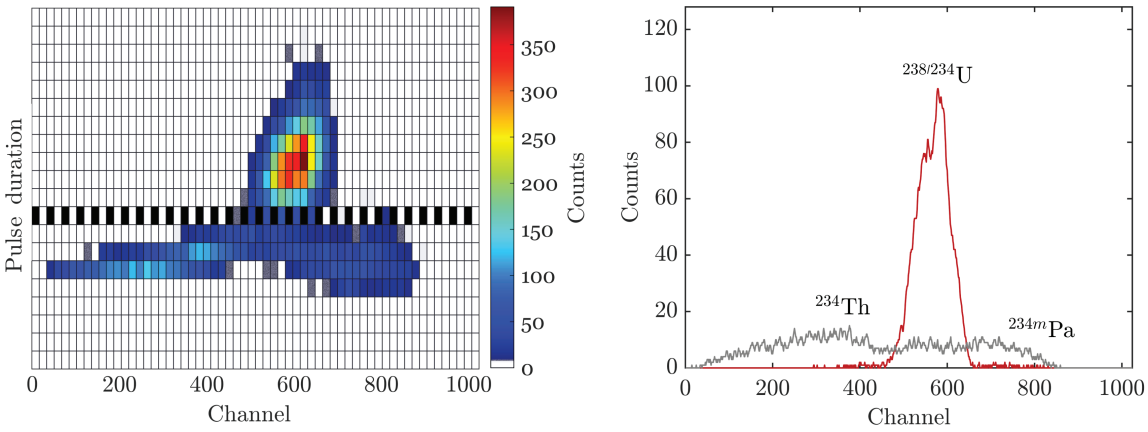

Figure 1.13: *Pulse duration analysis in α/β-separated LSC measurement of a [$^{238/234}$U]uranyl acetate solution (left): the number of detected photon pulses per bin (heat map) are plotted against channels and pulse duration bins. By defining a α/β-discriminator line (black dotted line), separated α- and β- spectra are constructed (right). The measurement was performed with a Hidex SL600 in AquaLight+ cocktail. Acquisition time was set to 5 min.*

As one can see in figure 1.13 (right), the spectral resolution for many LSC measurements is limited. This is particularly clear when comparing the spectrum in figure1.13 (right) with figure 1.10: as one can see, there is no peak separation between the ^{238}U and the ^{234}U peak in the LSC spectrum, due to the lower resolution. The same amount of stock solution was used for both measurements. When the sample is measured with a Si-detector, there is no β-background and the ^{238}U and ^{234}U spectra are clearly distinguishable. On the other hand, the long measurement time (here 5 min LSC vs. 6 h with a Si detector) is omitted with the LSC measurement. In addition, sample preparation is easier with the LSC measurement, as long as the sample mixes homogeneously with the cocktail and causes no strong quenching effect.

In summary, for α-LSC, as the radionuclide is mixed with the primary detection material, the scintillation cocktail, the geometric efficiency of the measurement is up to 100 % (4π geometry). But, the multi step procedure of transferring the kinetic energy of the decay radiation into an analog signal can be disturbed by quench effects, which reduce the number of photons, which reach the PMT. This results in a reduced overall efficiency. Due to the different decay times of the photon pulses, time circuits can be used to separate the photons produced by α - radiation from those produced by β - radiation. Even though α-spectrometry with Si semiconductor detectors still dominates in standardized methods such as ISO standards, LSC methods with α / β - separation also begin to be established as standard methods. However, due to the lower spectral resolution, compared to Si detectors [71], the LSC technique is currently mainly used for gross α-measurements in the ISO methods [72]. Nonetheless, this technique eliminates the need to prepare ultra-thin samples because the α-emitters are dissolved in a scintillation cocktail, as the α-radiation deposits all of its kinetic energy in the cocktail, allowing it to be measured with nearly 100 % counting yield.

1.4 Alpha-spectrometry in superheavy element (SHE) research

In commercial α spectrometry applications, the time it takes to produce a high-quality sample is primarily an economic issue. In SHE ($Z \geq 104$) experiments, time is a decisive factor for the success of an experiment, as the artificially generated nuclei typically have half-lives in the range from minutes to fractions of seconds. In addition, the overall efficiency is of central importance for the success of an experiment, due to the low production rates of the superheavy elements (SHEs). In this section, the essential steps of α-spectrometry applications for experiments with short-lived radionuclides ($t_{1/2} \leq 2$ min) are described for SHE research. As discussed in section 1.1.2, transfermium elements are only accessible through particle accelerators. In contrast to the production of radionuclides for pharmacy, such as ^{18}F, which can be produced from [^{18}O]H_2O in a (p,n) reaction, medium-heavy ion beams and targets from heavy elements are required for the production of SHE. In addition to a suitable reaction, many technical aspects must also be established in order to identify the SHE with the help of a chemical separation and the characteristic α-decay energy. These technical aspects include, the heavy ion beam, the production of a suitable target and the transfer of the generated SHE from the target to a chemical experiment. To do this, the SHE must first be transferred to the gas- or aqueous phase, pass a separation experiment, followed by the preparation of a sample and then performing spectrometry of the SHE. In the following sections, the individual steps of an experiment are described briefly.

1.4.1 Production and transfer of SHE to a chemical experiment

The target consists of a highly enriched nuclide, deposited on a thin supporting foil (e.g. titanium). The production yield of the nuclide in question depends, on the target material, the beam nuclei and on the projectile energy (see equation 1.3). The projectile beam transfers its momentum onto the produced nuclide. If the product has a sufficient recoil momentum, it leaves the target material and is transported into the experimental setup. After the recoil nuclei leave the target, there are basically two options for the following setup. Either the recoils are stopped directly in a recoil chamber (stopping before separation) or the recoils first pass a preseparator before they are stopped (stopping after preseparation).

Stopping before separation

In this method, the recoil nuclide exits the target and enters a recoil chamber (RC), filled with a gas (e.g. helium) at about atmospheric pressure where the recoil nuclides are thermalized [73]. After thermalization, the produced nuclides adsorb on aerosol particles (such as KCl or C), which is injected into the chamber with He carrier gas. Due to negative pressure at the gas outlet of the RTC, the aerosol particles (with the adsorbed SHE) will be flushed out of the chamber in order to be transported to the chemical experiment using a gas jet transport system. Transport efficiencies of $\geq$ 50 % have been achieved routinely with gas jet systems [10] (see figure 1.14). A major disadvantage of this technology is that side-products of the fusion reaction are extracted from the target chamber using the He / KCl gas jet and transported to the chemical experiment. These side-products are usually generated with a higher cross section than the desired SHE. This can lead to the need for a complex chemical separation and may lead to increased background in subsequent spectrometry. However, most of the liquid phase chemistry experiments were performed with this approach.

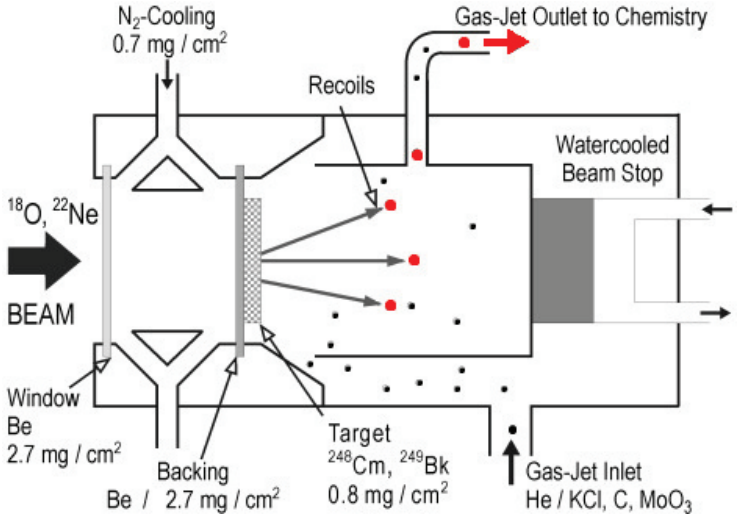

Figure 1.14: *Stationary target, coupled with a recoil chamber [10]. After the ion beam has penetrated the backing, a fusion reaction can occur in the target in which SHE are formed (red dots). The recoil nuclei are transferred to the recoil chamber by conservation of momentum. After thermalization, the fusion products can adhere to aerosol particles to be transported via gas jet to a chemical experiment. Reprinted with the permission of Wiley.*

Stopping after preseparation

The advantage of a physical preseparator is the separation of the desired radionuclide from high yield side-products of the fusion reaction and from the primary beam. The separation of the different ejectiles behind the actinide target is performed with the aid of electrostatic fields or electromagnets in different arrangements. Depending on the type of separator, the ejectiles are separated based on different properties e.g. the ratio of recoil energy or momentum to charge state. By separating the unwanted side-products, the spectral background is massively suppressed in the subsequent decay measurement [74] [75]. Pioneering experiments were performed at Lawrence Berkeley National Laboratory with the Berkeley Gas-filled Separator (BGS) [76]. The experimental setup of the BGS is shown in figure 1.15. The products in the nuclear reaction are transferred from the target to a He atmosphere (0.7 mbar). Using a quadropole and two dipole magnets, the target ejectiles are separated so that only the desired transactinides reach the end of the BGS system. Subsequently, the radionuclides are thermalized in a recoil transfer chamber (RTC) and, as in the "stopping before separation method", transported to a chemical experiment using aerosols and a gas jet system [77]. This advanced method has been introduced also at other recoil separators and has been used for both liquid phase experiments with Rf and gas phase chemistry with transseaborgium elements [78].

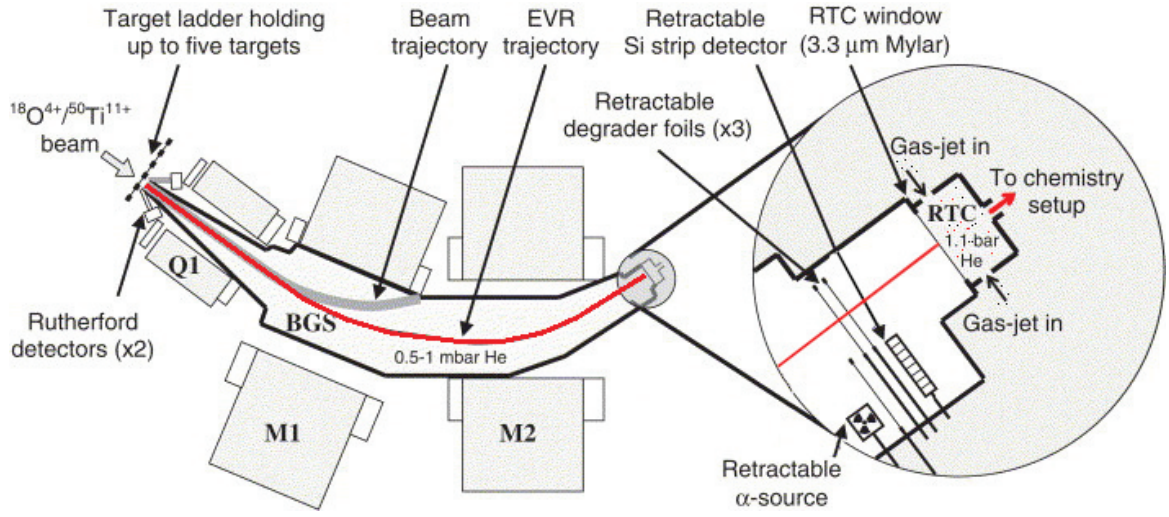

Figure 1.15: *Schematic representation of the BGS [77]. Bombarding a target with $^{18}O^{4+}$ or $^{50}Ti^{11+}$ ions generates heavy ions, which evaporate neutrons, resulting in evaporation residues (EVR). Due to conservation of momentum, the target ejectiles are transported into the BGS. The reaction products are first focused by a quadrupole magnet (Q1) and then separated by dipole magnets (M1 & M2). After passing through the BGS, the EVRs are transferred to a recoil transfer chamber. Reprinted and adapted with the permission of Elsevier.*

1.4.2 Apparatus for chemical experiments in the liquid phase

In both cases (stopping before and after separation), the SHE is transported to a chemical experiment by a gas jet system. Here, too, a distinction can be made between two types of experiment. On the one hand, there are discontinuous experiments, in which the SHE is collected on a surface or a filter, followed by transfer to a chromatographic column. On the other hand, the SHE can also be continuously analyzed for their chemical properties. Both strategies are discussed briefly in the following.

Discontinuous experiments

The first experiments with the SHE rutherfordium were performed in the 70's by Zvara et al. in Dubna [79] and Silva et al. in Berkeley [80]. These pioneering experiments were carried out manually. For example, in the experiment of Silva et al., ^{261}Rf was collected on platinum disks coated with NH_4Cl and then rinsed from the disks in small volumes and complexed with 2-hydroxy-2-methyl-propionic acid. The complexes were then chromatographically separated, evaporated, and measured with Si detectors. Even with the comparatively long half-life of 75 ± 5 s, the authors stated that they were only able to observe about 10 % of all Rf decays. Manual experiments would therefore mean even lower yields for shorter-lived radionuclides. In addition, since the production rate becomes smaller and smaller as the number of protons increases, the manual processes had to be automated. In addition to the required time savings, the automated systems also guaranteed constant repeatability of the experimental steps in order to achieve good statistics. Systems like ARCA (automated rapid chemistry apparatus) and its upgrade ARCA II [81] or AIDA [82] (automated ion-exchange separation apparatus coupled with the detection system for α-spectroscopy) used this type of batch-wise collection and elution to perform experiments up to seaborgium Sg (Z = 106), which was identified by its decay progeny.

Although the individual systems differed in their design, the experimental procedure can be generalized [83]: The radionuclides are continuously transferred by means of a gas jet system from a recoil transfer chamber to a surface for accumulation. The surface can be e.g. filters, frits or disks. The aerosol particles (together with the adsorbed SHE) are detached from the collection surface in small volumes. The SHE are then loaded onto a micro chromatography column. After chemical separation, the individual sample fractions are collected on metal plates (such as tantalum) and evaporated to dryness. Subsequent measurement by α-spectrometry allows nuclide identification via the particle energy (see figure 1.16).

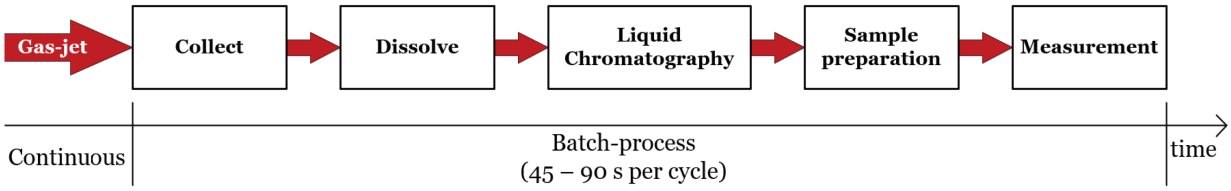

Figure 1.16: *Discontinuously operated systems for liquid phases SHE chemistry. Schematic representation of the individual process steps: Continuous collection of aerosol particles (with adsorbed SHE), discontinuous transfer of sample fractions into the aqueous phase, chemical separation, sample preparation, and spectrometric measurement.*

With the help of such discontinuous chemistry devices, the chemical properties of Rf and Db could be determined including the direct spectrometric measurement of α-radiation [84]. Even the properties of Sg [85] in aqueous solution could be investigated with the ARCA II system. However, the half-life was already too short to measure the α-decay of Sg directly. The identification was carried out via the measurement of its progeny.

Continuous experiments

The major disadvantage of the discontinuous methods is the time that is required before the separated sample fractions can be measured. Therefore, continuous systems have been developed that eliminate the need for collection times. Continuous systems with column chromatographic separation were used,

for example, in experiments with ^{262}Db ($t_{1/2}$ = 34 s). A three column technique was used for the investigation of its chemical properties [86]. As an alternative to column chromatography experiments, continuous liquid-liquid extraction experiments were performed using the SISAK (Short-lived Isotopes Studied by the AKUFVE-technique, where AKUFVE is a Swedish acronym for an arrangement for continuous investigations of distribution ratios in liquid-liquid extraction) system [87]. In order to transfer the radionuclide-transporting aerosol particles from the gas phase into the aqueous phase, membrane degasser (MDG) systems [88] are used (see figure 1.17).

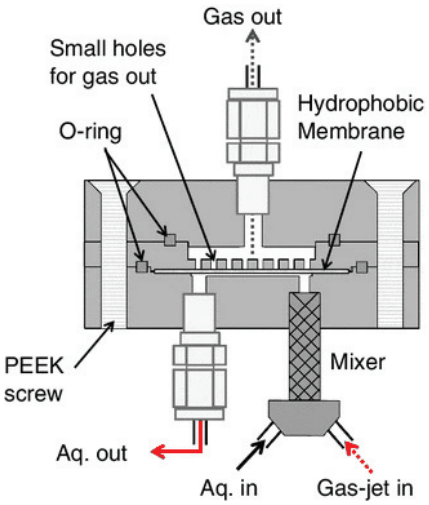

Figure 1.17: *Membrane degasser system, adapted from [88]. A gas jet, containing aerosol particles on which SHE are adsorbed, is mixed with an aqueous phase. The liquid phase is then transferred to the chemistry experiment. Reprinted with permission of Springer Nature.*

To transfer the aerosol particles to the aqueous phase, the gas jet is fed into a mixer with an aqueous phase. Dissolution efficiencies were determined for the system shown in figure 1.17 in experiments with $^{91m/93m}$Mo and ^{176}W as a function of the flow velocity of the media. Hereby the flow velocity of the liquid phase mainly has an influence on the dissolution efficiency. Depending on the flow velocity of the liquid phase, dissolution efficiencies up to 80 % were determined at a flow-rate around 25 ml/min. The gas/liquid mixture is passed through a PTFE membrane. By applying a vacuum on the gas side of the membrane, the gas is separated from the liquid. The aqueous solution including the SHE is then fed into the SISAK system [88]. Here, the aqueous solution is mixed with an organic solvent in order to perform liquid-liquid extraction. The organic phase also contains a complexing agent. After mixing the two phases, a phase separation is carried out by microcentrifuges. If necessary, quenching substances are removed from the organic phase with a washing step. As a final step, a scintillation cocktail suitable for alpha/beta separation is added to the organic phase. The α-/β- radiation is then measured with scintillation detectors equipped with flow cells [87], as schematically shown in figure 1.18. The α/β- separation is carried out via pulse shape discrimination (PSD) of the individual events, as described in section 1.3.2. One advantage of this system over discontinuous systems is the total time of an experimental process. Transport time measurements showed a mean residence time of 11 s for accelerator produced radionuclides from the RTC to the detector for the SISAK system, which is much shorter than for example a batch cycle in ARCA II (around 60 s). However, the type of detection is a problem, since β-radiation is detected in addition to α-radiation (see section 1.3.2). Since in SHE experiments α- and β- emitting by-products are generated with much higher yields, the spectral background is too high for a successful measurement.

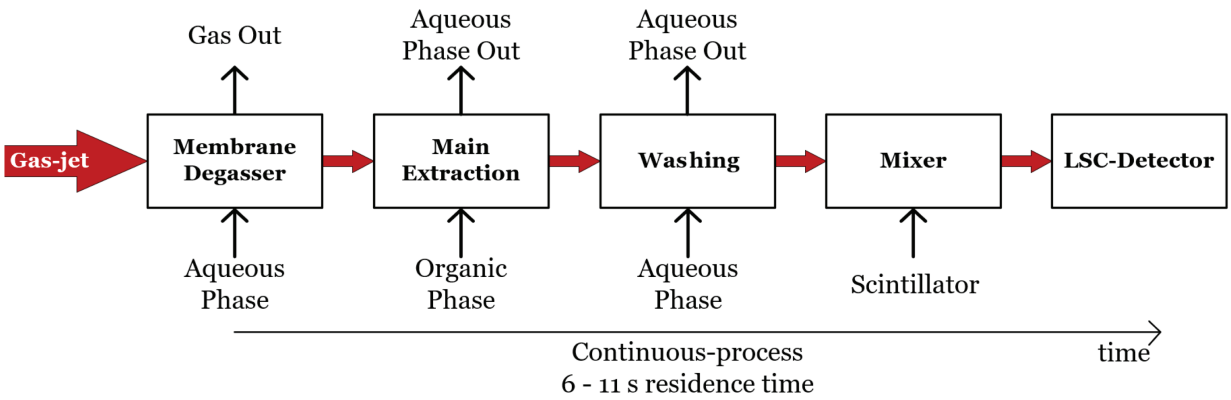

Figure 1.18: *Schematic structure of a SISAK experiment: after the SHE has been transferred to the liquid phase by the membrane degasser, the SHE is transferred to the organic phase in liquid-liquid extractions (depending on the chemical properties). After addition of a scintillator, LSC measurements are performed in flow cells.*

To suppress the increased background caused by by-products, the SISAK system was connected to the Berkeley Gasfilled Separator in a "stopping after preseparation" approach [89]. The transport between the RTC and the membrane degasser was done via gas jet. In this proof of concept experiment, it was possible to chemically separate ^{257}Rf ($t_{1/2}$ = 4.4 s) and to measure its decay radiation, due to the suppressed background. As an alternative to physical preseparation, efforts were made to suppress the β-background in the LSC spectra by PSD. A neural network was trained to distinguish the pulse shapes from α- and β-pulses [90]. This made it possible to filter out 95 % of all background events in an experiment with ^{261}Rf ($t_{1/2}$ = 68 s).

By developing the different systems (with continuous and discontinuous methods), it was possible to investigate the chemical properties of the first three superheavy elements Rf, Db and Sg in the aqueous phase. A detailed overview of the different experiments is described in [9]. Both methods to investigate SHE in the aqueous phase have their advantages and disadvantages. In the case of discontinuous systems, the main disadvantage is the maximum time elapsing between the start of aerosol particle collection and the final measurement of the chromatographically separated fractions. The advantage of discontinuous systems, on the other hand, is the measurement of the sample fractions with Si detectors. This allows the acquisition of high-resolution α-spectra. The identification, including the correlation of α-events in decay chains, is additionally easier, since the spectral background is significantly lower than in LSC-based measurements. The reason for this is the very low response of Si detectors for β-and γ-radiation.

However, despite the further developments of the different systems, seaborgium is still the heaviest element whose chemical properties have been studied in the aqueous phase. Since the half-lives of currently producible transseaborgium elements are too short to allow experiments in the aqueous phase, all heavy elements could only be studied in the gas phase. One major advantage of gas-phase experiments over liquid-phase experiments is the higher transport speed of the SHE. This makes it possible to study the chemical properties of shorter-lived transseaborgium elements as well. Therefore, the scientific focus of the past years has been on the development of new and efficient technologies for the chemical properties of the trans actinide elements in the gas phase. One of the state of the art systems for these research applications is the TransActinide Separator and Chemistry Apparatus (TASCA) preseparator at GSI (Darmstadt) [91],

coupled with the Si detector based Cryo-Online Multidetector for Physics And Chemistry of Transactinides (COMPACT) detector array, as recently used for the chemical studies of Flerovium Fl (Z=114) [28] (see figure 1.19). Its operation will be explained shortly by using the example of the Fl experiments.

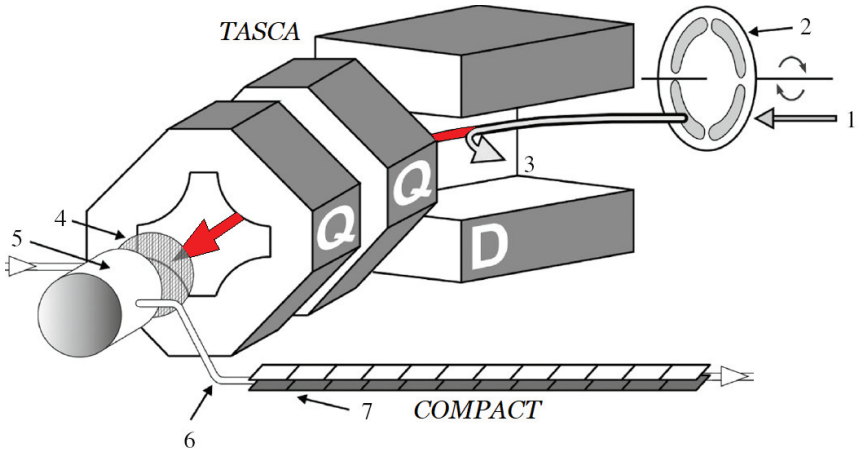

Figure 1.19: *Schematic drawing of the "TransActinide Separator and Chemistry Apparatus" (TASCA) preseparator, coupled to a detector array. A ^{48}Ca ion beam passes through a rotating ^{244}Pu target (2). The primary beam and unwanted by-products of the fusion reaction (3) are separated by a dipole magnet (D). The desired SHE (red arrow) are then focused by two quadrupole magnets (Q) and transported through a Mylar window (4) into the RTC (5). Via gas transport (6) the thermalized SHE are transported to a "COMPACT" Si detector array (7). Adapted from [28]. Reprinted with permission of American Chemical Society.*

Fl was synthesized in the ^{48}Ca(^{244}Pu,3-4 n)^{288,289}Fl reaction. For this purpose, a [^{244}Pu]PuO_2 target was irradiated with $^{48}Ca^{10+}$ ions of 259.4 MeV kinetic energy. After the compound nucleus has evaporated 3 to 4 neutrons, ^{288,289}Fl are produced. The Fl recoil out of the target into the TASCA setup [91], which is filled with a 0.8 mbar helium atmosphere. A dipole magnet is used to separate the Fl ions from the Ca beam and unwanted nuclear reaction products. Due to this separation, the background could be massively suppressed compared to experiments without preseparator [92]. After focusing in the vertical and horizontal axis by two quadropole magnets, the Fl nuclides are guided through a Mylar foil into the RTC for thermalization. Subsequently, the thermalized nuclides are transported with the carrier gas into the COMPACT detector array [93]: in the detector structure, individual Si detectors are arranged in arrays. The detector section acts as a gas chromatography column, whereby the detector surface is either covered with 30 - 50 nm of a SiO_2- or gold layer. Experiments with such a setup can be performed in an approach with constant COMPACT array temperature (isothermal) or with a negative temperature gradient. If the adsorption enthalpy is high enough, the SHE are deposited in a diffusion-controlled process on one of the detector sectors (SiO_2- or Au- covered), where subsequently the radioactive decay is detected. In addition to the decay of the SHE in question, the radioactive decays of the progeny are also recorded (decay chain). Based on the experimental conditions under which the SHE was deposited, absorption enthalpies can then be obtained using Monte Carlo code based simulations [25]. The data obtained in this way, in combination with experimental results of the lighter homologs, can then be compared with theoretical calculations to draw conclusions about the chemical properties of the (new) element in question [94].

In addition to the deposition of SiO_2 and gold layers to provide specific surfaces for the SHE interaction, silicon-based detectors in particular can be modified with a variety of organic functional groups. Depending

on the functional group, other types of surface processes are possible. If such a chemically modified Si detector is designed to function in the aqueous phase, complexation or ion exchange reactions are also possible. The various types of silicon surface modifications are discussed in the following chapter.

1.5 Surface modification techniques

1.5.1 Silicon and silicon dioxide surfaces

If pure silicon is exposed to air it undergoes passivation under the formation of a silicon dioxide (SiO_2) layer. The topmost layer of such passivated surfaces consists of chemical inert siloxane groups, where two silicon atoms are bridged by an oxygen atom (Si-O-Si). In addition to the siloxane groups, the surface also contains reactive silanol groups, where a hydroxy group is attached to a silicon atom (Si-OH). The theoretical silanol density on a SiO_2 surface is 4 - 5 Si-OH groups per nm² [95]. Due to condensation reactions of silanol groups in siloxanes, the silanol density on a SiO_2 surface is typically lower. However, these silanol groups are required for the chemical modification of a silicon based substrate. For these surface modifications, a clean and highly hydroxylated surface is required. There are several methods available for cleaning and converting siloxane to silanol groups (often referred as "activation") [96]. The general scheme is shown in figure 1.20.

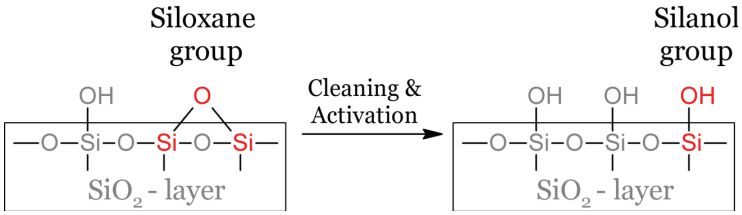

Figure 1.20: *Cleaning and activation of the topmost layer of a silicon dioxide structure: conversion of siloxan groups (Si-O-Si) into silanol groups (Si-OH).*

A widely applied technique is cleaning the substrate in a so called RCA-approach [97]. The RCA refers to the Radio Corporation of America, as this technique was developed by this company. The RCA procedure comprises two steps. First, the substrate is placed in a bath of ammonium hydroxide, hydrogen peroxide and distilled water. This first step is applied to remove organic molecules, as organic contaminations are always present when a surface is handled in other than cleanroom conditions [98]. In a second step, the surface is placed in a bath of hydrochloric acid, hydrogen peroxide and distilled water in order to remove metallic contaminations from the substrate. For a subsequent activation of the surface, a strong oxidizing agent, like Caro's acid (a mixture of hydrogen peroxide and sulfuric acid) or chromosulfuric acid (a mixture of sulfuric acid and chromium trioxide) is used. Many other wet chemical cleaning and activation methods have been developed for glass and silicon surfaces and therefore, other chemical cleaning processes such as treatment with methanol/HCl, isopropanol/KOH or NaOH solutions have been established, too [99]. However, the chemical cleaning and activation methods are all aggressive and remove parts of the topmost substrate surface layers [100]. In the case of glass and silicon wafer substrates this is acceptable, but it is not possible to treat electrical parts, like Si detector chips (already equipped with metallic contacts) with this method without damaging them. In addition to the established wet chemical methods, "dry"

methods have also been developed. One method is irradiation with a UV light source in an oxygen-rich atmosphere [101]. UV light has enough energy to break the chemical bonds in organic molecules and those of siloxane bridges. In addition, the oxygen is converted into reactive species such as atomic oxygen and ozone, which oxidize the organic molecules (mainly in H_2O and CO_2), resulting in an activated surface, without organic contaminations.

A similar principle is used in plasma treatment [102]. Plasma, as the fourth aggregate state, is a gas with free charge carriers (ions and electrons), as well as radicals. In this process, chemically reactive species are also generated, which then break chemical bonds on a substrate surface. For the treatment of sensitive surfaces a low-pressure plasma is typically used. For this purpose, a substrate to be treated is placed in a vacuum chamber. After the chamber has been evacuated, the remaining gas atmosphere is converted to a non thermal plasma by applying a high alternating voltage to a gas [103]. The plasma is referred to as non thermal because the temperatures of the components contained in the plasma differ greatly from one another (they are not in a thermal equilibrium). Here, the electrons are primarily accelerated. The comparably much heavier ions experience less acceleration. Nevertheless, there is also a secondary effect of UV radiation emission, due to particle collisions in the gas phase. The collisions of charged particles on the substrate surface (and the irradiation by UV light) also cause chemical bonds to break. Depending on the choice of process gas, the fragments are then oxidized (O_2 / air plasma) or reduced (H_2/Ar plasma). The resulting fragments are then extracted by a vacuum pump. Siloxane groups are also broken up on the substrate surface. In the presence of an oxidative atmosphere and water, these can then be converted into silanol groups [104].

1.5.2 Modification with organosilanes

Organosilanes are silicon-based molecules, with a covalent bond between the silicon and a carbon atom [105]. In general, organosilanes can be divided into three parts. The general structure is shown in figure 1.21.

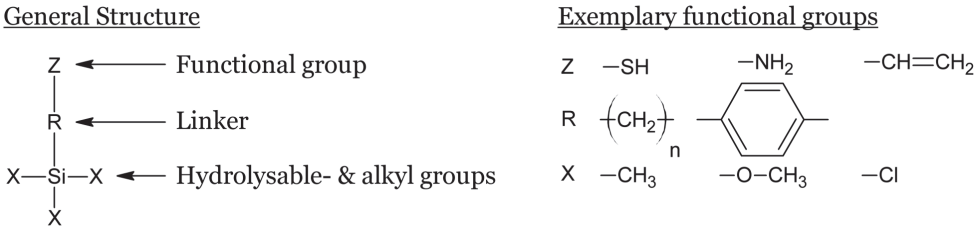

Figure 1.21: *General structure of organosilane compounds. X refers to a non-hydrolysable group e.g. methyl groups or to a hydrolysable group like alkoxy groups or halogenides. The linker group R is either an alkyl chain of various length or a phenyl group. Z represents a functional group like thiols, amino groups or halogenides which can be further modified.*

The hydrolysable part X of the organosilane molecule is able to form covalent bonds with reactive groups, e.g., hydroxide groups (R-OH), of a surface. Due to this silanization process, the substrate surface is covered with alkyl groups and a functional group Z, resulting in a change of the physical and chemical surface properties. The organosilane density on a surface varies with the amount of hydrolysable groups, the sterical properties of the silane molecule and the type of substrate [106]. In case of one hydrolysable

group, the density of covalently bound silanol the surface is at maximum as high as the initial amount of reactive sites on the substrate. If two or three hydrolysable groups are present in a molecule, the silane molecules can also undergo polymerisation reactions. On one hand, this is advantageous, as these polymerization reactions anchor the silane stronger to the surface. On the other hand, these polymerization reactions can result in the formation of bulk structures and thick silane layers deposited onto the surface. However, if the reaction conditions are chosen properly, these type of molecules are able to from self assembling monolayers (SAM) on a substrate. A widely applied technique for surface modifications is the silanization in solution. Here, the clean and acitvated substrate is submerged in a diluted silane solution, where the specific silanization conditions depend on the substrate, the organosilane and the degree of silane coverage [107]. The main reaction steps of surface silanization are described in the example of a silicon dioxide modification with (3-Mercaptopropyl)trimethoxysilane (MPTMS) [108] (see figure 1.22), as this is one of the main organosilanes utilized in this thesis.

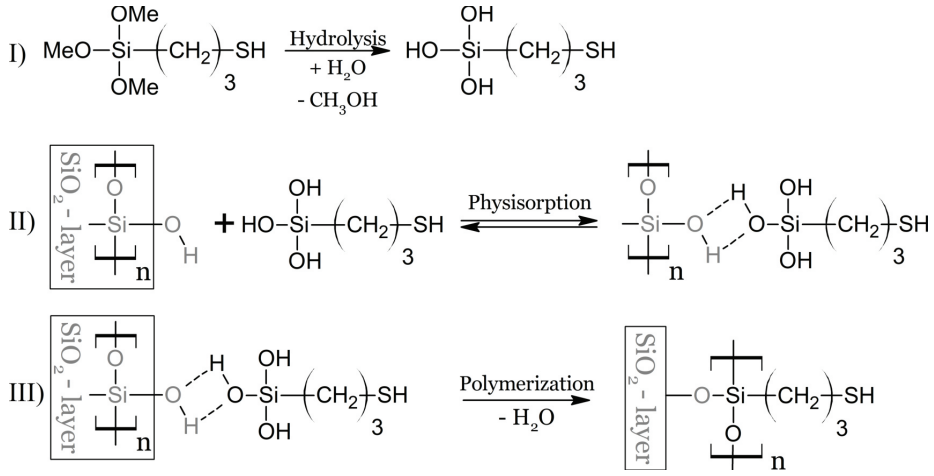

Figure 1.22: *Modification of silanol (Si-OH) bearing surfaces with MPTMS in solution. I) Hydrolysis of methoxy groups, yielding (3-Mercaptopropyl)trihydroxysilan (MPTHS). II) Polymerization of MPTHS in solution. III) Covalent attachment of polymerized organosilane structures.*

The influence of water on the formation of SAM structures with this type of liquid phase reactions is still under discussion [109]. In case of a completely water free reaction (water free solvent & organosilane and no physically adsorbed water on the substrate) the silanol groups on the substrate could react with one hydrolysable group of the organosilane. This would lead to an incomplete reaction, as the two remaining alkoxy groups require one water molecule to form siloxane groups with other organosilanes. However, in case of excessive water amounts (and high silane concentrations), the polymerization in solution becomes the dominant reaction, resulting in the formation of bulky species in the liquid phase. These bulky species can form multilayer systems on the substrate, through adsorption of several polymers (see figure 1.23), but also through covalent bonding.

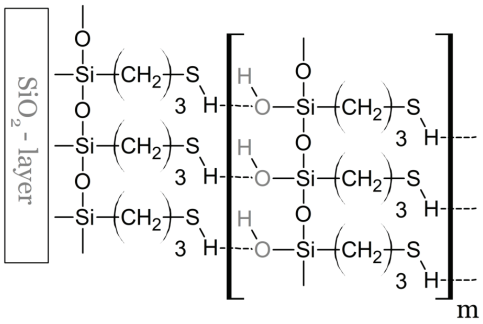

Figure 1.23: *Multilayer formation through adsorption of polymerized organosilane structures on a substrate.*

One way to avoid such multilayer formations is the chemical vapor deposition (CVD) method, where a suitable silane is vaporised at elevated temperatures and/or reduced pressure [110]. If an activated surface is exposed to this silane vapor, thin layers with heights in the order of nanometers form. At atmospheric pressure MPTMS has a boiling point of 214 °C. By applying a reduced pressure, e.g. of 54 mbar, the boiling point is set down to 93 °C [111], in case of temperature sensitive substrates, the pressure is further reduced, to 1-2 mbar for room temperatur applications, as done e.g. by Aswal et al. [112]. The inital steps of a silanization is shown in figure 1.24.

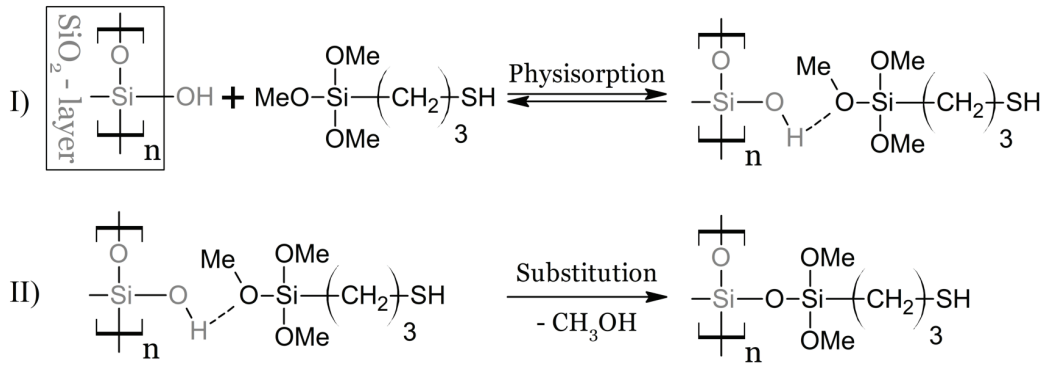

Figure 1.24: *First steps, involved in the surface modification of silicon dioxide with organosilanes: physisorption of (3-mercaptopropyl)trimethoxysilane (MPTMS) followed by covalent attachment to the surface.*

As the CVD process is performed in the absence of water, reactive alkoxy groups are still present on the surface. In order to increase the stability of the silane layer on the surface, the modified substrates are subsequently cured in a post-silanization process [113]. This curing process is typically performed at elevated temperatures in a hydrous atmosphere. Due to the elevated temperatures, the condensation product (in case of alkoxy groups an alcohol) is removed from the reaction, shifting the equilibrium to the product side.

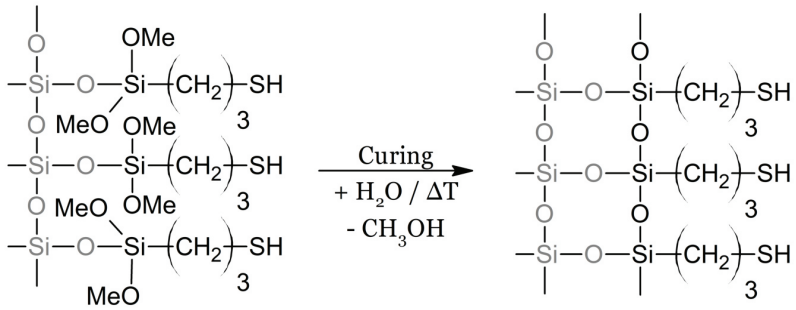

Figure 1.25: *Post-silanization process in the presence of water and at elevated temperatures: cross linking between surface-anchored organosilanes by addition of water and elimination of an alkohol.*

After the initial chemical surface modification with organo silanes, several strategies are available for the introduction of a specific functional group, which serves as an extraction agent in a radiochemical experiment. As an example for a subsequent modification of surface anchored thiol groups, the oxidation to sulfonic acid groups by the use of hydrogen peroxide [114] [115] [116] is shown in figure 1.26. This technique was used to introduce ion exchange groups on both silicon wafers [117] and silicon-based α-detectors [118].

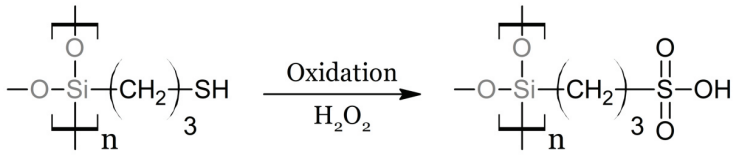

Figure 1.26: *Oxidation of thiol groups (R-SH) with hydrogen peroxide, yielding covalent attached sulfonic acid groups (R-SO_3H) on the substrate.*

1.5.3 Preparation of α samples with chemically modified surfaces

The general strategy of surface silanization with subsequent conversion in a selective extraction agent offers a large variety of possibilities for the preparation of thin layers of α-emitting radionuclides in thin layers on various substrates. However, until now this strategy has hardly been used for the production of high-resolution α-sources. Beside of the work done in this dissertation, there are few examples in the literature: one example of this technique is given by Mohamud et al. [119], who chemically modified silicon wafer to accumulate ^{226}Ra on the silanized surface from aqueous solution. In order to bind the extraction agent to the surface, the substrate was first silanized with 3-isocyanatopropyltriethoxysilane (ICPTES) in dry ethanol and then functionalized with 4'-aminodibenzo-18-crown-6 ether (ADB18C6) in dry tetrahydrofuran (THF) as shown in figure 1.27.

The modified Si-wafers were immersed in 5 ml of 0.01 M HNO_3 solution with 0.1 Bq ^{226}Ra for 24 h. According to the authors, around 3 % of the radium could be collected on the surface. However, this small amount of radium was collected in a monatomic layer on the wafer surface, which enabled high-resolution α-spectrometry of the ^{226}Ra. Another example of the simplified α-sample preparation through silanized surfaces is the work of Bilewicz [120]. In this work, neutrally charged TTA (thenoyltrifluoroacetone) complexes of Zr^{4+}, Hf^{4+}, Rf^{4+} and Po^{4+} were generated. The aim was to evaporate the samples as

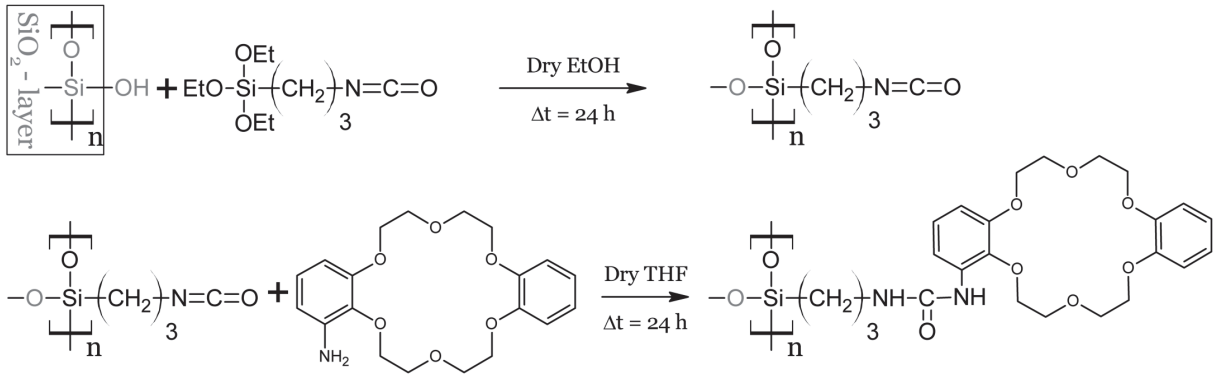

Figure 1.27: *Two step modification of a silicon wafer with a radium-extracting crown ether in the liquid phase. First, silanization with ICPTES in dry ethanol followed by addition of ADB18C6 in dry THF.*

quickly as possible and measure them using α spectrometry. However, these samples would also evaporate on untreated glass. Therefore, the glass substrates were hydropobized with diethyldichlorosilane and diphenyldichlorosilane to prevent the complexed compounds from evaporating.

In addition to silanized surfaces, other classes of organic substances can also be used to create thin layers of radionuclides on extractive surfaces. An example of this would be the production of thin polymer membranes on glass as described in [121]. Quaternary amino groups were used here as strong anion exchanger to extract ^{238}Pu as $[PuCl_6]^{2-}$ complexes on a glass surface for subsequent measurement in an α chamber. The anion exchange membranes were produced in a two step synthesis. First, a cleaned glass chip was immersed in a solution of polyvinyl benzyl chloride (PVBC) in chloroform and then slowly pulled out of the polymer solution so that a thin liquid film adhered to the glass surface. During the coating process, diazabicyclo [2.2.2] octane (DABCO) was added to crosslink individual PVBC chains and thus increase the adhesion of the polymer chains to the surface. By the same reaction, quaternary amino groups were added to the surface, too. The remaining chloro groups were also converted into quaternary amines by nucleophilic substitution with triethylamine (TEA) (see figure 1.28). In their publication, the authors state a minimum thickness of 180 nm that could be produced on glass surfaces using this process.

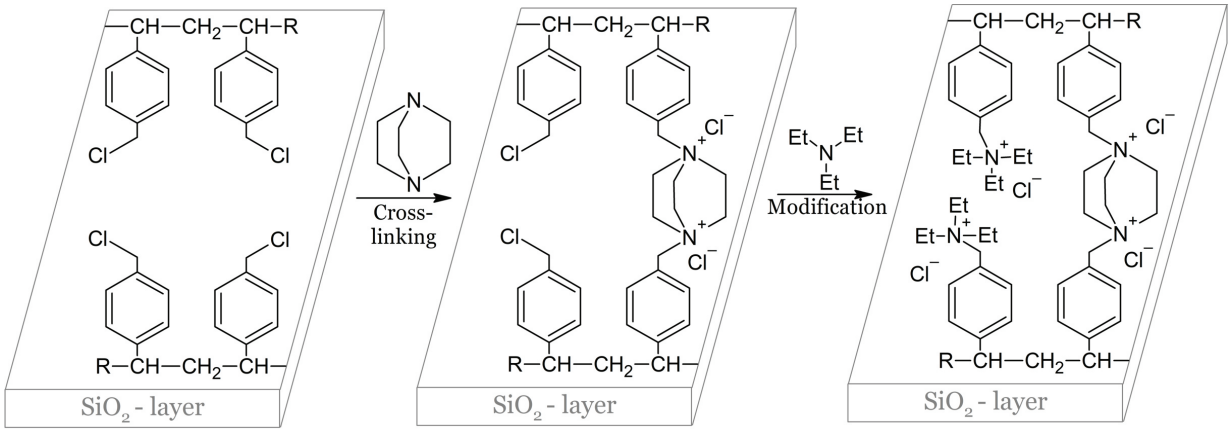

Figure 1.28: *Two step modification of a glass substrate with strong anion exchanger groups. First, DVBC chains are adsorbed on glass from solution and crosslinked by DABCO. Second, unreacted chloro groups are converted into quaternary amino groups with TEA.*

The polymer-coated surfaces were immersed in 9 M HCl for 3 days without showing any polymer desorption or swelling behavior. In extraction experiments, around 12 % of a plutonium solution with an activity concentration of 17 Bq / ml could be accumulated on the surface within 30 minutes.

By attaching a very thin film between a Si semiconductor detector and an aqueous solution, it is in principle possible to measure aqueous solutions of α-emitters directly if the α-emitters are close enough to the surface of the detector, separated by a polymer [122] or a thin air layer [123]. In experiments with 3-µm thick Mylar foils it could be shown that it is possible to measure α-emitters in aqueous solutions. The separation between the aqueous solution and the contacts of the α-detector by the Mylar foil enabled measurements without increased leakage currents. However, since the radionuclides were homogeneously distributed in aqueous solutions, only continuous α-spectra could be recorded, which makes nuclide identification of a complex sample impossible. In addition to Mylar foil, in other studies silicon detectors e.g., coated with thin polymer layers made of polytetrafluoroethylene or polyvinyl chloride have been used to enable radionuclide measurements in the aqueous phase. However, these coatings always required an additive, such as anion exchange resin [124] or di-2-ethylhexyl phosphoric acid [125] to accumulate radionuclides near the detector surface. However, no real covalent binding of extractive groups took place on the detector surfaces.

1.6 Outline of the dissertation

α-spectrometry plays an essential role in nuclide and activity determination, both for a large number of naturally occurring radionuclides and for artificially produced radionuclides. However, due to the short range of α-radiation, α-spectrometry is associated with a high sample preparation effort. This is primarily expressed by the high time expenditure associated with specimen preparation. This becomes particularly clear when investigating the chemical properties of SHE. SHE are produced with accelerators at rates of single atoms per hour or day. These individual nuclei usually have half-lives of a few minutes to fractions of a second. During this time, the nuclide must be examined for a chemical property in several stages of an experimental setup in order to detect it by means of energy-resolved α-spectrometry after the sample has been prepared as quickly as possible. With the already very small production rate, it is important that the individual steps have as low yield losses as possible in order not to significantly reduce the already very small number of potentially measurable decay events. However, in order to overcome the yield losses over the individual process steps, it is essential to develop new systems to enable experiments beyond Sg in the aqueous phase. The aim of this work is to develop new systems that make experiments in the liquid phase more efficient. This should lay the basis for future experiments of transseaborgium elements in the liquid phase. In addition, parts of this research can also be used in conventional fields of α-spectrometry to accelerate measurement procedures and reduce costs. An overview of existing systems for rapid analysis of SHE in the aqueous phase, in comparison with the techniques developed in this dissertation are shown in figure 1.29.

First, it was shown in a proof of concept that it is possible to modify detector surfaces with ultra thin covalently bonded organic functional groups to turn the surface of an α-detector into a stationary phase. This combines the sample preparation and the subsequent detection of the α-radiation (see chapter 2). In order to take advantage of physical preseparators such as TASCA, a transfer system has been developed that

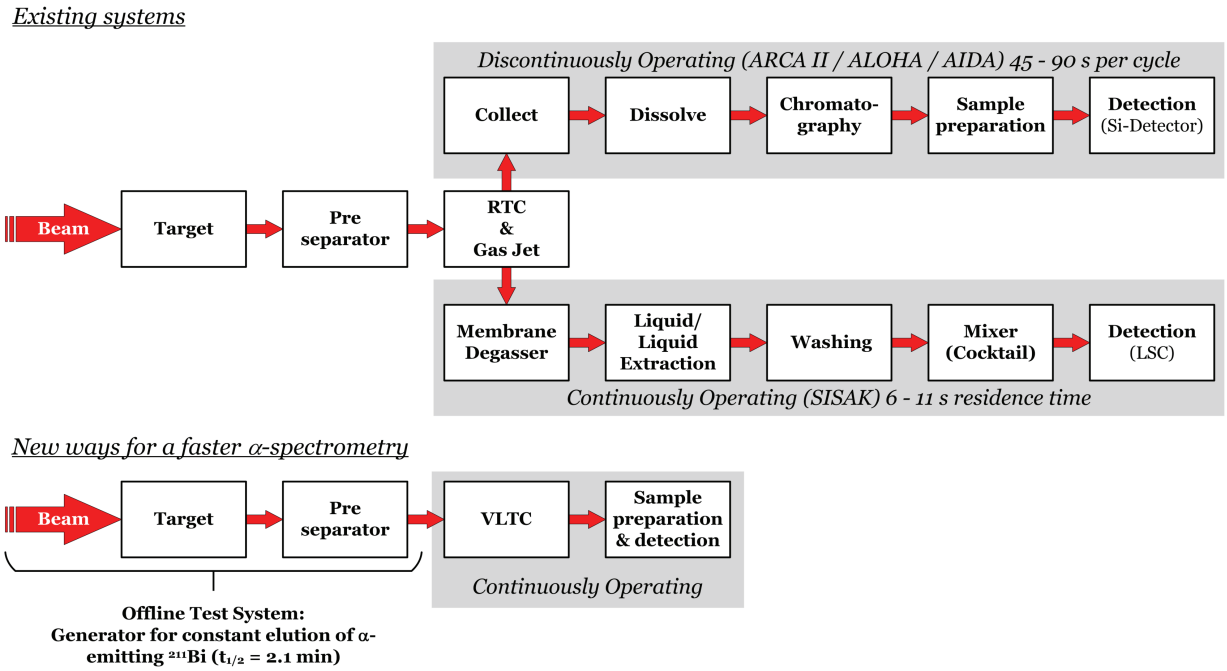

Figure 1.29: *Essential steps of existing systems for SHE-chemistry in the liquid phase compared to the technologies developed in this dissertation.*

transports SHE-recoils directly from the preseparator into the liquid phase, which a) eliminates the need for gas-jet and membrane degassing systems, and b) allows continuous flow experiments (see chapter 3). In order to be able to test such systems under similar conditions (short-lived α-emitters in the continuous flow of an aqueous phase) in preparation for experiments at accelerator facilities in the future, a generator system was developed that can generate pulsation-free continuous currents of the short-lived α-emitter ^{211}Bi ($t_{1/2}$ = 2.14 min) (see chapter 4). Finally, a brief summary and an based on this work is given in chapter 5.

1.7 References

[1] F. Flakus, "Detecting and measuring ionizing radiation- a short history." *IAEA bulletin*, vol. 23, no. 4, pp. 31–36, 1982.

[2] International Nuclear Structure and Decay Data Network, "Nuclear data services: evaluated nuclear structure and decay data," 29.05.2020. [Online]. Available: https://www.nndc.bnl.gov/ensdf/

[3] P. Linsalata, "Exposure to long-lived members of the uranium and thorium decay chains," *International Journal of Radiation Applications and Instrumentation. Part C. Radiation Physics and Chemistry*, vol. 34, no. 2, pp. 241–250, 1989.

[4] S. K. Aggarwal, "Alpha-particle spectrometry for the determination of alpha emitting isotopes in nuclear, environmental and biological samples: past, present and future," *Analytical methods*, vol. 8, no. 27, pp. 5353–5371, 2016.

[5] Y. Koma and E. Murakami, "Contamination of fukushima daiichi nuclear power station with actinide elements," *Radiochimica Acta*, vol. 107, no. 9-11, pp. 965–977, 2019.

[6] G. B. Saha, *Fundamentals of nuclear pharmacy*. Springer, 2010, vol. 6.

[7] M. Miederer, D. A. Scheinberg, and M. R. McDevitt, "Realizing the potential of the Actinium-225 radionuclide generator in targeted alpha particle therapy applications," *Advanced drug delivery reviews*, vol. 60, no. 12, pp. 1371–1382, 2008.

[8] M. G. Ferrier, V. Radchenko, and D. S. Wilbur, "Radiochemical aspects of alpha emitting radionuclides for medical application," *Radiochimica Acta*, vol. 107, no. 9-11, pp. 1065–1085, 2019.

[9] Y. Nagame, J. V. Kratz, and M. Schädel, "Chemical studies of elements with Z $\geq$ 104 in liquid phase," *Nuclear Physics A*, vol. 944, pp. 614–639, 2015.

[10] M. Schädel, "Chemistry of superheavy elements," *Angewandte Chemie International Edition*, vol. 45, no. 3, pp. 368–401, 2006.

[11] Y. Oganessian, "Heaviest nuclei from ^{48}Ca-induced reactions," *Journal of Physics G: Nuclear and Particle Physics*, vol. 34, no. 4, p. 165, 2007.

[12] J. Khuyagbaatar, A. Yakushev, Ch. E. Düllmann, D. Ackermann, L.-L. Andersson, M. Asai, M. Block, R. Boll, H. Brand, D. Cox *et al.*, "Search for elements 119 and 120," *Physical Review C*, vol. 102, no. 6, p. 064602, 2020.

[13] A. Türler, R. Eichler, and A. Yakushev, "Chemical studies of elements with Z ≥ 104 in gas phase," *Nuclear Physics A*, vol. 944, pp. 640–689, 2015.

[14] G. Choppin, J.-O. Liljenzin, J. Rydberg, and C. Ekberg, *Radiochemistry and nuclear chemistry*. Academic Press, 2013.

[15] W. F. McDonough and S.-S. Sun, "The composition of the earth," *Chemical geology*, vol. 120, no. 3-4, pp. 223–253, 1995.

[16] D. Peppard, G. Mason, P. Gray, and J. Mech, "Occurrence of the (4n+ 1) series in nature," *Journal of the American Chemical Society*, vol. 74, no. 23, pp. 6081–6084, 1952.

[17] H. Bateman, "The solution of a system of differential equations occurring in the theory of radio-active transformations," *Proc. Cambridge Phil. Soc., 1908*, vol. 15, pp. 423–427, 1908.

[18] D. Hoffman, F. Lawrence, J. Mewherter, and F. Rourke, "Detection of plutonium-244 in nature," *Nature*, vol. 234, no. 5325, pp. 132–134, 1971.

[19] A. Wallner, M. Froehlich, M. Hotchkis, N. Kinoshita, M. Paul, M. Martschini, S. Pavetich, S. Tims, N. Kivel, D. Schumann *et al.*, "^{60}Fe and ^{244}Pu deposited on Earth constrain the r-process yields of recent nearby supernovae," *Science*, vol. 372, no. 6543, pp. 742–745, 2021.

[20] Y. Nagame, "Nuclear and chemical characterization of heavy actinides," *Radiochimica Acta*, vol. 107, no. 9-11, pp. 803–819, 2019.

[21] S. M. Robinson, D. E. Benker, E. D. Collins, J. G. Ezold, J. R. Garrison, and S. L. Hogle, "Production of Cf-252 and other transplutonium isotopes at Oak Ridge National Laboratory," *Radiochimica Acta*, vol. 1, no. ahead-of-print, 2020.

[22] A. T. Chemey and T. E. Albrecht-Schmitt, "Evolution of the periodic table through the synthesis of new elements," *Radiochimica Acta*, vol. 107, no. 9-11, pp. 771–801, 2019.

[23] J. Roberto and K. Rykaczewski, "Actinide targets for the synthesis of superheavy nuclei: Current priorities and future opportunities," in *Fission and Properties of Neutron-Rich Nuclei: Proceedings of the Sixth International Conference on ICFN6*. World Scientific, 2018, pp. 129–135.

[24] W. Świątecki, K. Siwek-Wilczyńska, and J. Wilczyński, "Fusion by diffusion. II. Synthesis of transfermium elements in cold fusion reactions," *Physical Review C*, vol. 71, no. 1, p. 014602, 2005.

[25] L. H. Lens, "Advanced chemical investigations of the volatile element flerovium (Fl, Z= 114)," "Ph.D.-Thesis", Johannes Gutenberg-Universität Mainz, 2018.

[26] J. Hamilton, S. Hofmann, and Y. Oganessian, "Search for superheavy nuclei," *Annual Review of Nuclear and Particle Science*, vol. 63, pp. 383–405, 2013.

[27] A. Türler and V. Pershina, "Advances in the production and chemistry of the heaviest elements," *Chemical reviews*, vol. 113, no. 2, pp. 1237–1312, 2013.

[28] A. Yakushev, J. M. Gates, A. Türler, M. Schädel, C. E. Düllmann, D. Ackermann, L.-L. Andersson, M. Block, W. Brüchle, J. Dvorak *et al.*, "Superheavy element flerovium (element 114) is a volatile metal," *Inorganic chemistry*, vol. 53, no. 3, pp. 1624–1629, 2014.

[29] A. T. Kruppa, M. Bender, W. Nazarewicz, P.-G. Reinhard, T. Vertse, and S. Ćwiok, "Shell corrections of superheavy nuclei in self-consistent calculations," *Physical Review C*, vol. 61, no. 3, p. 034313, 2000.

[30] M. Schädel and D. Shaughnessy, *The chemistry of superheavy elements*. Springer, 2013.

[31] Y. Oganessian, "Nuclei in the "Island of Stability" of Superheavy Elements," in *Journal of Physics: Conference Series*, vol. 337, no. 1. IOP Publishing, 2012, p. 012005.

[32] A. Vértes, S. Nagy, Z. Klencsár, R. G. Lovas, and F. Rösch, *Handbook of Nuclear Chemistry: Vol. 4: Radiochemistry and Radiopharmaceutical Chemistry in Life Sciences.* Springer Science & Business Media, 2010.

[33] V. J. Molinski, "A review of ^{99m}Tc generator technology," *The International Journal of Applied Radiation and Isotopes*, vol. 33, no. 10, pp. 811–819, 1982.

[34] F. Rösch, "Past, present and future of ^{68}Ge/^{68}Ga generators," *Applied Radiation and Isotopes*, vol. 76, pp. 24–30, 2013.

[35] J. Weiss, *Handbook of Ion Chromatography, 3 Volume Set*. John Wiley & Sons, 2016, vol. 1.

[36] J. D. Despotopulos, K. N. Kmak, N. Gharibyan, R. A. Henderson, K. J. Moody, D. A. Shaughnessy, and R. Sudowe, "Characterization of the homologs of flerovium with crown ether based extraction chromatography resins: studies in hydrochloric acid," *Journal of radioanalytical and nuclear chemistry*, vol. 310, no. 3, pp. 1201–1207, 2016.

[37] J. D. Despotopulos, K. N. Kmak, K. J. Moody, and D. A. Shaughnessy, "Development of a ^{212}Pb and ^{212}Bi generator for homolog studies of flerovium and moscovium," *Journal of Radioanalytical and Nuclear Chemistry*, vol. 317, no. 1, pp. 473–477, 2018.

[38] E. Rutherford, "VIII. Uranium radiation and the electrical conduction produced by it," *The London, Edinburgh, and Dublin Philosophical Magazine and Journal of Science*, vol. 47, no. 284, pp. 109–163, 1899.

[39] M. F. L'Annunziata, *Handbook of radioactivity analysis*. Academic press, 2012.

[40] H. Geiger and J. Nuttall, "LVII. the ranges of the α particles from various radioactive substances and a relation between range and period of transformation," *The London, Edinburgh, and Dublin Philosophical Magazine and Journal of Science*, vol. 22, no. 130, pp. 613–621, 1911.

[41] R. Eisberg and R. Resnick, *Quantum physics of atoms, molecules, solids, nuclei, and particles*. John Wiley & Sons, 1985.

[42] G. Gamow, "Zur Quantentheorie des Atomkernes," *Zeitschrift für Physik*, vol. 51, no. 3-4, pp. 204–212, 1928.

[43] J.-V. Kratz and K. H. Lieser, *Nuclear and Radiochemistry*. Wiley Online Library, 2013.

[44] J. Tanaka, Z. Yang, S. Typel, S. Adachi, S. Bai, P. van Beek, D. Beaumel, Y. Fujikawa, J. Han, S. Heil *et al.*, "Formation of α clusters in dilute neutron-rich matter," *Science*, vol. 371, no. 6526, pp. 260–264, 2021.

[45] J. F. Ziegler, M. D. Ziegler, and J. P. Biersack, "SRIM- The stopping and range of ions in matter (2010)," *Nuclear Instruments and Methods in Physics Research Section B: Beam Interactions with Materials and Atoms*, vol. 268, no. 11-12, pp. 1818–1823, 2010.

[46] T. Siiskonen and R. Pöllänen, "New approach to alpha spectrum analysis: iterative Monte Carlo simulations and fitting," *Prog. Nucl. Sci. Technol*, vol. 2, pp. 437–441, 2011.

[47] G. F. Knoll, *Radiation detection and measurement*. John Wiley & Sons, 2010.

[48] E. Riedel and C. Janiak, *Anorganische Chemie*. De Gruyter, 2007.

[49] C. Williamson, J. Boujot, and J. Picard, "Tables of range and stopping power of chemical elements for charged particles of energy 0.5 to 500 MeV," Commissariat a l'Energie Atomique, Tech. Rep., 1966.

[50] ISO 13166, *Water quality — Uranium isotopes — Test method using alpha-spectrometry*. International Organization for Standardization, Switzerland, 2020.

[51] ISO 18589-4, *Measurement of radioactivity in the environment - Soil - Part 4: Plutonium 238 and plutonium 239 + 240 - Test method using alpha spectrometry*. International Organization for Standardization, Switzerland, 2019.

[52] F. Monroy-Guzmán, "Isolation of uranium by anionic exchange resins," *J. Chem. Chem. Eng*, vol. 10, pp. 90–95, 2016.

[53] O. Alhassanieh, A. Abdul-Hadi, M. Ghafar, and A. Aba, "Separation of Th, U, Pa, Ra and Ac from natural uranium and thorium series," *Applied radiation and isotopes*, vol. 51, no. 5, pp. 493–498, 1999.

[54] P. Blanco, J. Lozano, and F. V. Tomé, "On the use of ^{225}Ra as yield tracer and Ba (Ra) so_4 microprecipitation in ^{225}Ra determination by α-spectrometry," *Applied radiation and isotopes*, vol. 57, no. 6, pp. 785–790, 2002.

[55] P. D. Sawant, S. Wankhede, S. A. Kumar, S. Chaudhary, and S. P. Prabhu, "Alpha source preparation of actinides by micro-precipitation," *Journal of Radioanalytical and Nuclear Chemistry*, vol. 319, no. 1, pp. 109–113, 2019.

[56] K. Sekine, T. Imai, and A. Kasai, "Liquid—liquid extraction separation and sequential determination of plutonium and americium in environmental samples by alpha-spectrometry," *Talanta*, vol. 34, no. 6, pp. 567–570, 1987.

[57] E. P. Horwitz, R. Chiarizia, M. L. Dietz, H. Diamond, and D. M. Nelson, "Separation and preconcentration of actinides from acidic media by extraction chromatography," *Analytica Chimica Acta*, vol. 281, no. 2, pp. 361–372, 1993.

[58] K. Šťastná, V. Fiala, and J. John, "Preparation of samples for alpha-spectrometry by direct evaporation of extracted species," *Journal of radioanalytical and nuclear chemistry*, vol. 286, no. 3, pp. 735–739, 2010.

[59] G. Küppers, "Fast source preparation for alpha-spectrometry of uranium and transuranium isotopes," *Journal of radioanalytical and nuclear chemistry*, vol. 230, no. 1-2, pp. 167–174, 1998.

[60] R. Haas, S. Lohse, Ch. E. Düllmann, K. Eberhardt, C. Mokry, and J. Runke, "Development and characterization of a Drop-on-Demand inkjet printing system for nuclear target fabrication," *Nuclear Instruments and Methods in Physics Research Section A: Accelerators, Spectrometers, Detectors and Associated Equipment*, vol. 874, pp. 43–49, 2017.

[61] S. Bajo and J. Eikenberg, "Electrodeposition of actinides for alpha-spectrometry," *Journal of radioanalytical and nuclear chemistry*, vol. 242, no. 3, pp. 745–751, 1999.

[62] N. Talvitie, "Electrodeposition of Actinides for Alpha Spectrometric Determination," *Analytical Chemistry*, vol. 44, no. 2, pp. 280–283, 1972.

[63] M. Lee and C. Lee, "Preparation of alpha-emitting nuclides by electrodeposition," *Nuclear Instruments and Methods in Physics Research Section A: Accelerators, Spectrometers, Detectors and Associated Equipment*, vol. 447, no. 3, pp. 593–600, 2000.

[64] W. Parker and R. Falk, "Molecular plating: A method for the electrolytic formation of thin inorganic films," *Nuclear Instruments and Methods*, vol. 16, pp. 355–357, 1962.

[65] A. Vascon, N. Wiehl, T. Reich, J. Drebert, K. Eberhardt, and C. E. Düllmann, "The performance of thin layers produced by molecular plating as α-particle sources," *Nuclear Instruments and Methods in Physics Research Section A: Accelerators, Spectrometers, Detectors and Associated Equipment*, vol. 721, pp. 35–44, 2013.

[66] W. J. McDowell and B. L. McDowell, "Liquid Scintillation Alpha Spectrometry," *Radiocarbon*, vol. 36, no. 2, 1994.

[67] W. J. McDowell and B. L. McDowell, *Liquid Scintillation Alpha Spectrometry*. CRC Press, 1984.

[68] J. Thomson, "Quench & quench curves," in *Advances in Liquid Scintillation Spectrometry*. Citeseer, 2002, pp. 65–73.

[69] I. Stojković, B. Tenjović, J. Nikolov, and N. Todorović, "Radionuclide, scintillation cocktail and chemical/color quench influence on discriminator setting in gross alpha/beta measurements by lsc," *Journal of environmental radioactivity*, vol. 144, pp. 41–46, 2015.

[70] S. Möbius and T. L. Möbius, *Flüssigszintillation - Stand der Technik und neuere Entwicklungen zur Bestimmung natürlicher Radionuklide*. Karlsruher Institut für Technologie, 2008.

[71] G. Jia and J. Jia, "Determination of radium isotopes in environmental samples by gamma spectrometry, liquid scintillation counting and alpha spectrometry: a review of analytical methodology," *Journal of environmental radioactivity*, vol. 106, pp. 98–119, 2012.

[72] ISO 11704, *Water quality - Measurement of gross alpha and beta activity concentration in non-saline water - Liquid scintillation counting method*. International Organization for Standardization, Switzerland, 2010.

[73] H. Zimmermann, M. Gober, J. Kratz, M. Schädel, W. Brüchle, E. Schimpf, K. Gregorich, A. Türler, K. Czerwinski, N. Hannink *et al.*, "Chemical properties of element 105 in aqueous solution: back extraction from triisooctyl amine into 0.5 M HCl," *Radiochimica Acta*, vol. 60, no. 1, pp. 11–16, 1993.

[74] M. Leino, "Gas-filled separators - An overview," *Nuclear Instruments and Methods in Physics Research Section B: Beam Interactions with Materials and Atoms*, vol. 204, pp. 129–137, 2003.

[75] Ch. E. Düllmann, "Physical preseparation: a powerful new method for transactinide chemists," *The European Physical Journal D*, vol. 45, no. 1, pp. 75–80, 2007.

[76] G. KE and V. Ninov, "Superheavy elements with the Berkeley gas-filled separator," *Journal of Nuclear and Radiochemical Sciences*, vol. 1, no. 1, pp. 1–4, 2000.

[77] Ch. E. Düllmann, C. M. Folden III, K. E. Gregorich, D. C. Hoffman, D. Leitner, G. K. Pang, R. Sudowe, P. M. Zielinski, and H. Nitsche, "Heavy-ion-induced production and physical preseparation of short-lived isotopes for chemistry experiments," *Nuclear Instruments and Methods in Physics Research Section A: Accelerators, Spectrometers, Detectors and Associated Equipment*, vol. 551, no. 2-3, pp. 528–539, 2005.

[78] Ch. E. Düllmann, "Superheavy element studies with preseparated isotopes," *Radiochimica Acta*, vol. 99, no. 7-8, pp. 515–526, 2011.

[79] I. Zvara, Y. T. Chuburkov, R. Tsaletka, T. Zvarova, M. Shalaevskii, and B. Shilov, "Chemical properties of element 104," *Soviet Atomic Energy*, vol. 21, no. 2, pp. 709–710, 1966.

[80] R. Silva, J. Harris, M. Nurmia, K. Eskola, and A. Ghiorso, "Chemical separation of rutherfordium," *Inorganic and Nuclear Chemistry Letters*, vol. 6, no. 12, pp. 871–877, 1970.

[81] M. Schädel, W. Brüchle, E. Jäger, E. Schimpf, J. Kratz, U. Scherer, and H. Zimmermann, "ARCA II—a new apparatus for fast, repetitive HPLC separations," *Radiochim. Acta*, vol. 48, p. 171, 1989.

[82] Y. Nagame, K. Tsukada, M. Asai, A. Toyoshima, K. Akiyama, Y. Ishii, T. Kaneko-Sato, M. Hirata, I. Nishinaka, S. Ichikawa *et al.*, "Chemical studies on rutherfordium (Rf) at JAERI," *Radiochimica Acta*, vol. 93, no. 9-10, pp. 519–526, 2005.

[83] J. V. Kratz, "Aqueous-phase chemistry of the transactinides," *Radiochimica Acta*, vol. 99, no. 7-8, pp. 477–502, 2011.

[84] M. Schädel, "The Chemistry of Transactinide Elements-Experimental Achievements and Perspectives," *Journal of Nuclear and Radiochemical Sciences*, vol. 3, no. 1, pp. 113–120, 2002.

[85] M. Schädel, W. Brüchle, B. Schausten, E. Schimpf, E. Jäger, G. Wirth, R. Günther, J. Kratz, W. Paulus, A. Seibert *et al.*, "First Aqueous Chemistry with Seaborgium (Element 106)," *Radiochimica Acta*, vol. 77, no. 3, pp. 149–160, 1997.

[86] G. Pfrepper, R. Pfrepper, A. Kronenberg, J. V. Kratz, A. Nähler, W. Brüchle, and M. Schädel, "Continuous on-line chromatography of short lived isotopes of tungsten as homolog of seaborgium (element 106)," *Radiochimica Acta*, vol. 88, no. 5, pp. 273–276, 2000.

[87] J. P. Omtvedt, J. Alstad, T. Bjørnstad, Ch. E. Düllmann, K. Gregorich, D. Hoffman, H. Nitsche, K. Opel, D. Polakova, F. Samadani *et al.*, "Chemical properties of the transactinide elements studied in liquid phase with SISAK," *The European Physical Journal D*, vol. 45, no. 1, pp. 91–97, 2007.

[88] K. Ooe, M. Attallah, M. Asai, N. Goto, N. Gupta, H. Haba, M. Huang, J. Kanaya, Y. Kaneya, Y. Kasamatsu *et al.*, "Development of a new continuous dissolution apparatus with a hydrophobic membrane for superheavy element chemistry," *Journal of Radioanalytical and Nuclear Chemistry*, vol. 303, no. 2, pp. 1317–1320, 2015.

[89] J. P. Omtvedt, J. Alstad, H. Breivik, D. JE, K. Eberhardt, F. I. CM, T. Ginter, G. KE, H. EA, M. Johansson *et al.*, "SISAK liquid-liquid extraction experiments with preseparated 2^{57}Rf," *Journal of Nuclear and Radiochemical Sciences*, vol. 3, no. 1, pp. 121–124, 2002.

[90] G. Langrock, N. Wiehl, H.-O. Kling, M. Mendel, A. Nähler, U. Tharun, K. Eberhardt, N. Trautmann, J. V. Kratz, J. P. Omtvedt *et al.*, "Digital liquid-scintillation counting and effective pulse-shape discrimination with artificial neural networks," *Radiochimica Acta*, vol. 103, no. 1, pp. 15–25, 2015.

[91] A. Semchenkov, W. Brüchle, E. Jäger, E. Schimpf, M. Schädel, C. Mühle, F. Klos, A. Türler, A. Yakushev, A. Belov *et al.*, "The TransActinide Separator and Chemistry Apparatus (TASCA) at GSI–Optimization of ion-optical structures and magnet designs," *Nuclear Instruments and Methods in Physics Research Section B: Beam Interactions with Materials and Atoms*, vol. 266, no. 19-20, pp. 4153–4161, 2008.

[92] R. Eichler, N. Aksenov, Y. V. Albin, A. Belozerov, G. Bozhikov, V. Chepigin, S. Dmitriev, R. Dressler, H. Gäggeler, V. Gorshkov *et al.*, "Indication for a volatile element 114," *Radiochimica Acta*, vol. 98, no. 3, pp. 133–139, 2010.

[93] A. Yakushev, "Chemical Characterization of Element 108, Hassium and Synthesis of New Hassium Isotopes," Habilitation, Technische Universität München, München, 2009.

[94] V. Pershina, "Reactivity of superheavy elements Cn, Nh, and Fl and their lighter homologues Hg, Tl, and Pb, respectively, with a gold surface from periodic DFT calculations," *Inorganic chemistry*, vol. 57, no. 7, pp. 3948–3955, 2018.

[95] P. K. Jal, S. Patel, and B. K. Mishra, "Chemical modification of silica surface by immobilization of functional groups for extractive concentration of metal ions," *Talanta*, vol. 62, no. 5, pp. 1005–1028, 2004.

[96] W. Kern, "The evolution of silicon wafer cleaning technology," *Journal of the Electrochemical Society*, vol. 137, no. 6, p. 1887, 1990.

[97] W. Kern, "Cleaning solution based on hydrogen peroxide for use in silicon semiconductor technology," *RCA review*, vol. 31, pp. 187–205, 1970.

[98] H. Habuka, N. Ono, A. Sakurai, and T. Naito, "Molecular adsorption and desorption behavior on silicon surface in a complex ambient atmosphere containing vapors of Diethylphthalate, acetic acid and water," 2013.

[99] J. Cras, C. Rowe-Taitt, D. Nivens, and F. Ligler, "Comparison of chemical cleaning methods of glass in preparation for silanization," *Biosensors and bioelectronics*, vol. 14, no. 8-9, pp. 683–688, 1999.

[100] Y. Han, D. Mayer, A. Offenhäusser, and S. Ingebrandt, "Surface activation of thin silicon oxides by wet cleaning and silanization," *Thin Solid Films*, vol. 510, no. 1-2, pp. 175–180, 2006.

[101] J. Fan, G. Y. Chong, and C. S. Tan, "Study of hydrophilic Si direct bonding with ultraviolet ozone activation for 3D integration," *ECS Journal of Solid State Science and Technology*, vol. 1, no. 6, p. P291, 2012.

[102] D. Mattox, "Surface cleaning in thin film technology," *Thin Solid Films*, vol. 53, no. 1, pp. 81–96, 1978.

[103] J. Meichsner, M. Schmidt, R. Schneider, and H.-E. Wagner, *Nonthermal plasma chemistry and physics*. CRC press Boca Raton, FL, 2013.

[104] S. Kaya, P. Rajan, H. Dasari, D. C. Ingram, W. Jadwisienczak, and F. Rahman, "A systematic study of plasma activation of silicon surfaces for self assembly," *ACS applied materials & interfaces*, vol. 7, no. 45, pp. 25 024–25 031, 2015.

[105] S. F. Thames and K. G. Panjnani, "Organosilane polymer chemistry: A review," *Journal of Inorganic and Organometallic Polymers*, vol. 6, no. 2, pp. 59–94, 1996.

[106] C. A. Schlecht and J. A. Maurer, "Functionalization of glass substrates: mechanistic insights into the surface reaction of trialkoxysilanes," *Rsc Advances*, vol. 1, no. 8, pp. 1446–1448, 2011.

[107] D. Aswal, S. Lenfant, D. Guerin, J. Yakhmi, and D. Vuillaume, "Self assembled monolayers on silicon for molecular electronics," *Analytica chimica acta*, vol. 568, no. 1-2, pp. 84–108, 2006.

[108] J. Wu, L. Ling, J. Xie, G. Ma, and B. Wang, "Surface modification of nanosilica with 3-mercaptopropyl trimethoxysilane: Experimental and theoretical study on the surface interaction," *Chemical Physics Letters*, vol. 591, pp. 227–232, 2014.

[109] A. V. Krasnoslobodtsev and S. N. Smirnov, "Effect of water on silanization of silica by trimethoxysilanes," *Langmuir*, vol. 18, no. 8, pp. 3181–3184, 2002.

[110] F. Zhang, K. Sautter, A. M. Larsen, D. A. Findley, R. C. Davis, H. Samha, and M. R. Linford, "Chemical vapor deposition of three aminosilanes on silicon dioxide: surface characterization, stability, effects of silane concentration, and cyanine dye adsorption," *Langmuir*, vol. 26, no. 18, pp. 14 648–14 654, 2010.

[111] Gelest Inc, "Silane Coupling Agents: Connecting Across Boundaries," *Morrisville PA*, vol. 2, 2014.

[112] D. K. Aswal, S. Lenfant, D. Guerin, J. V. Yakhmi, and D. Vuillaume, "A Tunnel Current in Self-Assembled Monolayers of 3-Mercaptopropyltrimethoxysilane," *Small*, vol. 1, no. 7, pp. 725–729, 2005.

[113] C. R. Vistas, A. C. Águas, and G. N. Ferreira, "Silanization of glass chips - A factorial approach for optimization," *Applied surface science*, vol. 286, pp. 314–318, 2013.

[114] E. Cano-Serrano, G. Blanco-Brieva, J. Campos-Martin, and J. Fierro, "Acid-functionalized amorphous silica by chemical grafting- quantitative oxidation of thiol groups," *Langmuir*, vol. 19, no. 18, pp. 7621–7627, 2003.

[115] R. D. Badley and W. T. Ford, "Silica-bound sulfonic acid catalysts," *The Journal of Organic Chemistry*, vol. 54, no. 23, pp. 5437–5443, 1989.

[116] S. Jeenpadiphat, E. M. Björk, M. Odén, and D. N. Tungasmita, "Propylsulfonic acid functionalized mesoporous silica catalysts for esterification of fatty acids," *Journal of Molecular Catalysis A: Chemical*, vol. 410, pp. 253–259, 2015.

[117] R. Haas, M. Hufnagel, R. Abrosimov, Ch. E. Düllmann, D. Krupp, C. Mokry, D. Renisch, J. Runke, and U. W. Scherer, "Alpha spectrometric characterization of thin ^{233}U sources for ^{229m}Th production," *Radiochimica Acta*, vol. 108, no. 12, pp. 923–941, 2020.

[118] D. Krupp and U. W. Scherer, "Prototype development of ion exchanging alpha detectors," *Nuclear Instruments and Methods in Physics Research Section A: Accelerators, Spectrometers, Detectors and Associated Equipment*, vol. 897, pp. 120–128, 2018.

[119] H. Mohamud, E. van Es, T. Sainsbury, P. Ivanov, B. Russell, P. Regan, and N. Ward, "Progress towards the development of a rapid analytical approach for separation of ^{226}Ra using dibenzo-18-crown-6 ether functionalised silica (SiO_2) disks," *Radiation Physics and Chemistry*, vol. 140, pp. 57 – 60, 2017.

[120] A. Bilewicz, "Adsorption of Zr^{4+}, Hf^{4+}, Rf^{4+} and Po^{4+} diketonate complexes on hydrophobized glass surface," *Journal of Radioanalytical and Nuclear Chemistry*, vol. 247, no. 2, pp. 407–410, 2001.

[121] J. M. Mannion, W. D. Locklair, B. A. Powell, and S. M. Husson, "Alpha spectroscopy substrates based on thin polymer films," *Journal of Radioanalytical and Nuclear Chemistry*, vol. 307, no. 3, pp. 2339–2345, 2016.

[122] R. S. Addleman, M. J. O'Hara, T. Marks, J. W. Grate, and O. B. Egorov, "Direct actinide assay with surface passivated silicon diodes," *Journal of radioanalytical and nuclear chemistry*, vol. 263, no. 2, pp. 295–300, 2005.

[123] O. B. Egorov, R. S. Addleman, M. J. O'Hara, T. Marks, and J. W. Grate, "Direct measurement of alpha emitters in liquids using passivated ion implanted planar silicon (PIPS) diode detectors," *Nuclear Instruments and Methods in Physics Research Section A: Accelerators, Spectrometers, Detectors and Associated Equipment*, vol. 537, no. 3, pp. 600–609, 2005.

[124] L. Hughes and T. DeVol, "Characterization of a Teflon coated semiconductor detector flow cell for monitoring of pertechnetate in groundwater." *Journal of Radioanalytical & Nuclear Chemistry*, vol. 267, no. 2, 2006.

[125] R. S. Addleman, M. J. O'Hara, J. W. Grate, and O. B. Egorov, "Chemically enhanced alpha-energy spectroscopy in liquids," *Journal of radioanalytical and nuclear chemistry*, vol. 263, no. 2, pp. 291–294, 2005.

Chapter 2

Protoype Development of Ion Exchanging Alpha Detectors

D.Krupp [1] and U.W. Scherer[1]

[1] Institut für Physikalische Chemie und Radiochemie, Hochschule Mannheim - University of Applied Sciences, 68163 Mannheim, Germany

Published in: Nuclear Instruments and Methods in Physics Research Section A: Accelerators, Spectrometers, Detectors and Associated Equipment 897, 120-128 (2018)

DOI: https://doi.org/10.1016/j.nima.2018.04.038

The following article was submitted as full article to Nuclear Instruments and Methods in Physics Research Section A: Accelerators, Spectrometers, Detectors and Associated Equipment in 2018. The publication deals with a feasibility study in which it is to be shown that measurements of α emitting radionuclides from aqueous solutions are possible with the aid of chemically modified Si-detectors. The detector surfaces are coated with thin organosilane layers which, when chemically modified, form covalently bonded cation exchangers on the detector surface. With sufficiently thin layers, the alpha radiation can penetrate the silane layers without losing significant kinetic energy. This has been shown both in theoretical SRIM and AASI simulations and in practical experiments with $^{238/234}$U. By modifying the detector surface into a chemically selective stationary phase, sample preparation is significantly simplified and accelerated.

Own contributions

Both the theoretical calculations and the practical experiments, including evaluation, were carried out in a self-directed manner. Likewise, the writing of the publication was self-directed.

Abstract

In contemporary alpha particle spectrometry, the sample preparation is separated from the detection of the radionuclides. The sample preparation itself requires much time and the equipment of a radiochemistry lab. If sample preparation and detection could be combined in one step, a huge time-saving potential becomes available. One way to realize such a combination is described here. The concept was explored by simulations with the well-established computer programs SRIM and AASI. In a proof of concept, the active surface of commercially available alpha detectors was modified with sulfonic acid groups as a well-known type of cation exchanger. It was shown, that in contrast to a pristine detector, a chemically modified detector is able to extract uranium-238 and -234 selectively as uranyl cations onto the detector surface from a diluted [$^{238/234}$U]uranyl acetate solution. It was possible to measure directly in the sample solution for one week or to prepare the modified detector surfaces within 30 s for measurements in conventional alpha chambers. In either case, the full width at half maximum of the measured spectra was around 100 keV, allowing a clear nuclide identification. After regenerating the cation exchanger surfaces by rinsing with hydrochloric acid the typical uranium spectra had disappeared, proving chemical bonding of the uranium. Due to the large variety of potential functional groups this new way of alpha spectrometry could be beneficial for all fields of alpha particle spectrometry, from environmental analysis, over security measurements to studies of the heaviest elements.

2.1 Introduction

Alpha particle spectrometry is a challenging field for many reasons: the procedure to prepare samples, which allows high-quality spectra, requires a lot of time, expensive chemicals and technical equipment like electrodeposition apparatus and vacuum pumps. However, these quite complex preparation methods are accepted due to the resulting fingerprint information obtained in the subsequent measurement. When going to the extremes e.g. in the chemical separation of short-lived nuclides produced in heavy-ion bombardments with low cross sections one reaches the limits. Even the fastest chemical separation systems like ARCA II [1], AIDA [2] or the extraction based SISAK system [3] follow the subsequent steps of chemical preparation and detection. Radiochemical experiments in aqueous solutions cannot be performed effectively when the half-life is below ~ 20 s. By combining the individual stages in one step alpha particle spectrometry would become much more efficient. To that end, the detector surface needs to be modified with a chemically active agent. Based on the grafted functional group, established radiochemical separation processes e.g. [4] can be done directly on the detector surface. As a proof of principle silicon detectors were modified with sulfonic acid groups, a well-known class of strong cation exchangers (CIX). A typical procedure to prepare such a cation exchanger is a two-step reaction, in which a thiol-functionalized silane is grafted onto a surface followed by subsequent oxidation to sulfonic acid groups [5].

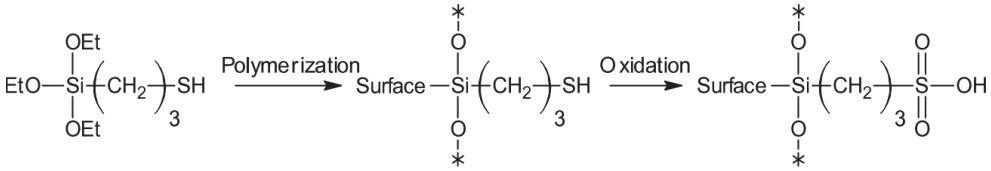

Figure 2.1: *Two-step surface modification to obtain CIX surfaces (EtO = Ethoxygroup; * = polymerized bond).*

Subsequently, such modified detectors can directly be placed in the solution to be analyzed. Here, a cation exchange reaction takes place between the detector surface present functional group (-SO_3H) and a dissolved cationic species (X^+) in which a proton (H^+) is substituted by the species X^+. The general reaction is described by the following equation:

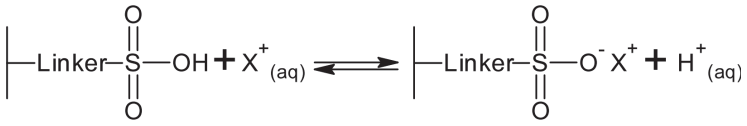

Figure 2.2: *General equation — ion exchange reaction.*

The resulting chemical equilibrium is described by the law of mass action. Ion exchange experiments of actinide ions like uranyl cations ($UO_2^{2+}{}_{(aq)}$) with this type of functional group are well studied [6]. Diamond et al. report equilibrium constants K » 1 in weakly acidic aqueous solutions [7] leading to complete adsorption. However, due to the small range of an alpha particle, the extraction agents need to be deposited in extremely thin layers onto the detector surface to allow high-resolution spectra. As a first step simulation models were created with the programs SRIM and AASI to test the feasibility of the approach of a combined separation/detection system.

2.2 Material and Methods

2.2.1 Simulation tools

Stopping power simulations for different materials were performed using the SRIM-Code version 2013.00, developed by James F. Ziegler [8]. More complex simulations of alpha spectra and detector properties were accomplished by using AASI-FIT version 2.0, developed and provided by the company STUK [9]. Additionally, the full width at half maximum (FWHM) of simulated and measured spectra was determined by the curve fitting program Fityk version 0.9.8 [10] [11].

2.2.2 Measurement set-up

All measurements were done with “ULTRATM Ion Implanted Silicon Charged Particle Radiation Detectors” (active window 25 mm²), manufactured by Ortec. The detectors were linked through a “SMA58 RG-58A/U” coaxial cable (Ortec) with an alpha spectrometer “Model 7401” (Canberra) for measurements outside of the vacuum chamber or mounted directly in the chamber for conventional measurements. Alpha

particle spectra were recorded with the multichannel analyzer system "Multiport II" in combination with the alpha acquisition software "Genie 2000 version 3.2" from Canberra. The whole system was mounted in a "4001M" Minibin & Power Supply from Ortec. A ^{239}Pu / ^{241}Am / ^{244}Cm calibration source (Amersham) was used for energy and efficiency calibration as well as a reference source for AASI simulations.

2.2.3 Chemicals

All reagents were used without further purification. Uranyl acetate dihydrate and conc. hydrochloric acid was obtained from Merck, both in p.a. quality. Mercaptopropyltrimethoxysilane (MPTMS) was purchased by Alfa Aesar with a purity of ≥ 95 %. Hydrogen peroxide (w = 30 %) was purchased by Roth with Ph. Eur. quality. Methanol was bought in p.a. quality from Th. Geyer. The detectors were modified by a procedure similar to that described in [12]. The subsequent oxidation of thiol groups to sulfonic acid groups was adapted to a procedure as described in [5]. Chemical processing is described elsewhere [13].

2.3 Experimental

General feasibility of a detector system to measure alpha particles from aqueous solution was initially studied by different nuclear simulation tools. In order to ensure comparability of the two simulation tools, both models use the same basic set-up. In an ideal model, the maximum amount of functional groups present on a surface is limited to ~10^{15} molecules per square centimeter [14]. These molecules are completely polymerized and attached to the surface by covalent bonds in a uniform manner. If the number of molecules is greater than 10^{15}, an additional layer is formed which is homogeneously attached on top of the previous layer by physisorption. Radionuclides adsorbed by a functional group, are also homogeneously distributed across the surface. Radionuclides dissolved in aqueous solution are equally distributed across the whole solution. As an initial step, the stopping power of each material was calculated by SRIM (Stopping and Range of Ions in Matter) [15] which utilizes the Bethe-Formula. The stopping power of the individual materials (water, ion exchange resin and silicon dioxide) were calculated in a range from 7 to 1 MeV. The required material properties for water and silicon dioxide are well known. The relevant properties of the silane layers need to be estimated. In general, the three hydrolyzable ethoxy groups would result in a three-dimensional polymerization of the silane with covalent- and hydrogen bonding, yielding an inhomogeneous silane density over the detector area and roughness fluctuations on top of the surface. These differences depend strongly on the preparation method. In order to allow a first prediction, the simulation is based on an ideal system in which the surface is homogeneously covered with the grafted molecule. The theoretical length of a mercaptopropyl chain is 0.77 nm [14]. Each further layer is attached by hydrogen bonding only (theoretical length is 0.81 nm). For estimating the density of the silane layers, similar density to that of silicone was assumed which varies between 0.94 to 1.07 g/cm³. Dietrich et. al. [16] estimated a density of 0.81 g/cm³ for a similar but smaller molecule. Such data are not available for MPTMS, therefore the lower density limit for silicone was chosen. Multilayer formation occuring during polymerization and the subsequent oxidation step would only affect the topmost layer in an ideal system, therefore the slightly different last (oxidized) layer are ignored as a model simplification (Figure 2.3).

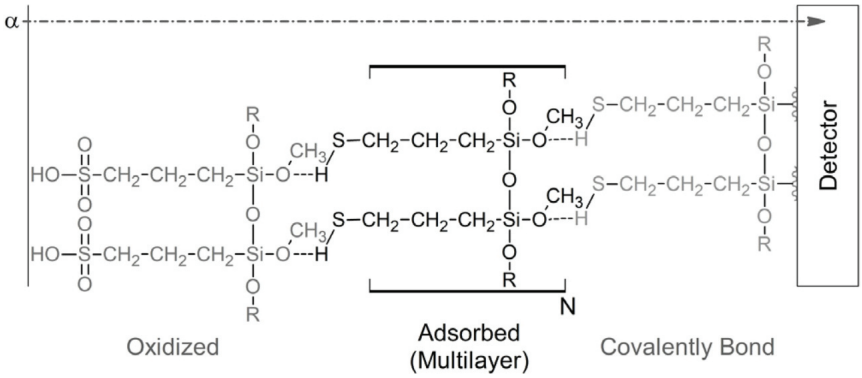

Figure 2.3: *SRIM Model Buildup—Transport of alpha particles through a multilayer silane system.*

The SRIM simulations predicted favorable energy loss of alpha particles when passing the multilayer. Instead of using the corresponding TRIM (Transport of Ions in Matter) software which is mainly used for target development, AASI (Advanced Alpha spectrometric Simulation) was used for more complex detector simulations. AASI is a Monte Carlo method based simulation software where alpha spectra can be simulated under a wide range of parameter sets [17] [18]. The ability to simulate the alpha particles, interacting with different adsorbing layers, is of special interest to predict the detector surface modification limits and to understand the resulting spectra on modified detectors. The simulations were done in three steps. The first step was to adjust the AASI parameters to simulate spectra compatible with spectra measured by a pristine detector in a vacuum chamber. Subsequently, an adsorbing monolayer, consisting of ion exchange material was simulated. Based on this simulation, multiple monolayers were stacked to evaluate the critical layer thickness after which unacceptable peak broadening and energy shift occur. In order to have a worst case scenario, it is assumed that decay takes place from the outermost layer, only. Finally, a supernatant solution, containing an alpha-emitting radionuclide at different concentrations, was simulated. This approach is depicted in Figure 2.4.

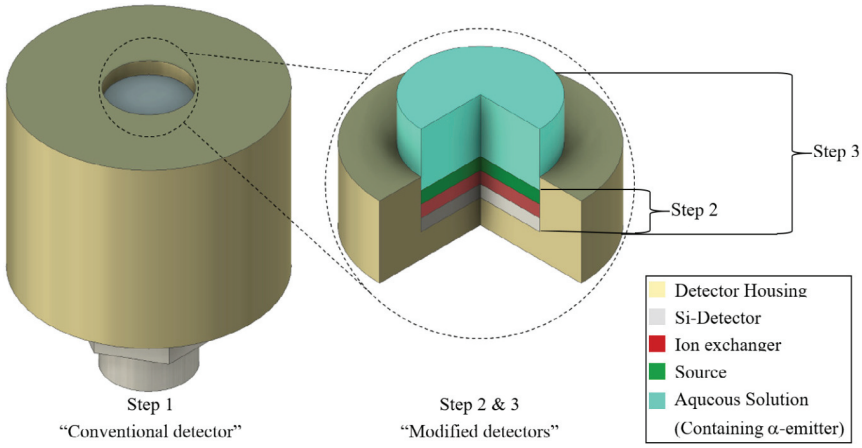

Figure 2.4: *AASI simulation steps.*

All chemical detector modification approaches were done on Ortec ULTRATM alpha detectors. Therefore a measurement was done with this type of detector in a conventional vacuum chamber with a ^{239}Pu / ^{241}Am / ^{244}Cm calibration source. The source was placed at a distance of 17 mm to the detector and measured for 3 hours in order to get good statistics at $1.4 \cdot 10^{-2}$ mbar. Subsequently, an AASI model of the Ortec alpha detector was created with the following parameters set:

Detector parameters

· Active detector area is 25 mm²
· Source-detector distance is 17 mm
· Intrinsic resolution is 17 keV
· Energy bin size is 4.0 keV
· Integration steps were 0.02 µm (AASI requires a value greater than 0.01 µm)

Source parameters

· Source diameter is 7 mm
· Source consists of ^{239}Pu / ^{241}Am / ^{244}Cm
· No self-absorption of alpha particles in the source
· Source activity ratio is (^{239}Pu / ^{241}Am / ^{244}Cm) 2.5 : 1.8 : 1

As discussed in chapter 3, a chemically modified detector is, under optimized conditions, grafted with a monomolecular polymer layer. This ideal modified detector is compared with an unmodified detector. The AASI detector characteristic, as described in this section, was also used for the subsequent models. However, geometric aspects, as well as source properties, were changed. The source diameter was reduced to 5.64 mm in order to match exactly the active detector surface. The source was placed at a distance of 20 µm to the detector. This was the minimum distance to ensure stable simulation conditions. Based on this source parameters, the geometric efficiency was computed with a relative standard deviation of 0.04 ‰, resulting in a geometric efficiency of 48.64 %. This value is still close enough to assume a source placed "directly" on a detector surface. In the next simulation step, the influence of silane layers present on a detector surface was investigated. The radionuclide was changed to ^{238}U, with the intention to make the simulations more compatible with measurements, as discussed in the experimental section. The optimized monomolecular grafted detector was simulated with all three decay lines of ^{238}U. The subsequent multilayer studies were done with an energy of the emitted alpha particle which was set to 4.2 MeV, which represents the main decay line of ^{238}U. This was done to reduce the simulation and analyzing time.

The stopping power calculations in SRIM suggest that a spectrum measured from solution consists of two parts: Events caused by the alpha emission of radionuclides adsorbed close to the detector surface and events caused by alpha emissions of radionuclides, which are coincidentally close enough to the detector surface. In case of water, the range of a 4.2 MeV alpha particle is about 30 µm, according to SRIM. Therefore a water layer, with the same area as the detector and a height of 30 µm was simulated to predict the influence of radionuclides, dissolved in solution. The influence was calculated for a solution containing a 4.2 MeV radionuclide with a concentration of 0.01 mol/l. Assuming a detector surface completely covered with radionuclide in the same number as functional groups the relative radionuclide partitioning P between the surface and the solution was estimated as follows:

$$
\begin{aligned}
N_{Solution} &= N_A \cdot c \cdot A_{Detector} \cdot h_{Solution} \\
&= 6.022 \cdot 10^{23} \frac{1}{mol} \cdot 1 \cdot 10^{-18} \frac{mol}{mm^3} \cdot 25\ mm^2 \cdot 0.03\ mm \\
&= 4.52 \cdot 10^{15} [/] \\
N_{Surface} &= N_{max} \cdot A_{Detector} = 1.00 \cdot 10^{13} \frac{1}{mm^2} \cdot 25 mm^2 \\
&= 2.5 \cdot 10^{14} [/] \\
P &= \frac{N_{Solution}}{N_{Surface}} = 18.10 \approx 18
\end{aligned}
\tag{2.1}
$$

From this estimate, eighteen times more decays from solution (background) than from the surface are anticipated. Both spectra were simulated individually. In order to have good statistics, 20,000 decays of 4.2 MeV alpha particles were simulated on the detector surface and 360,000 in solution, respectively. The ratio between simulated particles was subsequently changed to 180 and 1.8 in order to simulate a supernatant solution of higher or lower concentration respectively. The background contribution in the sum spectrum of both simulations was calculated by the following equation:

$$
w[\%] = \frac{ROI_{Solution}}{ROI_{Solution} + ROI_{On\ Detector}} \tag{2.2}
$$

In either case, the region of interest was a window from 4.2 to 4.0 MeV. The number of particles, which were absorbed by a non-detector medium was calculated by the following equation:

$$
Absorbed\ particle[\%] = \frac{N_{Absorbed\ particle}}{N_{Total\ number\ of\ simulated\ particle}} \cdot 100 \tag{2.3}
$$

In conclusion, a detector immersed in a solution containing 0.01 mol/l ^{238}U and its daughter nuclide ^{234}U was simulated with its main decay lines For short contact experiments 15 µl of a uranyl acetate solution (c = 0.01 mol/l) was spread on a modified detector surface. The solution was retracted from the surface after 30 seconds. Subsequently, the detector surface was washed extensively with distilled water, dried and mounted in an alpha chamber. The spectrum was recorded for 48 hours, subsequently, the detector was disassembled from the vacuum chamber. The surface was carefully rinsed with 20 µl concentrated hydrochloric acid and several milliliters of distilled water to remove the uranyl cations from the cation exchanger. The detector was dried again and mounted in the vacuum chamber for 48 hours measurement. This procedure was repeated with a pristine detector under the same conditions. In order to measure in solution and outside of a vacuum chamber, a modified detector was linked by a coaxial cable with the alpha chamber. Afterward, the wired detector was placed in a beaker, filled with a 100 ml of uranyl acetate solution (c = 0.01 mol/l), slightly below the surface of the sample. The measurement was carried out for 24 hours. Afterward, the detector was retracted from solution and washed extensively with distilled water, dried and mounted in a vacuum chamber for a conventional measurement for 24 hours. Next, the detector surface was regenerated with 20 µl concentrated hydrochloric acid and washed with distilled water. After this desorption step, the detector was measured again in the vacuum chamber for 24 hours. With the intention to study the long-term stability, a wired modified detector was placed in 100 ml of uranyl acetate

solution (c = 0.01 mol/l) for 7 days.

2.4 Results and Discussions (Simulation)

2.4.1 Stopping power calculations (SRIM)

Figure 2.5 shows the projectile range in µm versus the projectile energy in MeV. As expected, the projectile range in water (ρ = 1.0 g/cm³) and silicon dioxide (ρ = 2.2 g/cm³) is lower than in silane multilayers (ρ = 0.94 g/cm³). However, the projectile range is still high enough to allow an alpha particle to penetrate several silane layers. As an example, a 4 MeV alpha particle is absorbed within ~ 32 µm. This is equal to around 40,675 adsorbed silane layers. This result suggests, that alpha particles can be detected through a sufficiently thin silane film, even with an underlying silicon dioxide dead layer without a significant energy loss. Nevertheless, because of the high projectile range in water, it is highly probable, that radionuclides dissolved in the solution but not bonded to the cation exchanger can be close enough to the detector to cause background events, too. This could result in a raised background spectrum and a peak shape broadening.

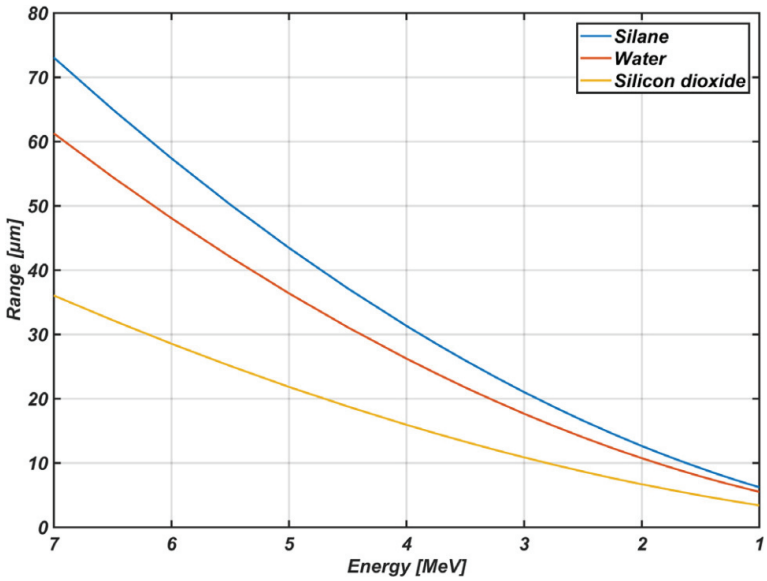

Figure 2.5: *SRIM Results — Energy depletion of alpha particles in different materials.*

2.4.2 Advanced alpha simulations (AASI)

The simulation the spectrum of a standard sample is in good agreement with the measured result. The best AASI parameter set with the lowest residuum achieved is shown in (Figure 2.6). The peak maxima of the individual decay lines are slightly shifted to lower energies, however, the relative peak positions are compatible in both, simulation and measurement. Nevertheless, AASI seems to underestimate the intrinsic resolution of the simulated detector. This gets clearer by looking especially at the peak resolution between the line with the highest intensity and the second intense line of each nuclide. However, due to the high coverage of the simulation, this parameter set was used as a conservative model fundament for further simulations.

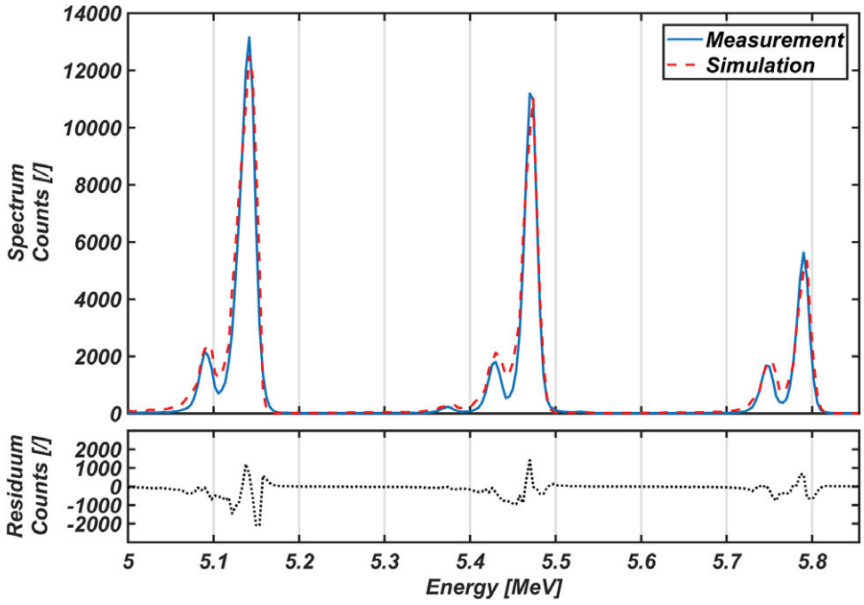

Figure 2.6: *Comparison between simulation and measurement of a ^{239}Pu, ^{241}Am, ^{244}Cm source in a conventional alpha chamber.*

The influence of an increasing number of silane layers to a spectrum of 4.2 MeV alpha particle emitters is summed up in Table 2.1. Additionally, Figure 2.7 shows examples of simulation results for various numbers of silane layers on the surface.

Table 2.1: *Influence of increasing silane layers ta a 4.2 MeV spectrum.*

Sim Nr.	Layer Nr.	h_{Layer} [nm]	Rel. Absorption [%]	FWHM [keV]	E at R_{max} [MeV]	200 keV ROI [/]
1	0	0	0.01	28.86	4.180	91988 ± 303
2	1	0.77	0.01	29.16	4.176	92190 ± 304
3	2	1.58	0.01	29.00	4.176	91466 ± 302
4	10	8.06	0.01	29.82	4.176	91610 ± 303
5	50	40.46	0.02	32.60	4.172	90313 ± 301
6	100	80.96	0.02	36.17	4.172	88916 ± 298
7	250	202.46	0.09	45.37	4.156	83781 ± 289
8	500	404.96	0.28	60.53	4.136	77311 ± 278
9	750	607.46	0.52	76.21	4.116	71531 ± 267
10	1000	809.96	0.73	90.28	4.100	65830 ± 257
11	3000	2429.96	2.87	193.70	3.948	41340 ± 203
12	5000	4049.96	5.26	286.88	3.792	29376 ± 171
13	7000	5669.96	7.61	372.32	3.644	21879 ± 148
14	9000	7289.96	9.98	438.06	3.492	17279 ± 131
15	11000	8909.96	12.40	517.83	3.332	13410 ± 116

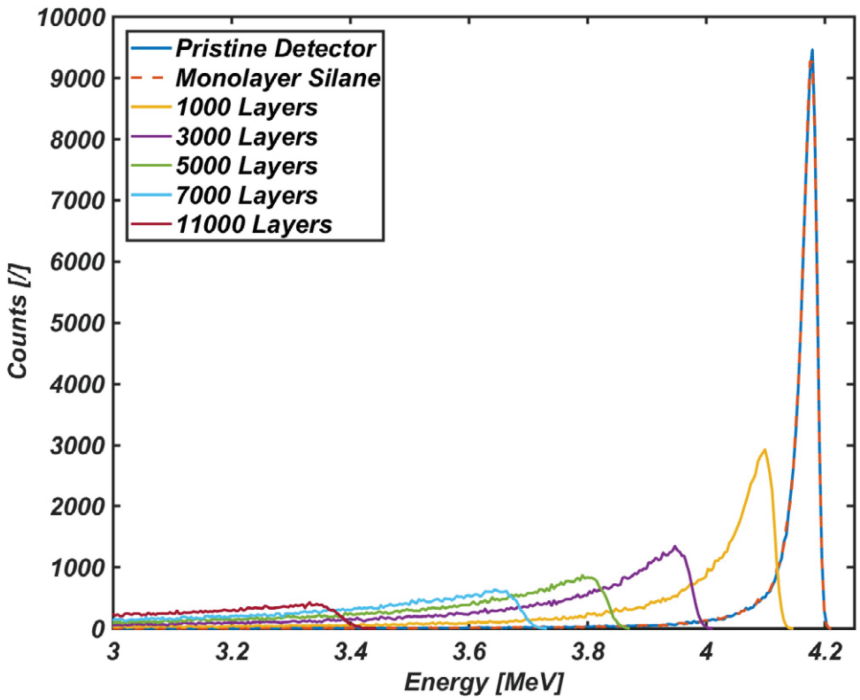

Figure 2.7: *AASI Simulation of N = 200,000 decays on a pristine detector compared with a silane-grafted detector.*

As already predicted by previous SRIM simulations, in chapter 4.1, the stopping power of a monomolecular silane layer is too small to cause a notable effect. It also shows that several tens of additional silane layers would be acceptable for measurements on a detector surface. However, this corresponds to a thickness of around 40 nm, only. With further increase of the film thickness, several effects become more significant: an increasing number of the initially 200000 alpha particles is completely absorbed. This results in a lower number of counts per 200 keV region of interests (starting at the high-energy edge of the peaks). An additional effect is the shift of the peak maximum, down to lower energies. Special consideration should be taken to a comparison with the SRIM simulation. According to the SRIM code, 4.2 MeV alpha particles are completely absorbed within 35 µm. However, this does not take into account the properties of the resulting spectrum. The AASI code demonstrates a nearly continuous spectrum from 3000 to 5000 silane layers, already. 5000 silane layers represent a thickness of only 4.05 µm, i.e. ~ 10 % of the SRIM result. This clearly indicates that the silane thickness needs to be much less than initially estimated by SRIM to allow high-resolution spectra. There is an additional effect, which needs to be taken into account: The energy of the alpha particle was set to 4.2 MeV because it represents the main decay line of ^{238}U. However, most of the known alpha-emitting radionuclides, like ^{238}U itself, are not decaying by monoenergetic alpha emission, so the resulting peak in a spectrum is a multiplet of individual decay lines. This results in an additional peak broadening when measuring on modified detectors. If a detector with a chemically modified surface is placed in an aqueous solution of radionuclides, the sum spectrum is composed of two contributions: Decays, caused by radionuclides extracted from solution onto the surface. Such an event can be considered as “true” event, where the capacity depends on the number of functional groups on the surface (shown in red in Figure 2.8). The second contribution are decays, caused by dissolved radionuclides coincidently decaying when close enough to the detector surface (shown in blue in Figure 2.8). These events are “false” events which contribute mainly to the background of the spectrum. The

number of counts depends on the radionuclide concentration of the solution, where the relevant volume is set by the active detector area and the maximum distance to the detector surface, resulting from the stopping power of the solution. Figure 2.8 shows an example of such a simulation approach.

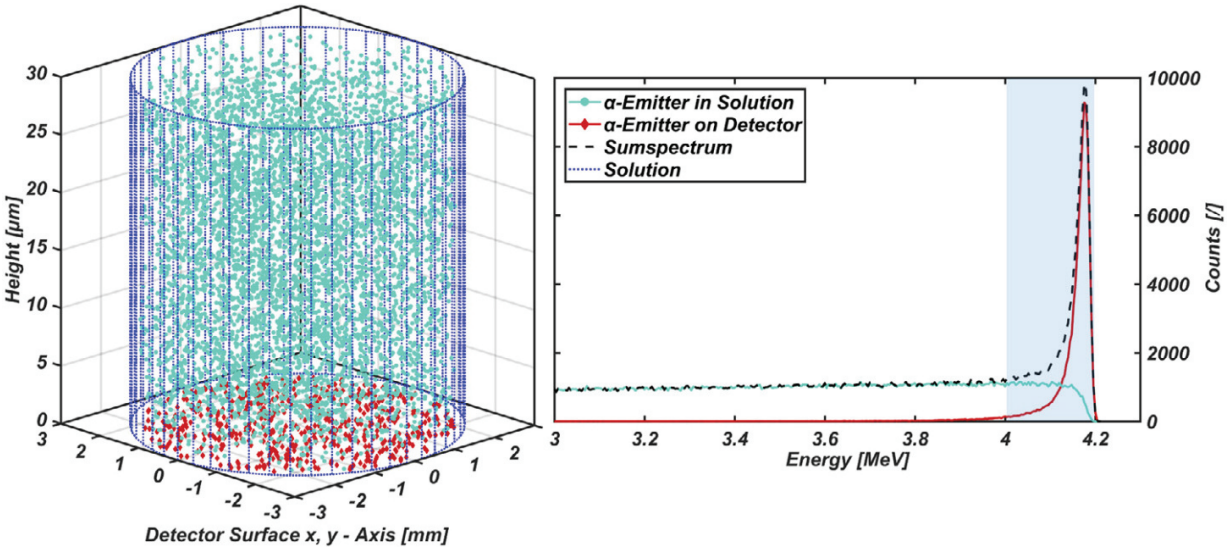

Figure 2.8: *Three dimensional (left) and two dimensional (right) distribution visualization of alpha decays, detected on a detector surface and through a solution with highlighted ROI.*

As one can see, the individual data points are randomly distributed in the solution and on the surface which fulfills the criteria of a homogeneous supernatant solution. The number of data points in this figure was reduced in order to make it better readable but the ratio between grafted and dissolved radionuclides is as described in chapter 3: The number of radionuclides is eighteen times higher in solution than on the surface for a 0.01 molar solution. Table 2.2 shows the simulation results of the simplified system, containing a hypothetical radionuclide emitting monoenergetic 4.2 MeV alpha particles.

Table 2.2: *Results of the simplified simulation approach with 4.2 MeV alpha particles in solutions with different concentrations.*

Concentration [mol/L]	$\frac{N_{Insolution}}{N_{Ondetector}}$	Adsorbed particle [%]		Counts in ROI [/]		BG contr.* w [%]
		In Solution	On Detector	In Solution	On Detector	
0.1	180	25.6	0.01	47928 ± 219	9207 ± 96	83.89 ± 0.85
0.01	18	25.6	0.14	47928 ± 219	92593 ± 305	34.11 ± 0.28
0.001	1.8	25.6	0.14	4856 ± 70	92593 ± 305	4.98 ± 0.09

**contr. = contribution*

The relative number of absorbed 4.2 MeV alpha particles remains constant, showing that the homogeneous distribution of solutions remains constant for all three simulated concentrations. The data also shows that a 0.1 molar solution would have a high background, making nuclide identification possible but difficult. However, measurements in a 0.01 molar solution represent an acceptable case where the peak to background ratio is low enough to allow a good nuclide identification and at even lower concentrations, the background contribution becomes negligible. In any way, Figure 2.8 clearly illustrates the necessity of a surface functionalization if one wants to measure alpha particle spectra directly in aqueous solution:

If an untreated detector is placed in solution, the obtained spectrum would be continuous without any clearly distinguishable peaks. But if the surface is able to extract radionuclides from solution, the obtained spectrum contains individual peaks. With the aim of subsequent prototype tests, a concentration of 0.01 mol/l in solution was chosen. This case was also simulated by substituting the 4.2 MeV emitting particles by ^{238}U and ^{234}U in a ratio of 2.5 (^{238}U/^{234}U). Figure 2.9 shows the result of this simulation approach.

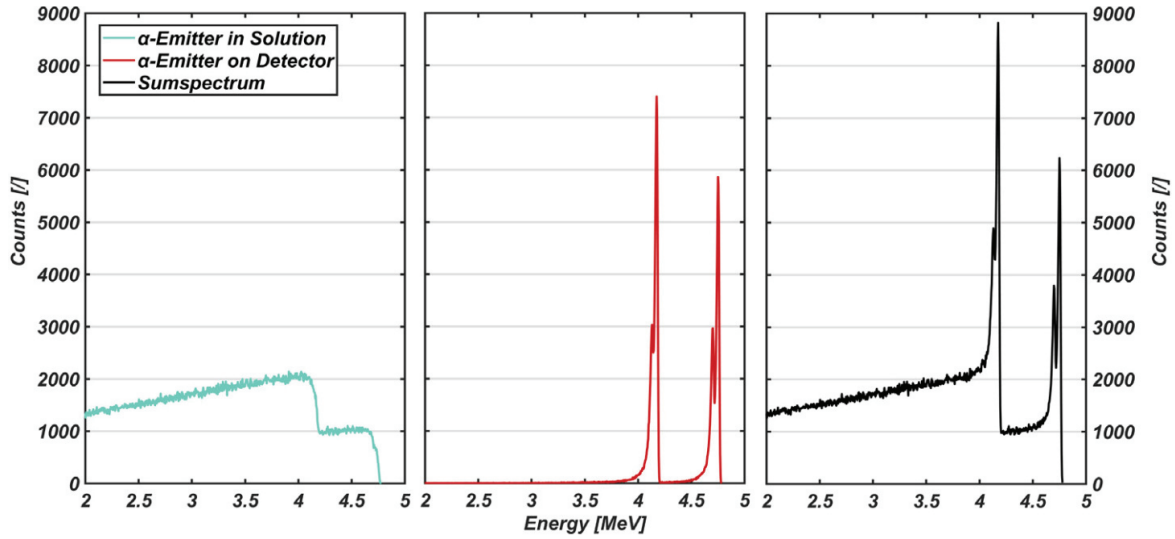

Figure 2.9: $^{238/234}$*U Simulation: In Solution (left), on the detector (middle) sum spectrum (right).*

The peaks are clearly distinguishable from the background, as already seen in the simplified model. However, these simulations do not cover several contributions, which would occur in a real measurement, like bonding of uranium on different silane layers (not only the topmost one), physisorption of uranium species on the detector surface, the contribution of decay products the spectrum and the potential roughness of the silane layers. These uncertainties make prototype tests necessary.

2.5 Results and Discussions (Experimental)

Table 2.3 shows the counts, recorded in the individual spectra, in two regions of interest (ROI): 4198 – 3998 keV for ^{238}U and 4775 – 4575 keV for ^{234}U, as well as the total number of counts, recorded over all channels for all detector experiments.

Table 2.3: *Counts and their uncertainties in regions of interests overall experimental stages.*

		ROI$_1$ (^{238}U) 4198 - 3998 keV	ROI$_2$ (^{234}U) 4775 - 4575 keV	Total number in 2048 channels
Short contact	Pristine detector (adsorbed)	2	0	11
	Modified detector (adsorbed)	1656 ± 41	771 ± 28	3662 ± 61
	Modified detector (desorbed)	108 ± 11	48 ± 7	288 ± 17
In solution	In solution	214 ± 15	118 ± 11	1052 ± 33
	In Vacuum	266 ± 17	128 ± 12	877 ± 30
	Regenerated	60 ± 8	27 ± 6	352 ± 19
	Long-term	2667 ± 52	1119 ± 34	10519 ± 103

A pristine detector was in contact with 15 µl uranyl acetate solution (c = 0.01 mol/l) for 30 s. After extensive rinsing with distilled water and drying, the detector was mounted in a conventional alpha chamber, where a spectrum was acquired for 48 h. Figure 2.10 shows the resulting spectrum of $^{238/234}$U on a pristine detector. 11 counts in total were recorded within 48 h, which proofs that literally, no adsorption took place (see Table 2.3 section "Short Contact").

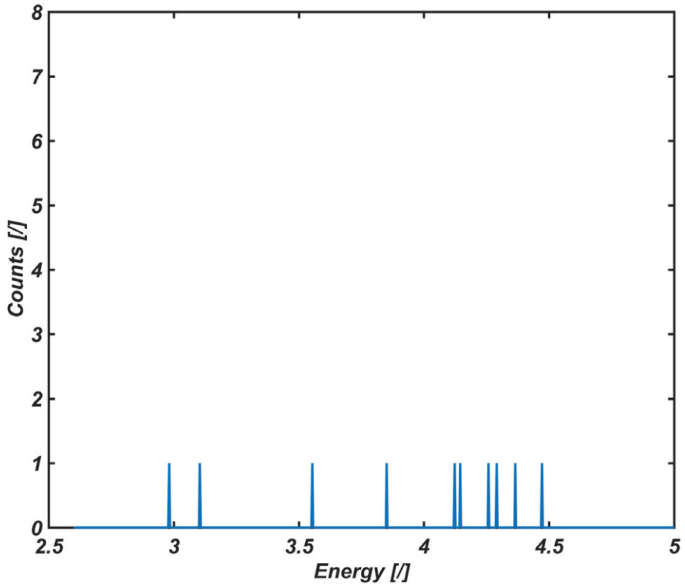

Figure 2.10: $^{238/234}$*U Spectra on a pristine detector.*

After a short contact (30 s) of 15 µl uranyl acetate solution (c = 0.01 mol/l) with a modified detector and subsequent extensive rinsing with distilled water, to remove chemically non-bonded uranyl cations, the detector was dried and a spectrum was acquired for 48 h in a conventional alpha chamber. The spectrum recorded on the modified detector (blue in Figure 2.11 left) shows the presence of uranium on the surface, with clearly identifiable peaks. The FWHM of the resulting spectrum was estimated by Fityk (Figure 2.11 right) with low residuals.

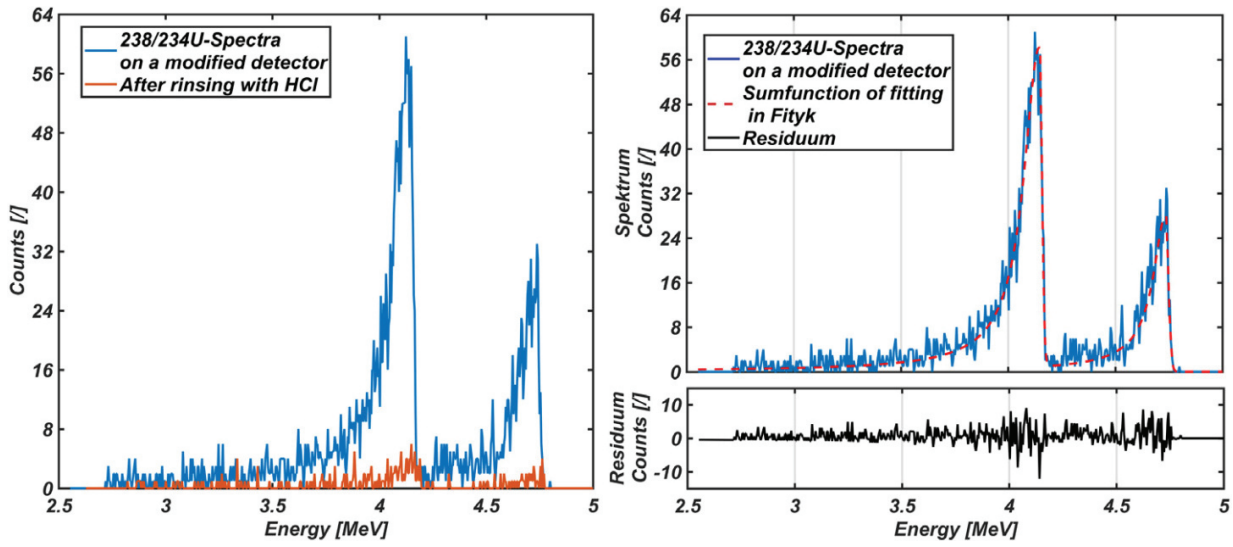

Figure 2.11: $^{238/234}$*U Spectra on a modified detector and Fityk Fit for FWHM estimation.*

The uranium concentration on the detector surface is estimated to be 25.90 ± 0.90 µmol/cm² (1.6 · 1016 ± 0.1 · 10^{15} molecules/cm²) which is by a factor 10 too high for a monomolecular cation exchanger layer. This observation is in agreement with the calculated full width at half maximum (FWHM) for the ^{238}U and ^{234}U multiplet. The FWHM is 104.2 keV for ^{238}U and 90.2 keV ^{234}U, respectively, indicating a multilayer system present on the detector. The FWHM difference between the two peaks is caused by low statistics and the ^{234}U tail influencing the ^{238}U peak. Nevertheless, the amount of uranium, present on the detector surface, was irremovable by rinsing the surface with distilled water, indicating a chemical adsorption of uranyl cations on the surface. This observation is supported by the quick and nearly complete desorption after contact of the surface with microliter quantities of concentrated hydrochloric acid (spectrum shown in red in Figure 2.10 left). After rinsing with the acid, the concentration of uranium on the surface drops down to 1.69 ± 0.23 µmol/cm². This is caused by two supplementary effects. First, hydrochloric acid has an acid constant of pKa = -6 where sulfonic acid groups have a pKa value of around 1.4 [19], so the deprotonated sulfonic acid groups are regenerated by the hydrochloric acid under releasing of the uranyl cations. Second, the uranyl cations are complexated by chloride ions under the formation of negatively charged tetrachlorouranate complexes [20]. Either effect results in irreversible desorption of uranium from the surface. Figure 2.12 shows three spectra of a $^{238/234}$U on another detector, modified with ion exchanger groups. All spectra have the same scale and are recorded for 24 h. The left spectrum was acquired while the detector was immersed in solution. The central spectrum was acquired from the same detector taken out of the solution and placed in a vacuum chamber. The spectrum to the right was acquired in a vacuum chamber after rinsing the detector with 20 µl $HCl_{(aq)}$ (see Table 2.3 section "In Solution").

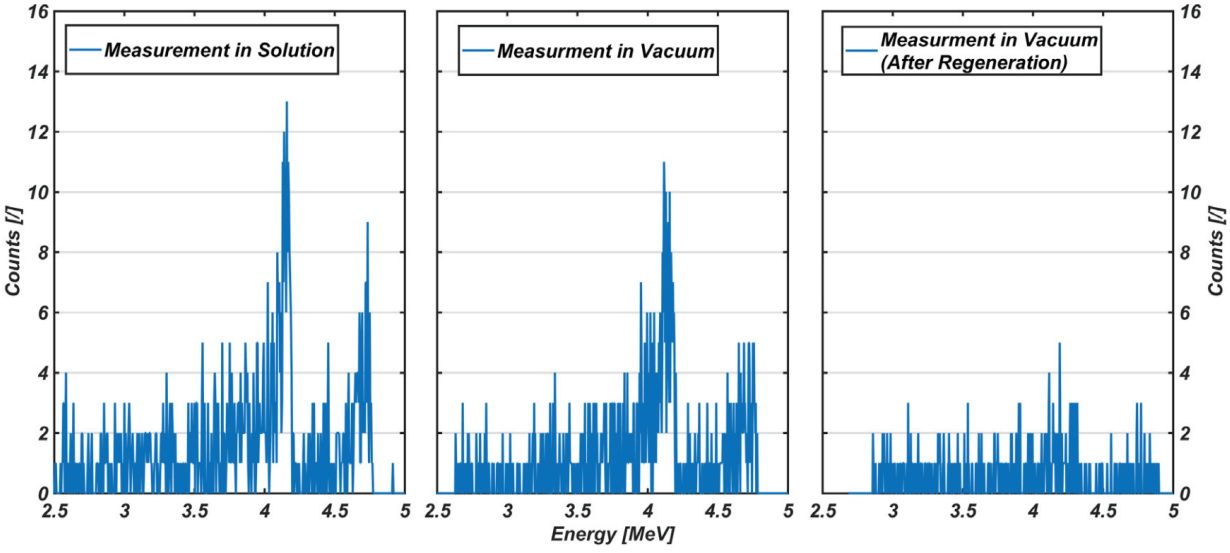

Figure 2.12: $^{238/234}$*U Spectra on the same detector: In Solution (left), in a vacuum chamber (middle) and after regeneration (right).*

Based on the ROI for both radionuclides, the amount of uranium, grafted on the surface, from aqueous solution is 6.69 ± 0.46 µmol/cm². This is the equivalent of 4.0 · 10^{15} ± 0.3 · 10^{15} uranium atoms per square centimeter. This value would be the equivalent of a completely modified surface and is in good agreement with the theoretical assumptions and the literature [12]. During the immersion experiment a small air bubble was caught at the edge of the silicon surface, next to the detector housing, resulting in incomplete contact of surface with solution. While removing the detector from solution the bubble was released and, thereafter, the complete surface was in contact with the solution. Subsequently, the

modified detector surface and the housing was washed with several hundred milliliters of water, to remove potentially physisorbed uranyl acetate solution. After drying the detector in a dry air stream, the detector was mounted in a vacuum chamber to detect the bonded uranium. The molar coverage was calculated to be 8.32 ± 0.51 µmol/cm² which corresponds to a coverage of $5.0 \cdot 10^{15} \pm 0.3 \cdot 10^{15}$ uranium atoms per square centimeter. This slight increase is thought to result from the incomplete contact of the detector while being in solution. However, it also shows, that literally all detected alpha particles in the region of interest originate from uranyl cations extracted by ion exchange from the solution to sulfonic acid groups. Physisorbed uranium should have been flushed away when rinsing the detector with water. The total number of counts, integrated over the whole spectrum, drops from 1052 ± 33 to 877 ± 30. This is in agreement with theoretical considerations and the simulations (Figure 2.8 and Figure 2.9) where the supernatant solution has an influence on the background. After placing 20 µl concentrated hydrochloric acid on the surface, retracting it after 30 seconds and additional rinsing the detector with distilled water to remove remaining acid traces, the sulfonic acid groups were regenerated and the uranium desorbed, resulting in a decrease in coverage to 1.88 ± 0.24 µmol/cm² ($1.3 \cdot 10^{15} \pm 0.1 \cdot 10^{15}$ uranium atoms per square centimeter). This proofs, that the uranyl cations were chemically bonded to the surface and that a detector with chemically modified surface is able to measure alpha particle spectra in solution with high resolution. A long-term stability test of another modified detector in solution was carried out for one week. This allows an estimation of background to peak and peak shape analysis with lower statistic variations.

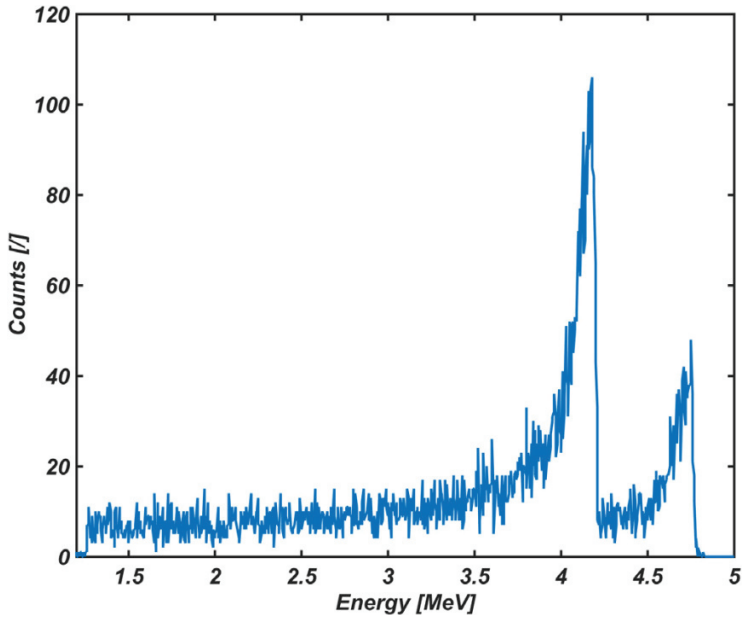

Figure 2.13: *Long-term test - detector seven days in contact with the solution.*

Assuming that all counts in the regions of interest would result from initially grafted uranyl cations, the concentration of active sides on the surface would be 11.92 ± 0.23 µmol/cm². However, due to the contribution of radionuclides, dissolved in aqueous solution and the interplay between the tailing of the ^{234}U Peak into the ^{238}U Peak, the true value should be below this value. In order to estimate the contribution of the solution background to the spectrum, the virtually linear offset at the low energy part of the spectrum was analyzed by separating the lower part into 200 keV regions of interest.

The background in the region between 1177 to 2000 keV is constant, within the statistical limits. Regions

at higher energies are inflicted by contributions of the peak tailings. Based on this background data, the relative background contribution was calculated by dividing a background ROI by the ROI of ^{234}U. Alpha-particles emitted from the solution contribute to the peak area to 25.6 ± 2.3 %.

Table 2.4: *Counts and their uncertainties in regions of interests over all stages of experiments in solution.*

	ROI_3 (BG 1)	ROI_4 (BG 2)	ROI_5 (BG 3)	ROI_6 (BG 4)	ROI_3 (BG 4)
Energy [keV]	1177 - 1379	1384 - 1586	1591 - 1793	1798 - 2000	2005 - 2207
Counts [/]	286 ± 17	271 ± 17	301 ± 18	278 ± 17	335 ± 19

2.6 Conclusion

This paper describes pioneering work in a new way of alpha spectrometry. It demonstrates the feasibility of measuring alpha particles in solution. This is done by combining sample preparation with the detection itself. The key for this combination is the chemical modification of a detector surface with functional groups, which are able to bond radionuclides from solution onto the detector surface, where the alpha particles are detected with almost 2 π geometric efficiency and high resolution enough to allow nuclide identification. The viability of this concept was proven by using the well-known and established simulation codes SRIM and AASI as well as by practical tests with three commercially available alpha detectors, modified with cation exchanger groups. At the current state of this research, the modification shows a high fluctuation of cation exchange capacities on the detector surface and FWHM in the order of 100 keV, indicating an unnecessary thick silane layer on top of the detector. This was acceptable for prototype tests, demonstrating a proof of principal of the concept. In future research, silicon detectors without housing will be used in order to study the silane grafting more precisely. At this point of research, it is only possible to say, that a short contact time of 30 seconds is enough to obtain spectra in sufficient quality to allow nuclide identification and nearly a complete regeneration of the detector. It is well known that ion exchange reactions are “fast” [21] but the time scales depend on the diffusion through the aqueous boundary layer. Uranyl ions have been observed to exchange with a rather low rate compared to ions of similar size and charge [22]. On the other hand, ion exchange reactions on nanoparticles have been reported to take place within milliseconds [23]. Simulations and kinetic measurements will be undertaken to investigate diffusion coefficients and the resulting time scales for ions exchanging with grafted detectors immersed in solutions over a wide concentration range. Additionally, different functional groups will be introduced, in order to extend the selectivity for certain nuclides and fields.

In principle, this new technology is advantageous. Due to the drastically reduced preparation time, no need for expensive chemicals and the absence of complex preparation devices (like an electrodeposition apparatus), this new and fast way of alpha spectrometry can be beneficial for all fields of alpha particle spectrometry, from environmental analysis, over security measurements to studies of the heaviest elements.

2.7 References

[1] M. Schädel, W. Brüchle, E. Jäger, E. Schimpf, J. Kratz, U. Scherer, and H. Zimmermann, "ARCA II - A new apparatus for fast, repetitive HPLC separations," *Radiochim. Acta*, vol. 48, p. 171, 1989.

[2] Y. Nagame, K. Tsukada, M. Asai, A. Toyoshima, K. Akiyama, Y. Ishii, T. Kaneko-Sato, M. Hirata, I. Nishinaka, S. Ichikawa *et al.*, "Chemical studies on rutherfordium (Rf) at JAERI," *Radiochimica Acta*, vol. 93, no. 9-10, pp. 519–526, 2005.

[3] F. Samadani, J. Alstad, T. Bjornstad, L. Stavsetra, and J. P. Omtvedt, "Development of a SISAK extraction system for chemical studies of element 108, hassium," *Radiochimica Acta*, vol. 98, no. 12, pp. 757–764, 2010.

[4] J.-V. Kratz and K. H. Lieser, *Nuclear and Radiochemistry*. Wiley Online Library, 2013.

[5] W. Van Rhijn, D. De Vos, B. Sels, and W. Bossaert, "Sulfonic acid functionalised ordered mesoporous materials as catalysts for condensation and esterification reactions," *Chemical communications*, no. 3, pp. 317–318, 1998.

[6] International Atomic Energy Agency, "Ion exchange technology in the nuclear fuel cycle," 1986.

[7] R. Diamond, K. Street Jr, and G. T. Seaborg, "An ion-exchange study of possible hybridized 5f bonding in the actinides 1," *Journal of the American Chemical Society*, vol. 76, no. 6, pp. 1461–1469, 1954.

[8] J. Ziegler, "Download srim software," 2018.

[9] STUK, "AASI - Program for simulating energy spectra in alpha spectrometry," 2018.

[10] M. Wojdyr, "Fityk: a general-purpose peak fitting program," *Journal of applied crystallography*, vol. 43, no. 5-1, pp. 1126–1128, 2010.

[11] M. Wojdyr, "Fityk - curve fitting and data analysis, http://fityk.nieto.pl/,2016 (accessed 16.02.2018)," 2018.

[12] D. Aswal, S. Lenfant, D. Guerin, J. Yakhmi, and D. Vuillaume, "Self assembled monolayers on silicon for molecular electronics," *Analytica chimica acta*, vol. 568, no. 1-2, pp. 84–108, 2006.

[13] D. Krupp and U. Scherer, "to be published," 2018.

[14] D. K. Aswal, S. Lenfant, D. Guerin, J. V. Yakhmi, and D. Vuillaume, "A Tunnel Current in Self-Assembled Monolayers of 3-Mercaptopropyltrimethoxysilane," *Small*, vol. 1, no. 7, pp. 725–729, 2005.

[15] J. F. Ziegler, M. D. Ziegler, and J. P. Biersack, "SRIM - The stopping and range of ions in matter (2010)," *Nuclear Instruments and Methods in Physics Research Section B: Beam Interactions with Materials and Atoms*, vol. 268, no. 11-12, pp. 1818–1823, 2010.

[16] P. M. Dietrich, C. Streeck, S. Glamsch, C. Ehlert, A. Lippitz, A. Nutsch, N. Kulak, B. Beckhoff, and W. Unger, "Quantification of silane molecules on oxidized silicon: are there options for a traceable and absolute determination?" *Analytical chemistry*, vol. 87, no. 19, pp. 10 117–10 124, 2015.

[17] T. Siiskonen and R. Pöllänen, "Advanced simulation code for alpha spectrometry," *Nuclear Instruments and Methods in Physics Research Section A: Accelerators, Spectrometers, Detectors and Associated Equipment*, vol. 550, no. 1-2, pp. 425–434, 2005.

[18] R. Pöllänen and T. Siiskonen, "High-resolution alpha spectrometry under field conditions - fast identification of alpha particle emitting radionuclides from air samples," *Journal of environmental radioactivity*, vol. 87, no. 3, pp. 279–288, 2006.

[19] I. K. Mbaraka and B. H. Shanks, "Acid strength variation due to spatial location of organosulfonic acid groups on mesoporous silica," *Journal of Catalysis*, vol. 244, no. 1, pp. 78–85, 2006.

[20] J. Ryan, "Anion exchange and non-aqueous studies of the anionic chloro complexes of the hexavalent actinides," *Inorganic Chemistry*, vol. 2, no. 2, pp. 348–358, 1963.

[21] F. C. Nachod and J. Schubert, *Ion exchange technology*. Academic Press, 1956.

[22] F. Mata-perez, F. A. Castro, and J. F. Perez-benito, "Kinetics of exchange reactions in a cation-exchange resin," *Journal of Macromolecular Science: Part A-Chemistry*, vol. 24, no. 2, pp. 155–165, 1987.

[23] E. M. Chan, M. A. Marcus, S. Fakra, M. ElNaggar, R. A. Mathies, and A. P. Alivisatos, "Millisecond kinetics of nanocrystal cation exchange using microfluidic X-ray absorption spectroscopy," *The Journal of Physical Chemistry A*, vol. 111, no. 49, pp. 12 210–12 215, 2007.

Chapter 3

Speeding up liquid-phase heavy element chemistry: development of a vacuum to liquid transfer chamber (VLTC)

D. Krupp [1], Ch. E. Düllmann[2,3,4], L. Lens[1], J. P. Omtvedt[5], A. Yakushev[3] and U.W. Scherer[1]

[1] Institut für Physikalische Chemie und Radiochemie, Hochschule Mannheim - University of Applied Sciences, 68163 Mannheim, Germany
[2] Department of Chemistry - TRIGA site, Johannes Gutenberg University, Fritz-Strassmann-Weg 2, 55128 Mainz, Germany
[3] GSI Helmholtzzentrum für Schwerionenforschung, Planckstr. 1, 64291 Darmstadt, Germany
[4] Helmholtz Institute Mainz, Staudingerweg 18, 55128 Mainz, Germany
[5] University of Oslo, 0315 Oslo, Norway

Accepted in: Nuclear Instruments and Methods in Physics Research Section A (2021)

DOI: https://doi.org/10.1016/j.nima.2021.165486

The following article was submitted as full article to Nuclear Instruments and Methods in Physics Research Section A: Accelerators, Spectrometers, Detectors and Associated Equipment in 2021. The publication deals with a feasibility study to show that it is possible to implant heavy ions from a low pressure region of a physical preseparator directly in a liquid phase. Simulations for this were carried out with the program SRIM. In addition, model experiments were performed with fission fragments of a ^{250,252}Cf source. The residence time in the VLTC was determined with ^{68}Ga tracer solutions. With the help of this system in combination with the chemically modified α detectors, it should be possible in the future to perform experiments with shorter-lived isotopes of the super heavy elements in the aqueous phase than is currently possible.

Own contributions

The system design (including experimental setup, DAQ Software development and simulations) were performed self-directed. The experiments and the corresponding analysis were performed self-directed. The writing of the publication was performed self-directed with input from the co-authors.

Abstract

We present a new system, which is suitable for performing fast liquid phase chemistry experiments and gives access to shorter-lived isotopes of super heavy elements (SHE) than accessible with current techniques. With this novel vacuum to liquid transfer chamber (VLTC), which is mounted behind a physical preseparator, the desired isotopes are transported from the low-pressure side of the recoil separator directly into the liquid phase of a chemical experiment. Simulations on the kinematics of evaporation residues were performed using SRIM, validating the general plausibility of the VLTC concept. Subsequently, the feasibility was demonstrated with ^{250,252}Cf fission fragments, which were collected in dilute nitric acid, separated on an ion exchange column and measured by γ-ray spectroscopy. Finally, tests on the mechanical and chemical stability of the system as well as measurements of the residence time in the liquid phase were performed.

3.1 Introduction

3.1.1 Liquid Phase Heavy Element Chemistry

The liquid phase chemical study of heavy elements of the transactinide (atomic number Z $\geq$ 104) series which are often also referred to as superheavy elements (SHE) has been a challenging research field for many decades [1]. The first reported experiments were performed with rutherfordium (Z = 104) by Zvara et al. in Dubna, Russia in 1966 [2]. Further experiments were performed, e.g., by Silva et al. [3] in Berkeley, USA. There, the relatively long-lived isotope ^{261}Rf ($t_{1/2}$ = 75 ± 7 s) [4] was produced by irradiating ^{248}Cm with 92-MeV ^{18}O ions in the ^{248}Cm(^{18}O,5n)^{261}Rf reaction. The reaction products were collected on a NH_4Cl-covered platinum foil, which was transferred to the chemical system. The half-life was long enough to I) dissolve the NH_4Cl (including the adsorbed Rf), II) perform chromatographic experiments, III) prepare a sample suitable for α spectrometry through evaporation, and IV) measure the resulting α emissions of the samples. In their paper the authors claimed to have observed only 10 % of the totally produced ^{261}Rf activity, due to "[. . .] decay, counting geometry and chemical losses" [3]. Discussing the decay losses, the authors propose potential optimizations to shorten transport times and to implement automated preparation steps. These pioneering experiments marked the starting point of the development of automated liquid phase experimental setups. With devices like "ARCA II" [5] (automated rapid chemistry apparatus), "AIDA" [6] (automated ion-exchange separation apparatus coupled with the detection system for alpha spectroscopy) and the continuous liquid-liquid extraction system "SISAK" [7], even the investigation of the heavier element dubnium Db (Z = 105) [8] was possible. For element 106, seaborgium Sg, liquid phase chemical studies were reported by Schädel et al. [9]. In contrast to the experiments with the longer-lived Rf and Db isotopes, the decay of which was detected in the experiments, the Sg isotope under study [9], which is now believed to have been exclusively ^{265}Sg [10], has a half-life of less than 15 s [11], which was too short for its detection. Accordingly, only its α-decay progenies ^{261}Rf and ^{257}No were detected in these experiments [9]. Till now, Sg is the heaviest element for which liquid phase chemistry data has been reported. Detailed overviews of these types of experiments are given, e.g., by Kratz et al. in [12] and by Nagame et al. in [13].

Each of the mentioned experimental setups is unique and was crucial for obtaining a deeper understanding

of the chemical properties of heavy elements in the liquid phase. Nonetheless, some aspects of the individual setups are comparable, i.e., all these experiments comprise the following six generalized steps:

- Accelerator-based production of the transactinide isotope of interest in fusion-evaporation reactions
- Thermalization of the evaporation residues in high-pressure gas atmosphere and transfer to the chemistry setup via a gas-jet seeded with aerosol particles
- Dissolution of the aerosol particles (with attached evaporation residues) in a liquid phase
- Chemical separation (e.g., ion exchange or liquid-liquid extraction)
- Sample preparation
- Detection of the nuclear decay

The time of each of these steps influences the overall detection yield of a liquid-phase SHE experiment. Optimizing each step individually to be as fast as possible is therefore paramount, but also the interplay of the steps has to be kept in mind to arrive at the highest possible overall yield. For an automated transfer from the gas to the liquid phase, two strategies have been pursued. In systems like in AIDA [6] or ALOHA [14], the aerosol particles were collected on foils and frits, with batch-wise elution. Another possibility is the use of membrane degasser systems [15] where the carrier gas and the SHE-bearing aerosol particles are mixed with a liquid upon entering the chemistry setup. The gas is removed by having the mixture passing a hydrophobic gas-permeable membrane, which retains the aqueous solution inside the setup. Thereafter, this separated liquid phase is transported to the chemical experiment. With both techniques, the batch-wise or continuous elution, not only the desired SHE but also unwanted side products of the nuclear reaction are transported to the chemical apparatus. This causes increased background levels, which complicates the nuclide identification. Improvements with respect to transport time, radionuclidic purity and dissolution efficiency are required in the step of the transfer of the fusion products from the target to a liquid phase. The isolation of the nuclide under study from unwanted background can be achieved by using the approach of physical preseparation [16] [17] [18] , e.g., in the "TransActinide Separator and Chemistry Apparatus" (TASCA) [19] [20]. This approach has been used recently for chemical studies of flerovium (Z = 114) in the gas phase [21]. In this approach, the isotope of interest passes and exits the recoil separator and enters a gas-filled volume installed in the separator's focal plane. The evaporation residues are thermalized in this so-called Recoil Transfer Chamber (RTC) [22], and then transported to the chemistry setup with rapidly flowing gas. For most efficient collection and thermalization of evaporation residues, the RTC should cover the whole image size of the separator and be sufficiently deep for complete thermalization. On the other hand, for the fastest possible transport to the chemistry setup, its volume should be as small as possible. Current setups therefore operate with gas flow rates in the L/min range, which is very difficult to efficiently mix with a liquid flowing at rates of 100 µL/s. The volume ratio is very unfavorable for ensuring efficient transfer from gas to liquid. To fundamentally overcome this problem, we developed a novel vacuum to liquid transfer chamber (VLTC), which is able to provide direct immersion of ions from the preseparator into liquid phase, without the need of stopping the ions in a gas, transporting them with the aid of an aerosol gas-jet to the liquid phase chemistry station, dissolve the particles and remove the gas.

3.2 Materials and Methods

3.2.1 ^{250,252}Cf and ^{68}Ga

The radioisotope ^{68}Ga ($t_{1/2}$ = 67.71 min) is a positron emitter (I_{β^+} = 89.01 %) [23]. It is constantly produced as the decay product of its parent nuclide ^{68}Ge ($t_{1/2}$ = 270.93 d) in secular equilibrium and available from a generator system. The two radioisotopes ^{250}Cf ($t_{1/2}$ = 13.08 a) and ^{252}Cf ($t_{1/2}$ = 2.645 a) are α emitters that also undergo spontaneous fission (SF) ($I_{SF,^{250}Cf}$ = 0.077 %; $I_{SF,^{252}Cf}$ = 3.092 %) [23]. In each fission process two fission fragments with asymmetric mass distribution are released, with two yield maxima (~ 6 %), in the regions between 104 - 110 atomic mass units (amu) and around 139 - 144 amu. Typical recoil energies for products of the light and heavy mass peak are around 105 MeV and 80 MeV, respectively [24].

3.2.2 Chemicals and devices

For residence time measurements, a NaI(Tl) scintillation detector type “51BP51/2M” with an endcap size of 4 cm x 6 cm (13 % efficiency at 351 keV) (Scionix) was used, for high resolution γ-ray spectroscopy a HPGe detector type 6530 (Ortec) (rel. efficiency 60 % at 1332.5 keV). The detectors were powered by a 3106D HV Power Supply from Canberra. The anode signal was amplified with a spectroscopy amplifier model 2022 from Canberra. For energy-resolved spectra, the analog signal was processed in a Multiport II multi channel analyzer (Canberra) in combination with the software package "Genie 2K - gamma acquisition and analysis" (Canberra). In case of residence time measurements, the amplified analog signal was subsequently sampled with its time stamp with a "NI 9239" (National Instruments) data acquisition device, mounted in a "NI cDAQ-9174" chassis. Data acquisition was controlled by a Matlab based script (Version R2020a) in combination with the data acquisition toolbox. Based on the signal processing toolbox the raw data were also processed in Matlab. Data acquisition and processing on a National Instrument / Matlab based interface is described in detail elsewhere [25].

3.2.3 Measurement Setup

For residence time measurements, a NaI(Tl) scintillation detector type “51BP51/2M” with an endcap size of 4 cm x 6 cm (13 % efficiency at 351 keV) (Scionix) was used, for high resolution γ-ray spectroscopy a HPGe detector type 6530 (Ortec) (rel. efficiency 60 % at 1332.5 keV). The detectors were powered by a 3106D HV Power Supply from Canberra. The anode signal was amplified with a spectroscopy amplifier model 2022 from Canberra. For energy-resolved spectra, the analog signal was processed in a Multiport II multi channel analyzer (Canberra) in combination with the software package "Genie 2K - gamma acquisition and analysis" (Canberra). In case of residence time measurements, the amplified analog signal was subsequently sampled with its time stamp with a "NI 9239" (National Instruments) data acquisition device, mounted in a "NI cDAQ-9174" chassis.

Data acquisition was controlled by a Matlab based script (Version R2020a) in combination with the data acquisition toolbox. Based on the signal processing toolbox the raw data were also processed in Matlab. Data acquisition and processing on a National Instrument / Matlab based interface is described in detail elsewhere [25].

3.2.4 Experimental Setup

The vacuum to liquid transfer chamber (VLTC) consists of five parts, which are made from different materials, as shown in figure 3.1. The stainless steel flange (A) is compatible with preseparator setups and can be mounted, e.g., behind the TASCA separator at GSI. The flange center has an entrance window of 1270 mm² (31 mm x 41 mm), which is covered with a metal grid (B) as mechanical foil support. The geometrical transparency of this plate is 80 % [22]. In order to separate the low pressure side from the liquid phase, a metal frame (C), covered with a 6-µm thick Mylar foil (D) is placed on top of the metal grid. The liquid phase chamber (E) was produced from a methacrylate-based polymer resin with a void of 635.5 µl (31 x 41 x 0.5 mm). It is mounted on top of the Mylar foil and linked with a peristaltic pump. In addition, two sealing rings are used: one between the flange (A) and the metal frame (C) and one between the metal frame (C) and the liquid phase chamber (E).

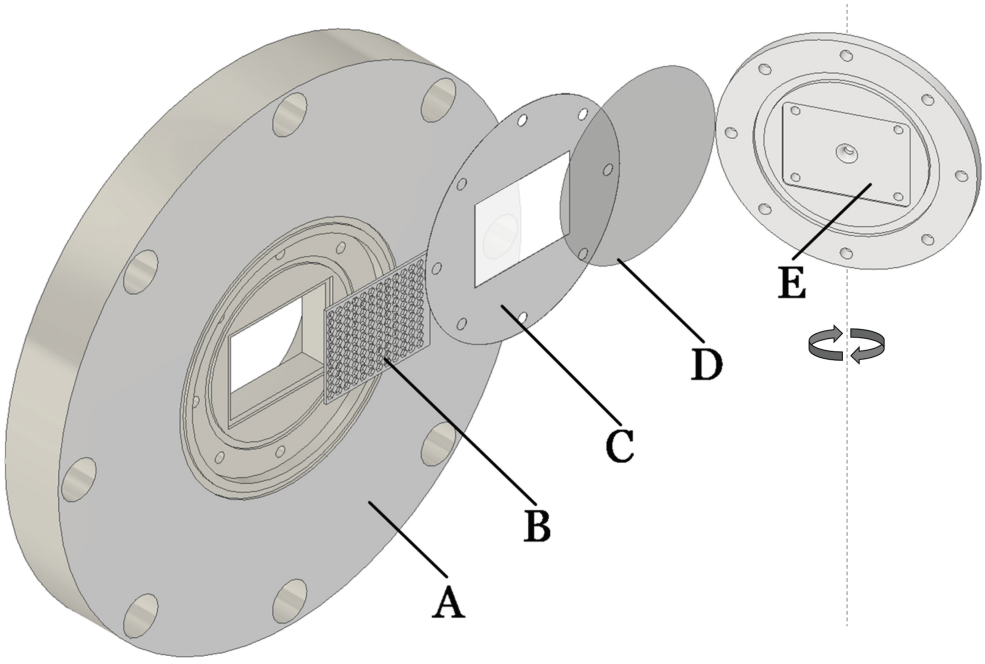

Figure 3.1: *Flange for vacuum to liquid transfer of heavy ions in individual parts from left to right: flange (A), metal grid (B), metal frame (C), Mylar foil (D) and liquid phase chamber (E). The part of the liquid phase has been rotated by 90 ° in the illustration to represent the flow chamber.*

The VLTC was used in two configurations. In the first configuration (case 1), systematic experiments were performed to investigate the conditions under which the Mylar foil can withstand the mechanical and chemical stress, which would occur during a heavy element chemistry experiment. To determine the mean residence time (MRT) of radionuclides in the liquid phase chamber, the assembled system (see figure 3.1) was arranged in a vertical position. The mobile phase was transported through the liquid phase chamber with a peristaltic pump. The backside of the flange was connected to a volume evacuated with a vacuum

pump and equipped with a digital pressure gauge. A lead-collimated scintillation detector was placed behind the flange in order to detect the ^{68}Ga decay in the liquid phase chamber. This experimental setup is shown in figure 3.2.

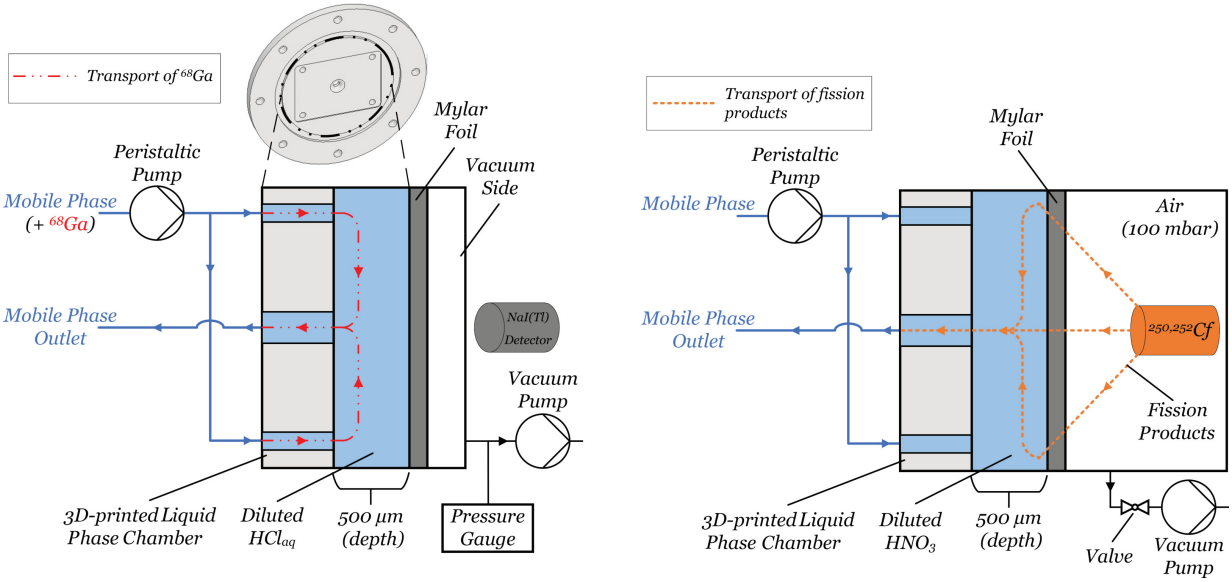

Figure 3.2: *Experimental setup for systematic studies of the residence time*

For Mylar foil stability tests, the vacuum side was evacuated to 100 – 75 mbar. The mobile phase (DI water or 0.2 M HCl) was circulated through the system for up to 24 hours. In case of residence time experiments, the Matlab/ National Instruments data acquisition was started before the ^{68}Ga sample was transported with DI water through the setup. The flow rate of the peristaltic pump was adjusted to 50 – 100 mL/min. A defined amount of ^{68}Ga (~ 10 MBq) was loaded to the inlet line of the peristaltic pump and transported through the liquid phase chamber as shown in the top panel in figure 3.2. The mobile phase, exiting the chamber, was transferred to a lead-shielded waste vessel. This measurement constitutes a reverse situation of an on-line experiment, in which the radionuclides will enter through the vacuum window and, after immersion in the liquid, will be transported out with the continuously flowing liquid and then enter the chemistry apparatus with subsequent detection. Proof of principal experiments with the ^{250,252}Cf source were performed in a similar setup (case 2), as shown in the bottom panel in figure 3.2. The VLTC was mounted on a stainless steel tube. Instead of the scintillation detector of case 1, the fission fragment source was placed at a distance of 9 mm from the Mylar foil in the tube. At the start of the experiments, the tube was evacuated to 100 mbar. After reaching this pressure, the valve between vacuum pump and steel tube was closed, so the only potential gas entrance into the steel tube was from the liquid phase chamber of the VLTC. Subsequently the liquid phase chamber was filled with 0.01 M nitric acid as stationary media. Afterwards, fission products were collected for 14 h and collected in a 10 mL sample vial. The solution containing the fission fragments was transferred from the liquid phase chamber by a peristaltic pump into a sample vial. The liquid phase chamber was additionally flushed with fresh 0.01 M nitric acid until the sample vial was filled. Afterwards the filled sample vial was measured with a HPGe detector. Subsequently, a new batch of fission products was collected for 14 h. This second batch was passed through a glass column filled with 2 mL Dowex 50Wx8 cation exchange resin. In total, 30 mL solution were passed through the column within 15 min. Afterwards, the cation exchange column was removed from the pumping system and measured with a HPGe detector.

3.3 Simulation

3.3.1 Fission Fragments

The stopping power of the different media for Cf fission fragments was calculated in SRIM [26] [27]. The candidates for range calculations were chosen based on an extended fission product study [28] [29]. In these studies, the authors list fission yields for fission products in a mass range from ^{78}As to ^{169}Er. The fission products with the highest cumulative fission yield, their individual half-lives and the most prominent γ lines are listed in table 3.1.

Table 3.1: $^{250/252}$*Cf cumulative fission yields [28] [29]*

Fission Product	$t_{1/2}$		γ-Ray Energy [keV]	Intensity [%]	Fission Yield ^{250}Cf [%]	Fission Yield ^{252}Cf [%]
^{105}Ru	4.44	h	724.30	47.3	6.69 ± 0.34	5.53 ± 0.55
^{106}Ru	371.80	d	no γ	-	6.68 ± 0.34	5.57 ± 0.58
^{109}Pd	13.59	h	88.03	3.7	6.37 ± 0.64	5.60 ± 0.56
^{111}Ag	7.45	d	342.13	6.7	4.97 ± 0.25	5.04 ± 0.25
^{139}Ba	82.93	min	165.86	23.7	6.23 ± 0.31	5.75 ± 0.55
^{140}Ba	12.75	d	537.26	24.4	5.17 ± 0.26	5.50 ± 0.28
^{141}Ce	32.51	d	145.44	48.4	5.87 ± 0.29	6.08 ± 0.61
^{143}Ce	33.04	h	293.27	42.8	4.66 ± 0.23	5.66 ± 0.28

For the corresponding ion range calculations of the light mass peak, ^{105}Ru was chosen as promising candidate to be observed in subsequent experiments. It is a nuclide with a high cumulative fission yield, a relatively short half-life of 4.44 h and a high-intensity γ line at 724.30 keV. For the same reasons, ^{139}Ba was chosen as a typical radionuclide of the heavy mass peak. Data for Q-value calculations were obtained from the Brookhaven National Nuclear Data Center (NNDC) [23]. Based on the work of Göök et al. [30] the average prompt neutron multiplicity for fission fragments with mass numbers of 105 – 110 amu and 139 - 144 amu is 1.5 each. The average kinetic energy of the neutrons was chosen as 2.348 MeV, based on the work of Meadows [31]. The kinetic energy of the fission products was calculated according to [24].

The simulation model was based on the intended experimental setup. After spontaneous fission of the ^{252}Cf, the fission fragments travel with their kinetic energy through 9 mm of 100 mbar air (density ρ = 0.1188 kg/m³). Subsequently, the fragments penetrate the 6.0 ± 0.2 µm thick Mylar foil (ρ = 1397 kg/m³) and are then stopped in a 500 µm thick water body (ρ = 998 kg/m³). The individual stopping power data points for the individual media were interpolated in the Scientific Data Analysis and Visualization program (SciDAVis) [19] Version 1.23 in order to calculate the kinetic energy of the fragments at the boundary between two media. As the exact thickness of the Cf-source is unknown, the stopping power of the fission products was calculated for Cf fission products ejected from the surface of the source, i.e., self-absorption was not taken into account.

3.3.2 Superheavy elements (SHE)

The SRIM simulation was performed for a scenario, where the VLTC is attached to the end of TASCA. Flerovium $^{289}_{114}$Fl ($t_{1/2} = 1.9^{+0.7}_{-0.4} s$ [32]) was chosen as example for SHEs, produced in the ^{244}Pu(^{48}Ca, 3n) reaction. Experimental data were taken from [33]. A 240.6 MeV ^{48}Ca beam passes through a 2.3 ± 0.1 µm thick Ti foil and enters a $^{244}PuO_2$ target (0.80 ± 0.01 mg/cm² ^{244}Pu). ^{289}Fl is formed in the $^{244}PuO_2$ target, where the kinetic energy of the Fl is calculated according to the equation:

$$E_{kin,Fl} = \frac{m_{Ca}}{m_{Ca} + m_{Pu}} \cdot E_{Ca} \tag{3.1}$$

The produced Fl-ions leave the target with their recoil energy. Subsequently the ions pass through TASCA (3.5 m at a He pressure of 0.8 mbar), penetrate the Mylar foil (3.3 ± 0.1 μm or 6.0 ± 0.2 μm) and are stopped in the water-filled liquid phase chamber. Since SRIM can only directly calculate the range of ions up to element 92 (uranium), the range of Fl in these materials had to be extrapolated. Therefore, for all materials through which Fl would pass, the ranges were calculated for a nuclide ^{289}Z in the range of Z = 20 - 92 (calcium to uranium). In order to be able to conservatively estimate the applicability of the VLTC system in SHE experiments by the aid of SRIM, these simulations were calculated for an average case where the materials have the mean thickness, as described [33], with Fl formed in the center of the target (Case II). In order to estimate the energy spread around the average value (Figure 3.3, center), additionally, two extreme cases, from the point of view of the overall Fl transport range were simulated. Case I: Fl is formed in the last PuO_2 target layer and is transported through the materials with their lowest given thickness i.e., mean value minus one standard deviation (Figure 3.3 top). Case III: Fl is formed in the first PuO_2 target layer and is transported through the materials with their highest given thickness i.e., mean value plus one standard deviation (Figure 3.3, bottom) (Case III). In these two cases the Fl nuclei have either maximum or minimum recoil energy. In order to estimate the stopping power of the PuO_2 target, the ion transport calculations were carried out for targets $^{244}_{Z}XO_2$ with Z = 88 - 92 and a fixed density of 11.5 g/cm^3 and extrapolated to Pu (Z = 94). The corresponding model for Fl range estimation is shown in figure 3.3.

For each ^{289}Z element, the kinetic energy at the end of a material was used as the starting value for the next material. To approximate the kinetic energy of a ^{289}Fl-ion, the data for Z = 20 - 92 were linearly fitted. From the fit, values for Z = 114 were extrapolated along with 1 σ prediction intervals. The residual kinetic energy of ^{289}Fl after passing the Mylar foil is completely dissipated in the water body. The same approach was performed for a setup with a Mylar foil of 6.0 ± 0.2 μm thickness (d_{Mylar} case I: 5.8 μm, case II: 6.0 μm and case III: 6.2 μm).

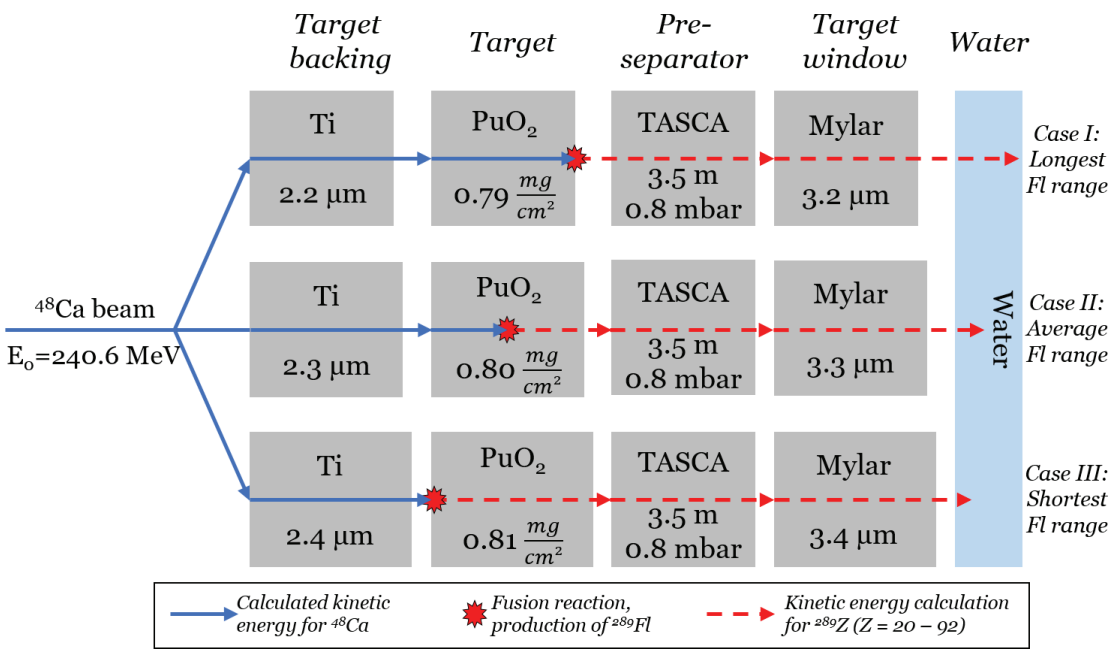

Figure 3.3: *SRIM simulation for the range of a SHE (^{289}Fl) in a TASCA - VLTC experiment, based on experimental data [33]. For Fl range estimations, three cases were considered. Case I) All materials were used with their lowest thickness and the ^{48}Ca undergoes the fusion reaction at the end of the PuO_2 target. Case II) All materials were used with their average thickness and the ^{48}Ca undergoes the fusion reaction in the middle of the PuO_2 target. Case III) All materials were used with their highest thickness and the ^{48}Ca undergoes the fusion reaction at the entrance of the PuO_2 target.*

3.4 Results and Discussion

3.4.1 Foil stability tests

In case of an accelerator-based experiment, an undetected foil rupture would lead to a situation, where the liquid pump pushes the aqueous phase into the low pressure or vacuum region of the preseparator. These experimental systems are typically used at pressures of at most a few mbar, which would therefore suck out all the liquid from the VLTC into the separator very rapidly. Depending on the liquid, this could result in a severe damage of an essential and hard to replace part of the separator setup. Therefore the first aspect of the systematical studies was the demonstration of a potential control value for an interlock system in a real experiment. For this purpose, the setup as described in figure 3.2 was operated with a constantly running vacuum pump, at 80 mbar on the gas side and with deionized water at a flow rate of 100 mL/min on the liquid-phase side. Close to the central liquid outlet, an additional hole with a diameter of 1 mm was drilled and sealed with Teflon tape. The pressure logging on the vacuum side pressure was started and then a needle was pierced through the Teflon tape that covered the hole and the Mylar foil. The pressure on the vacuum side showed a strong increase from the operating pressure of 80 mbar up to atmospheric pressure within 1 s, with a leakage rate of 1.17 $\frac{Pa \cdot m^3}{s}$, indicating a fast pressure response. For fission fragment experiments, the vacuum side was evacuated to 100 mbar. Afterwards, the gas side valve was closed and all experiments were performed without additional evacuation for one week. During this experiments no leakage above $1.52 \cdot 10^{-6}$ $\frac{Pa \cdot m^3}{s}$ was detected. Mechanically, the foil did not seem to be degraded over time by the contact with the dilute nitric acid during the experiments. To ensure that even a thinner Mylar foil

would meet the requirements of a VLTC-based experiment, a separate experiment was performed, in which a 3.3 µm foil was installed into the VLTC system. The vacuum side was pumped down to 0.1 mbar. The liquid phase side was filled with 0.01 M HNO_3. After one week, no leakage rate above $1.26 \cdot 10^{-7}$ $\frac{Pa \cdot m^3}{s}$ was observed, indicating that the thinner film can also be used for the VLTC. This observation is consistent with numerous experiments already performed using an RTC behind TASCA [21] [33] where Mylar films with thicknesses of 3.3 µm or less were stable for months in an experimental setup with pressures around 0.8 mbar He on one side and 900 - 1000 mbar on the other side.

3.4.2 Residence time in the liquid phase chamber

For the determination of the residence time in the liquid phase chamber, ^{68}Ga was loaded in 100 µL volume in front of the liquid phase chamber. The activity was injected into in the liquid phase chamber as a plug flow with rates of 50 mL/min and 100 mL/min. The ^{68}Ga activity was transported by a HCl solution and stored in a lead-shielded waste vial. The ^{68}Ga decay in the liquid phase chamber was measured with a NaI(Tl) detector as described in [25]. The experiments at both flow rates were performed three times. The mean values of the residence time, with their corresponding standard deviations are shown in figure 3.4, where the ^{68}Ga activity in the chamber is shown as a function of time. The count rates were normalized to the maximal detected count rate in each experiment.

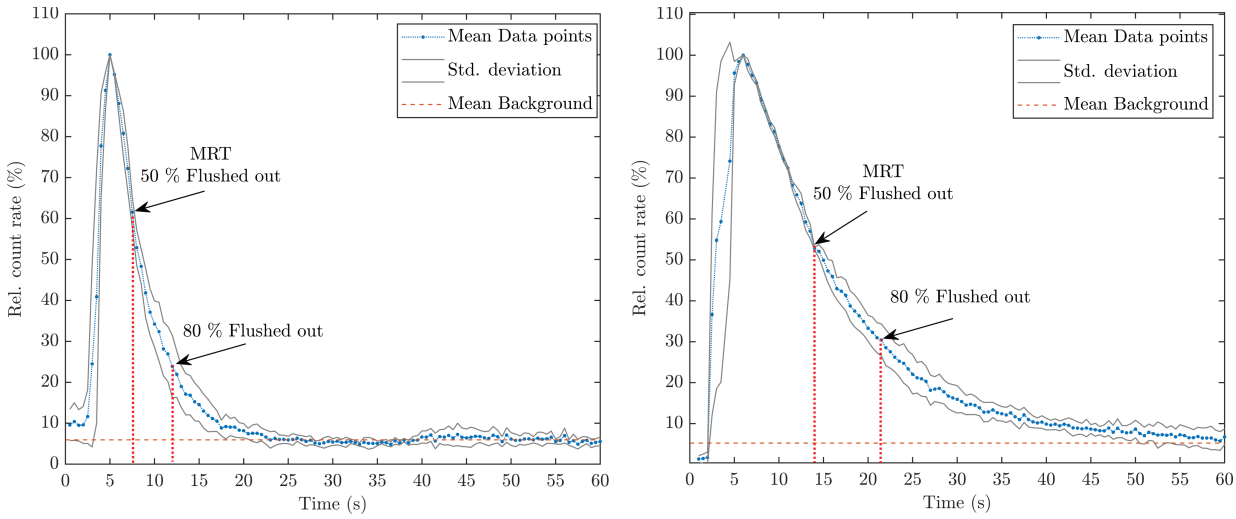

Figure 3.4: *Residence time of ^{68}Ga with mobile phase flow rates of 100 mL/min (left) and 50 mL/min (right). The data represent the mean count rates of three experiments with their corresponding standard deviations.The count rates of the individual experiments were normalized to the maximum detected count rate.*

The time to flush out 50 % (mean residence time, MRT), and 80 % of the ^{68}Ga activity from the liquid phase chamber were determined by a Matlab-based calculation of the total net area under the elution curve and subsequently the time, when 50 %, and 80 % of the total net area were reached. In order to obtain net count rates, the continuous background after 60 s of the experiments was used to calculate the mean background, which was then subtracted. Based on this approach, 50 % of the activity were flushed out within 7.7 s ± 1.0 s, and 80 % after 12.0 s ± 2.5 s at a flow rate of 100 mL/min. For a lower flow rate of 50 mL/min, 50 % were flushed out within 14.7 s ± 1.5 s, and 80 % within 21.5 s ± 3.0 s. When going from

100 mL/min to 50 mL/min the times nearly doubled, which indicates a consistency in the experimental setup. However, these MRT values were determined for a non-optimized liquid phase chamber geometry. In addition, the way the activity enters and exits the chamber does not represent the typical travel path in a fission-fragment or accelerator-based experiment: for tracer experiments with ^{68}Ga, the solution enters the chamber frontally, is distributed into an area extending to the corners of the chamber volume and leaves it again through the center. This represents the longest possible way a radionuclide would travel in this setup during a real experiment. In an accelerator-based experiment, the ion enters the chamber centrally through the Mylar foil with a small spatial spread. Therefore, the values determined here represent a conservative approximation of the residence time, which would be expected in a real experiment. However, at a flow rate of 100 mL/min, the MRT of the non-optimized liquid phase chamber is 7.7 s ± 1.0 s, nearly half as long as, e.g., the mean lifetime of ^{269}Hs ($\tau = 14.0^{+1.4}_{-0.5} s$) [23] or ^{266}Bh ($\tau = 14.4^{+3.8}_{-2.5} s$) [34] which would allow continuous flow chemistry with a fast chemical apparatus.

3.4.3 Fission Fragment Experiment

Based on the SRIM simulation results (see figure 3.7), an experimental setup was realized, in which the VLTC was placed in front of a ^{250,252}Cf source. The liquid phase chamber was filled with 0.01 M nitric acid and the gas side was evacuated to 100 mbar. As shown in figure 3.5, several γ lines above background were detected within 6 h of counting time. However, due to the fission source being relatively weak and the collection time of 12 h, only fragments with half-lives from minutes to several hours were observed. Besides, not all fission products with high fission yield and short half-life have highly intense γ lines, which could be detected with the HPGe detector. Nonetheless, several fission products were collected during the experiment and are highlighted with corresponding half-lives and γ lines in figure 3.5. These accumulated nuclides originate from both the heavy and light mass peak of the fission yield distributions of ^{250}Cf and ^{252}Cf.

The most prominent γ lines in figure 3.5 were used to estimate the yield of the collected fission products over 12 h, eluted with 10 mL solution. In order to calculate the fission yield of the mixed ^{250,252}Cf - source, the cumulative fission yields of Flynn et al. for ^{252}Cf [28] and ^{250}Cf [29] were used. For decay corrections and the state of the secular equilibrium, the half-lives of the nuclides and the gamma emission intensity were taken from the nuclear data section of the ENSDF compilation [23]. The HPGe detection efficiencies for the 10 mL sample geometry in a energy-range from 100 to 2000 keV were calculated with the ISOCS/LABSOCS module of Genie 2K [35]. Based on the HPGe measurements, the collection yields for the individual fission products were used to calculate a weighted mean value, where the uncertainty of the individual yields were used as weighting factors and are shown in table 3.2.

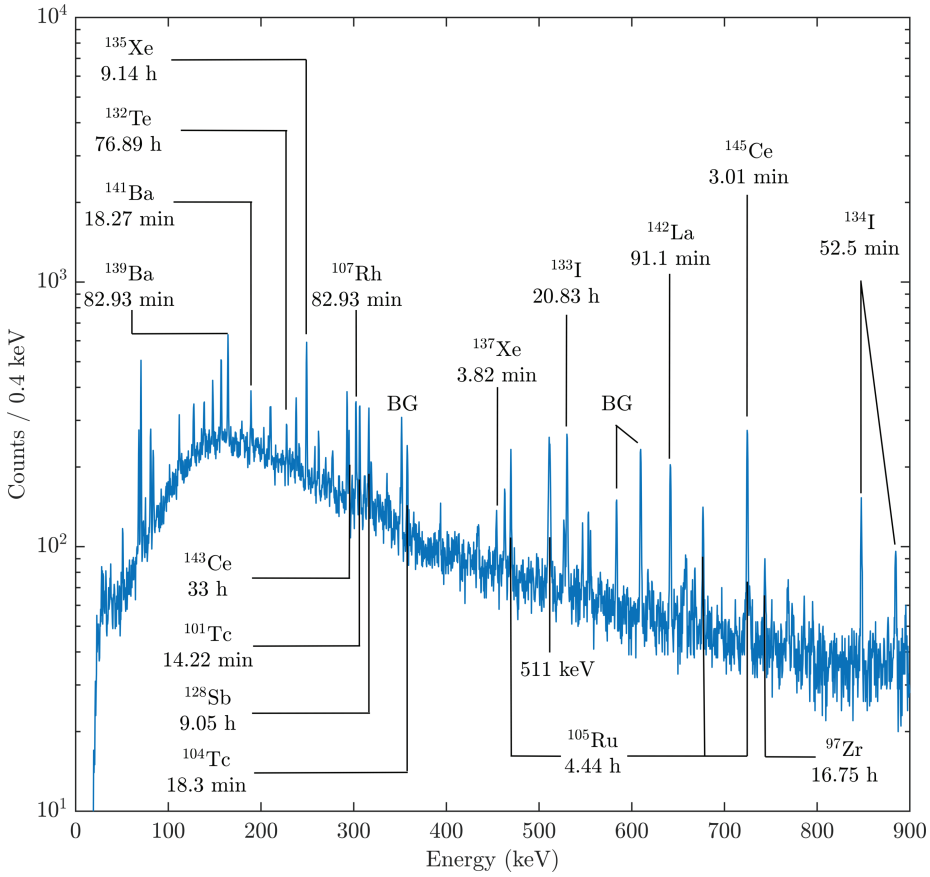

Figure 3.5: *Gamma spectrum of ^{250,252}Cf fission products, collected over 12 h with the VLTC, eluted in 10 mL and measured for 4 h. Lines originating from background radionuclides are labeled with BG.*

Table 3.2: *Collection yield of ^{250,252}Cf fission products, eluted in 10 mL 0.01 HNO_3*

Fission Product	Collected Yield [%]
^{97}Zr	41 ± 12
^{105}Ru	51 ± 16
^{132}Te	34 ± 9
^{139}Ba	35 ± 9
^{143}Ce	40 ± 7
Weighted mean	41 ± 9

As shown in the residence time experiments, 12.5 mL of solution are required to flush out 50 % of the activity, present in the liquid phase chamber. Based on these flush-out calculations, the 10 mL samples represent 40 % of the total activity, which was collected over 12 h by the VLTC.

Subsequently, a demonstration for a potential accelerator-based experiment was realized: a glass column filled with DOWEX 50Wx8 cation exchange resin was placed after the VLTC liquid phase outlet. The 0.01 M nitric acid was circulated through the setup for 1 h. Afterwards, the column was removed and placed in front of the HPGe detector and measured for 900 s. The result is shown in figure 7. The measurement of the ion exchange column was compared with a sample, where the fission products were collected for 1 h

in the liquid phase chamber and eluted in 10 mL 0.01 M HNO_3. The 10 mL sample was also measured for 900 s. The result is shown in figure 3.6. In comparison to the reference sample without chemical separation, several nuclides were not detected on the cation exchange column: ^{135}Xe, a noble gas, passing the column without retention. ^{133,134}I as iodide and ^{104}Tc, forming pertechnetate ions $[TcO_4]^-$, do not react with the cation exchange resin neither. In dilute HNO_3, ^{105}Ru forms anionic oxo complexes which do not interact with a cation exchange group [36] [37]. In contrast, ^{139}Ba as alkaline earth metal is bound to the cation exchange resin. In dilute nitric acid, cerium and lanthanum ions are also strongly bound to the ion exchange resin [38]. This proof of concept experiment demonstrated the feasibility of a transport system for radionuclides with high recoil energies from a low pressure region into a liquid phase with subsequent detection of the collected nuclides.

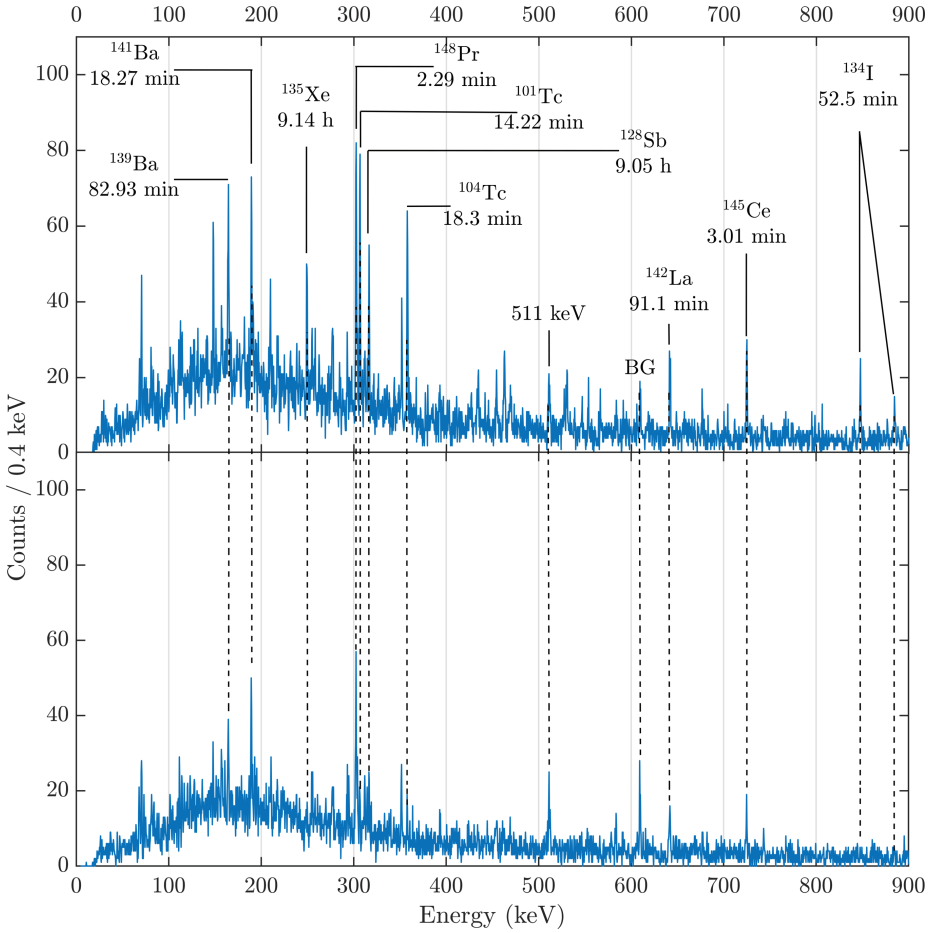

Figure 3.6: *Gamma spectrum as shown in figure 3.5, but measured for 900 s: fission product sample, collected in 10 mL 0.01 M Nitric acid for 1 h (top) and a on cation exchange column, loaded with fission products for 1 h (bottom). Only cationic species are observed in the lower spectrum.*

3.4.4 Simulation of fission fragments transmission

The result of the SRIM calculations is shown in figure 3.7. The calculated initial kinetic energy for the light-mass peak fragments (LMF) ^{105}Ru was 107.19 MeV. For the heavy-mass peak fragments (HMF) ^{139}Ba, this was 84.78 MeV. These values are in good agreement with the generalized literature values [24]. The fission fragments travel with their kinetic energy from the Cf-source surface through 9 mm of air at

a pressure of 100 mbar. Via the interaction with the low pressure gas the LMF lose 5.5% of their kinetic energy, and the HMF 6.5%. The Mylar foil is the medium with the highest density in this setup. Within the 6 µm of path length, the fission fragments lose around 50 % of their remaining kinetic energy. After traveling through the Mylar foil, the fission fragments enter the water body. The liquid phase chamber depth of 500 µm is ~30 times the maximum range of the 1simulated fragments: the ^{105}Ru had a maximum range of 16.5 µm ± 0.2 µm in water, and the heavier fragment ^{139}Ba one of 14.6 µm ± 0.2 µm. The uncertainty of the range derives from the variations of the foil thickness.

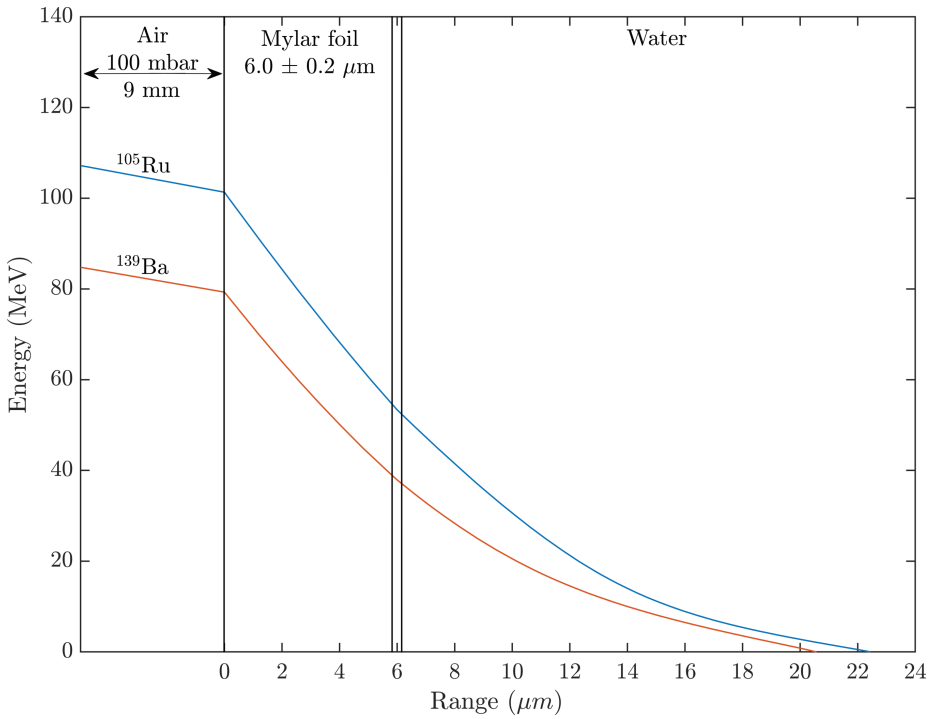

Figure 3.7: *SRIM results for the ion range of ^{105}Ru and ^{139}Ba as examples of typical ^{252}Cf fission fragments. The fission fragments travel through different media: 9 mm air at 100 mbar, 6.0 ± 0.2 µm Mylar foil, where the uncertainty is indicated as a double line in the graph, and a water body. The 9 mm air are indicated for better readability of the graph.*

3.4.5 Simulation of superheavy element transmission

In order to assess whether the VLTC could be used for SHE experiments SRIM calculations were performed for ^{289}Fl. These simulations were based on parameters from an recent experiment conducted at the TASCA pre separator [33]. Since SRIM only calculates ranges in materials for elements up to Z = 92, range calculations for transuranium elements were extrapolated, as described in figure 3.3. A similar extrapolation approach was already performed in [39]. If Fl penetrates the Mylar foil, it will be stopped in a few µm of the water layer. Therefore, the decisive result of this simulation is whether Fl is stopped in the Mylar foil or is able to penetrate this and passes into the water layer. Cases 1 and 3 were used to estimate the distribution of the kinetic energy of the Fl after passing through the Mylar foil. The results were expressed as average kinetic energy (case 2) plus highest kinetic energy + 1 σ of the prediction interval (case 1) minus lowest kinetic energy - 1 σ of the prediction interval (case 3). The stopping power calculations for ^{48}Ca for case I are shown in figure 3.8, left. In case I, it was assumed that Fl is formed at

the end of the target, therefore the extrapolation was only performed for ^{48}Ca. The ion transport through TASCA and the Mylar window was calculated for the ^{289}Z ions (Z = 20 - 92). The error bar represents the ± 1 σ prediction interval. In case III, Fl is formed at the beginning of the target. Therefore, the stopping power calculations were performed for a $^{244}_{Z_1}XO_2$ (Z_1 = 88 - 92) target with 11.5 g/cm^3 density and $^{289}Z_2$ ions (Z_2 = 20 - 92), yielding a three dimensional plot (figure 3.8, right). The results for a setup with 3.3 µm Mylar foil are shown in figure 3.9. For a better overview, only the results for the upper and lower limits of the simulation are shown. The illustrations describing TASCA in figure 3.3 could not be displayed on the same energy scale, as one of the two cases shown would no longer have been visible.

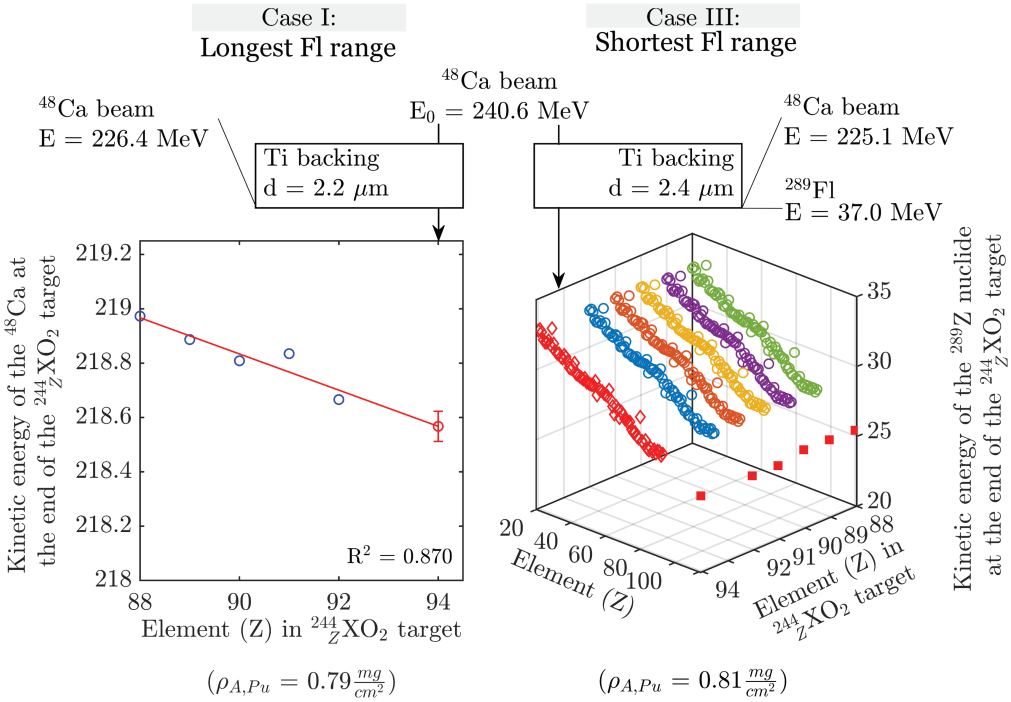

Figure 3.8: *SRIM based estimation of the residual kinetic energy of a ^{48}Ca ion after passing through a PuO_2 target (left), extrapolated from calculations with a $^{244}_{Z_1}XO_2$ (Z_1 = 88 - 92) target ± the 1 σ prediction interval. In case of a Fl formation at the begin of the target (case III), the residual Fl kinetic energy was extrapolated for the $^{244}_{Z_1}XO_2$ (Z_1 = 88 - 92) target and the $^{289}Z_2$ (Z_2 = 20 - 92) (right). The prediction interval is not shown for better readability.*

As can be seen in figure 3.9, even in the most unfavorable case, the Fl has a residual kinetic energy of more than 8 MeV after passing the Mylar 3.3 µm foil. Taking into account the other two cases also the kinetic energy of the ^{289}Fl would be 13.0 $^{+4.9}_{-5.0}$ MeV. This result is consistent with pre-separator experiments where Fl could be measured behind 3.0 µm and 3.3 µm Mylar foils [21] [39]. In the simulations of the fission products, the range of ^{139}Ba was estimated to be 14.6 ± 0.2 µm in water at a kinetic energy of 40 MeV. Fl with less than half of the kinetic energy and twice the mass will therefore be stopped within a much shorter range. In case of a SHE experiment, a liquid phase chamber depth of 500 µm, as used in this setup here, would be oversized. However, the minimal depth of a liquid phase chamber depends on the manufacturing method. In case of laser-based 3D printers minimal depths on the order of 50 µm can be achieved [40], which would reduce the volume of such a chamber by a factor of 10. However, from a practical point of view, it would not be very beneficial to make the liquid phase transfer chamber so small that it just matches the range of SHE. On the one hand, current commercial 3D printers are not capable of reliably printing

these structures with depths of approx. 10 µm, and on the other hand, the liquid phase back pressure in the chamber would increase considerably, which, together with other undesirable effects such as by capillary forces, could hinder the efficient transport of the SHE.

Recent studies have also shown that Fl and Moscovium (Mc, Z = 115) can be transferred into a transfer chamber in a setup with 6.0 µm Mylar foil [41]. This case was also mapped in the simulations. The experimental setup was not changed except for the thickness of the Mylar foil. Figure 3.10 shows the result of a simulation with average material thicknesses.

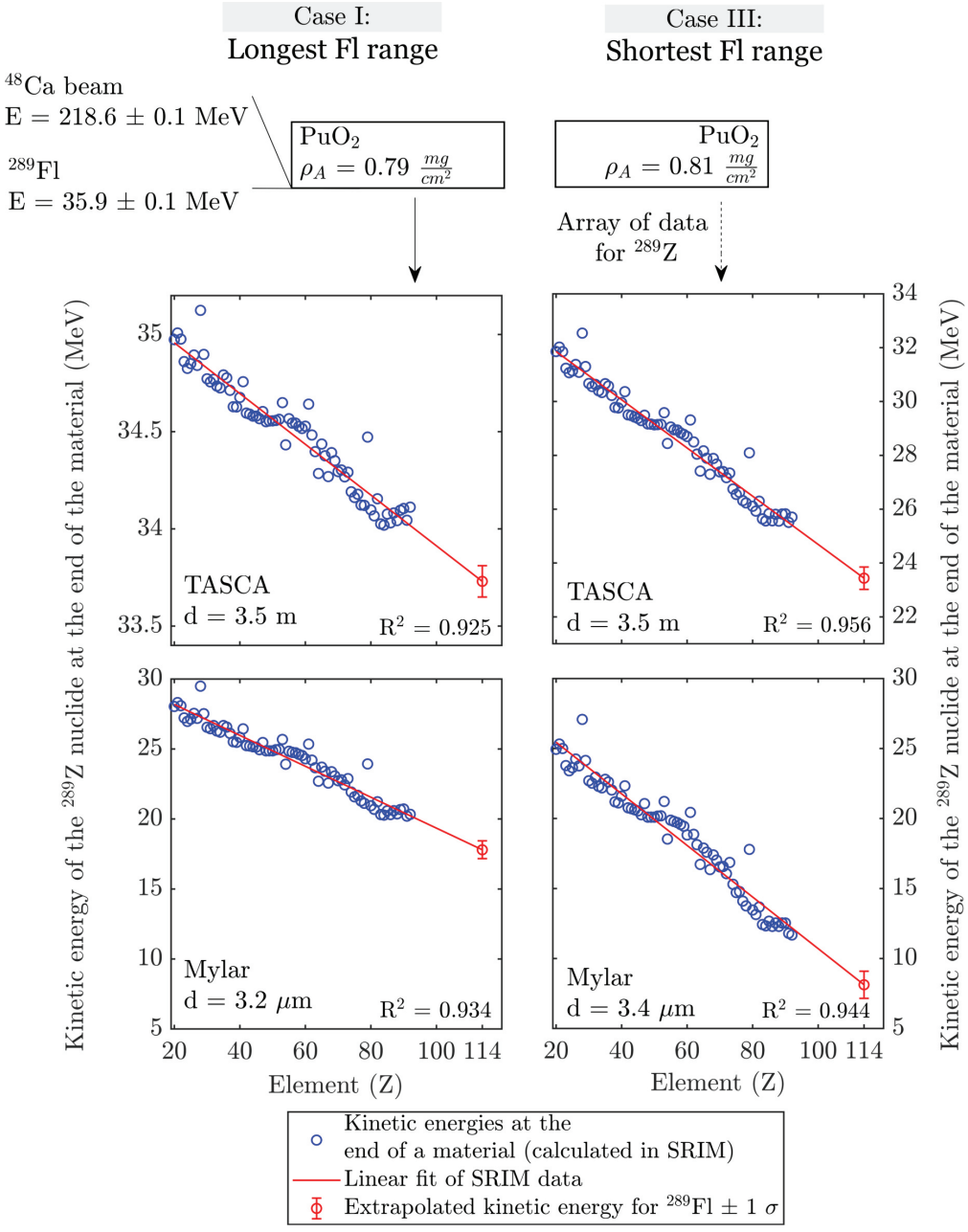

Figure 3.9: *SRIM simulation for the range of a SHE (^{289}Fl) in a TASCA-based VLTC experiment using a 3.3 µm ± 0.1 µm thick Mylar window, based of experimental data in [33]. For Fl range estimations, two cases were constructed. Case I) All materials were used with their lowest thickness and the ^{48}Ca undergoes the fusion reaction at the end of the PuO_2 target. Case II) All materials were used with their highest thickness and the ^{48}Ca undergoes the fusion reaction at the begin of the PuO_2 target. "E" denotes the kinetic energy of the respective particle.*

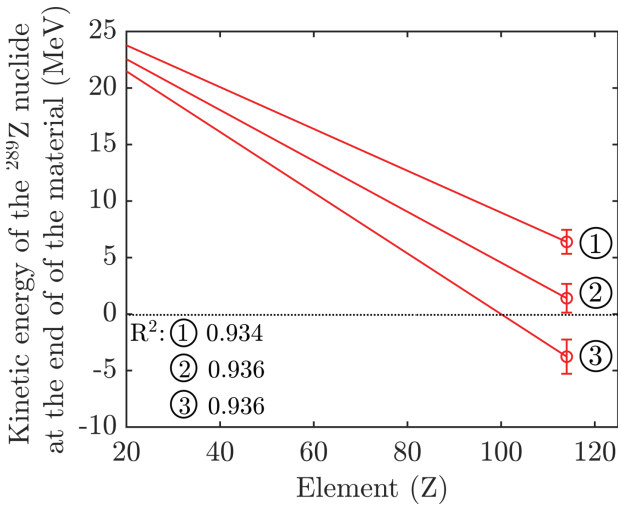

Figure 3.10: *Same as figure 3.8 but with average material thicknesses and 6 ± 0.2 µm Mylar foil. For better readability, only the linear data fits of SRIM data (including the regression parameters) are shown.* ①*: All materials have the minimum thickness, Fl is formed in the last PuO_2 layer and the mylar film has a thickness of 5.8 µm.* ②*: average material thicknesses, Fl forms in the target center and the Mylar foil is 6 µm thick.* ③*: maximum material thickness, Fl is formed in the first PuO_2 layer and the Mylar foil is 6.2 µm thick.*

As can be seen from the figure 3.10, ^{289}Fl would have enough kinetic energy on average to pass through a 6.0 µm Mylar foil. If one also considers the cases with the longest and the shortest Fl range (see figure 3.10), the energy after the Mylar foil as suggested by SRIM would be $1.4\ ^{+6.1}_{-6.7}$ MeV. Here, the negative kinetic energy indicates that the Fl would be absorbed in the Mylar foil in this case. As can be seen from this result, 6.0 ± 0.2 µm thick foil would represent the borderline case for such applications, since according to the SRIM simulations, a small fraction of the Fl atoms would be stopped in the Mylar foil.

The general applicability of the VLTC depends on the recoil energy of the radionuclide in question. A recent overview on the production of SHE, with the nuclear reaction, cross section and beam energy is given in [1]. Based on this overview, the recoil energies of SHEs with half-lives > 0.1 s in the range of atomic masses between 256 and 289 were calculated. Since the individual kinetic energy of an SHE after passing through a pre-separator and a Mylar foil depends very much on the experimental conditions, like the type and thickness of the target, only the recoil energies (according to equation 3.1) of the different SHEs are shown in figure 3.11.

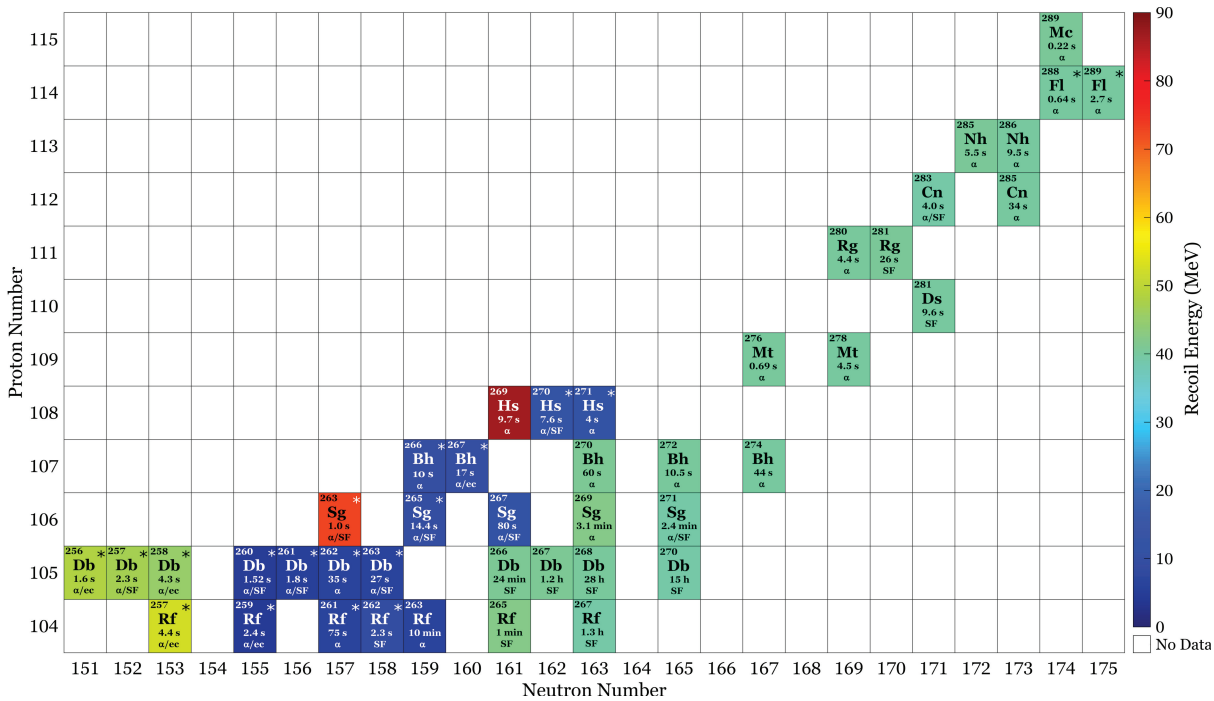

Figure 3.11: *Recoil energies (MeV) of isotopes of SHE from ^{257}Rf to ^{289}Mc with corresponding half-lives and most intense decay modes. For better readability, only known nuclides with a half-life above 0.1 s are mentioned in this chart. Nuclides highlighted with "*" are directly produced. The other nuclides are available as decay products of their directly producible precursors.*

Recoil energies around 35 MeV or above behind the target are enough to allow deposition of the SHE in the liquid phase, as shown for ^{289}Fl. For the isotopes with very low energies (blue color), the VLTC is not suitable in the current configuration. However, as one can see in figure 3.11, there is at least one isotope known for every SHE that is produced with a recoil energy that is high enough to enter the VLTC-setup. It should be emphasized that not all isotopes are directly produced. In many cases, a heavier precursor is first produced, because this is accessible with a higher cross section. The desired nuclide is then available through the decay of the precursor, as demonstrated for the production of nihonium (Z = 113) [42], where first moscovium (Z = 115) is produced: $^{243}_{93}$Am ($^{48}_{20}$Ca,3n) $^{288}_{115}$Mc. The $^{288}_{115}$Mc decays by emission of an α-particle into the $^{284}_{113}$Nh. Several of these directly and indirectly available SHE isotopes have also comparably long half-lives ($t_{1/2} > 5$ s), which makes them ideal candidates for a fast chemical experiment.

3.5 Conclusion

In liquid phase heavy element chemistry, the currently used techniques are multi-step procedures: First, the produced radionuclide enters through a high-pressure stopping cell, is thermalized and then transported with a KCl-gas-jet to a dissolution apparatus, where the gas phase is mixed with an aqueous phase. The KCl aerosol particles with adsorbed radionuclides dissolve in the liquid phase and the gas phase is removed by a degasser unit. After this multi-step procedure, the radionuclide is available for chemical study in the liquid phase. Each of these steps requires a certain amount of time which reduces the efficiency due to decay-losses. In this work, we introduced a new setup for faster liquid-phase heavy element chemistry

experiments. By transferring the radionuclide from the low pressure side of the preseparator unit directly into the liquid phase, a setup with gas stopper cell and the gas/liquid dissolving apparatus including the degassing unit becomes superfluous.

This vacuum to liquid phase transfer chamber (VLTC) separates the low pressure region of a physical preseparator from the liquid phase by a thin Mylar foil, supported by a metal grid. SRIM simulations were performed to demonstrate the theoretical feasibility and to design a liquid phase chamber with appropriate depth to stop radionuclides over a large mass and energy range. In order to ensure the mechanical stability of this system, the setup was first tested as a mock-up without the transfer of radionuclides between the gas and liquid phase. It was shown that the foil can withstand the high mechanical stress without rupturing for long periods of time. In addition, it was shown that the pressure on the vacuum side can be used as an indicator for an interlock system, as the pressure would rise in case of a foil rupture. Tracer experiments with ^{68}Ga were performed in order to estimate the flush-out time for the liquid phase chamber. In these experiments, the ^{68}Ga activity was injected through an additional inlet port into the liquid phase chamber. Mean residence times were determined to be 7.7 s ± 1.0 s at a flow rate of 100 mL/min with and 14.7 s ± 1.5 s for 50 mL/min. A constant decrease of the count rate was observed after the elution peak, indicating the absence of dead volumes, even in this rather simple chamber geometry. Finally, experiments with ^{250,252}Cf fission products were performed, where the Cf-source was placed in a 100 mbar vacuum chamber and fission fragments entered the VLTC through the Mylar foil and were collected in dilute nitric acid solution. In first instance, the collected solution with the accumulated fission products was measured directly with a HPGe detector. The flush-out yield of the collected fission products was 40.6 % ± 9.3 % in 10 mL solution, which is in good agreement with the results of the residence time measurements. Fission fragments from the light-mass peak and the heavy-mass peak region were identified by γ spectrometry. In addition, an ion exchange experiment was performed, in which the fission product solution was passed through a DOWEX 50Wx8 cation exchange column in order to chemically verify the identified nuclides of the first experiment and to demonstrate a potential setup for an accelerator based experiment with the novel VLTC. As shown by recoil energy calculations for the elements 104 - 115, there are many promising isotopes known that are suitable for liquid phase chemical studies of elements beyond dubnium and seaborgium.

3.6 References

[1] M. Schädel and D. Shaughnessy, Eds., *The Chemistry of Superheavy Elements*, 2nd ed. Springer Berlin Heidelberg, 2014.

[2] I. Zvara, Y. T. Chuburkov, R. Tsaletka, T. Zvarova, M. Shalaevskii, and B. Shilov, "Chemical properties of element 104," *Soviet Atomic Energy*, vol. 21, pp. 709–710, 1966.

[3] R. Silva, J. Harris, M. Nurmia, K. Eskola, and A. Ghiorso, "Chemical separation of rutherfordium," *Inorganic and Nuclear Chemistry Letters*, vol. 6, pp. 871–877, 1970.

[4] E. Sylwester, K. Gregorich, D. Lee, B. Kadkhodayan, A. Türler, J. Adams, C. Kacher, M. Lane, C. Laue, and C. McGrath, "On-line gas chromatographic studies of Rf, Zr, and Hf bromides," *Radiochimica Acta*, vol. 88, pp. 837–844, 2000.

[5] M. Schädel, W. Brüchle, E. Jäger, E. Schimpf, J. Kratz, U. Scherer, and H. Zimmermann, "ARCA II—a new apparatus for fast, repetitive HPLC separations," *Radiochim. Acta*, vol. 48, p. 171, 1989.

[6] Y. Nagame, K. Tsukada, M. Asai, A. Toyoshima, K. Akiyama, Y. Ishii, T. Kaneko-Sato, M. Hirata, I. Nishinaka, S. Ichikawa *et al.*, "Chemical studies on rutherfordium (Rf) at JAERI," *Radiochimica Acta*, vol. 93, pp. 519–526, 2005.

[7] P. O. Aronsson, B. E. Johansson, J. Rydberg, G. Skarnemark, J. Alstad, B. Bergersen, E. Kvåle, and M. Skarestad, "SISAK - A new technique for rapid, continuous (radio)chemical separations," *Journal of Inorganic and Nuclear Chemistry*, vol. 36, pp. 2397–2403, 1974.

[8] M. Schädel, W. Brächte, E. Schimpf, H. Zimmermann, M. Gober, J. Kratz, N. Trautmann, K. Gregorich, A. Türler, K. Czerwinski *et al.*, "Chemical properties of element 105 in aqueous solution: cation exchange separations with α-hydroxyisobutyric acid," *Radiochimica Acta*, vol. 57, pp. 85–92, 1992.

[9] M. Schädel, W. Brüchle, R. Dressler, B. Eichler, H. Gäggeler, R. Günther, K. Gregorich, D. Hoffman, S. Hübener, D. Jost *et al.*, "Chemical properties of element 106 (seaborgium)," *Nature*, vol. 388, pp. 55–57, 1997.

[10] Ch. E. Düllmann and A. Türler, "^{248}Cm (^{22}Ne, xn) $^{270-X}$Sg reaction and the decay properties of ^{265}Sg reexamined," *Physical Review. C, Nuclear Physics*, vol. 77, no. 6, pp. 064 320–064 320, 2008.

[11] H. Haba, D. Kaji, Y. Kudou, K. Morimoto, K. Morita, K. Ozeki, R. Sakai, T. Sumita, A. Yoneda, Y. Kasamatsu *et al.*, "Production of ^{265}Sg in the ^{248}Cm (^{22}Ne, 5 n) ^{265}Sg reaction and decay properties of two isomeric states in ^{265}Sg," *Physical Review C*, vol. 85, no. 2, p. 024611, 2012.

[12] J. V. Kratz, "Aqueous-phase chemistry of the transactinides," *Radiochimica Acta*, vol. 99, pp. 477–502, 2011.

[13] Y. Nagame, J. V. Kratz, and M. Schädel, "Chemical studies of elements with Z ≥ 104 in liquid phase," *Nuclear Physics A*, vol. 944, pp. 614–639, 2015.

[14] B. Wlodzimirska, K. Eberhardt, J. Kratz, S. Zauner, W. Brüchle, E. Jäger, M. Schädel, and E. Schimpf, "Reduction of Mo (VI) in ALOHA."

[15] K. Ooe, M. F. Attallah, M. Asai, N. Goto, N. S. Gupta, H. Haba, M. Huang, J. Kanaya, Y. Kaneya, Y. Kasamatsu, Y. Kitatsuji, Y. Kitayama, K. Koga, Y. Komori, T. Koyama, J. V. Kratz, H. V. Lerum, S. Miyashita, Y. Oshimi, V. Pershina, D. Sato, T. K. Sato, Y. Shigekawa, A. Shinohara, A. Tanaka, A. Toyoshima, K. Tsukada, S. Tsuto, T. Yokokita, A. Yokoyama, J. P. Omtvedt, Y. Nagame, and M. Schädel, "Development of a new continuous dissolution apparatus with a hydrophobic membrane for superheavy element chemistry," *Journal of Radioanalytical and Nuclear Chemistry*, vol. 303, pp. 1317–1320, 2015.

[16] Ch. E. Düllmann, C. M. Folden III, K. E. Gregorich, D. C. Hoffman, D. Leitner, G. K. Pang, R. Sudowe, P. M. Zielinski, and H. Nitsche, "Heavy-ion-induced production and physical preseparation of short-lived isotopes for chemistry experiments," *Nuclear Instruments and Methods in Physics Research Section A: Accelerators, Spectrometers, Detectors and Associated Equipment*, vol. 551, pp. 528–539, 2005.

[17] J. P. Omtvedt, J. Alstad, T. Bjørnstad, Ch. E. Düllmann, K. E. Gregorich, D. C. Hoffman, H. Nitsche, K. Opel, D. Polakova, F. Samadani, F. Schulz, G. Skarnemark, L. Stavsetra, R. Sudowe, and L. Zheng, "Chemical properties of the transactinide elements studied in liquid phase with SISAK," *The European Physical Journal D*, vol. 45, pp. 91–97, 2007.

[18] L. Stavsetra, K. E. Gregorich, J. Alstad, H. Breivik, K. Eberhardt, C. M. Folden III, T. N. Ginter, M. Johansson, U. W. Kirbach, D. M. Lee, M. Mendel, L. A. Omtvedt, J. B. Patin, G. Skarnemark, R. Sudowe, P. A. Wilk, P. M. Zielinski, H. Nitsche, D. C. Hoffman, and J. P. Omtvedt, "Liquid-scintillation detection of preseparated ^{257}Rf with the SISAK-system," *Nuclear Instruments and Methods in Physics Research Section A: Accelerators, Spectrometers, Detectors and Associated Equipment*, vol. 543, pp. 509–516, 2005.

[19] M. Schädel, "Superheavy element chemistry at GSI-status and perspectives," *The European Physical Journal D*.

[20] A. Semchenkov, W. Brüchle, E. Jäger, E. Schimpf, M. Schädel, C. Mühle, F. Klos, A. Türler, A. Yakushev, A. Belov *et al.*, "The TransActinide Separator and Chemistry Apparatus (TASCA) at GSI-Optimization of ion-optical structures and magnet designs," *Nuclear Instruments and Methods in Physics Research Section B: Beam Interactions with Materials and Atoms*, vol. 266, pp. 4153–4161, 2008.

[21] A. Yakushev, J. M. Gates, A. Türler, M. Schädel, Ch. E. Düllmann, D. Ackermann, L. Andersson, M. Block, W. Bruchle, J. Dvorak, et al., "Superheavy element flerovium (element 114) is a volatile metal," *Inorganic chemistry*, vol. 53, pp. 1624–1629, 2014.

[22] J. Even, J. Ballof, W. Brüchle, R. A. Buda, Ch. E. Düllmann, K. Eberhardt, A. Gorshkov, E. Gromm, D. Hild, E. Jäger, J. Khuyagbaatar, J. V. Kratz, J. Krier, D. Liebe, M. Mendel, D. Nayak, K. Opel, J. P. Omtvedt, P. Reichert, J. Runke, A. Sabelnikov, F. Samadani, M. Schädel, B. Schausten, N. Scheid, E. Schimpf, A. Semchenkov, P. Thörle-Pospiech, A. Toyoshima, A. Türler, V. Vicente Vilas, N. Wiehl, T. Wunderlich, and A. Yakushev, "The recoil transfer chamber - An interface to connect the physical preseparator TASCA with chemistry and counting setups," *Nuclear Instruments and Methods in Physics Research Section A: Accelerators, Spectrometers, Detectors and Associated Equipment*, vol. 638, pp. 157–164, 2011.

[23] International Nuclear Structure and Decay Data Network, "Nuclear data services: evaluated nuclear structure and decay data," 29.05.2020. [Online]. Available: https://www.nndc.bnl.gov/ensdf/

[24] G. R. Choppin, C. Ekberg, J.-O. Liljenzin, and J. Rydberg, *Radiochemistry and nuclear chemistry*, 4th ed. Amsterdam: AP Academic Press/Elsevier, 2013.

[25] D. Krupp, Ch. E. Düllmann, L. Lens, and U. W. Scherer, "Development of a fast characterization setup for radionuclide generators demonstrated by a ^{227}Ac-based generator," *Radiochimica Acta*, vol. 109, no. 3, pp. 205–214, 2021.

[26] J. F. Ziegler, "SRIM - The Stopping Range of Ions in Matter," Download, 01.07.2018. [Online]. Available: www.srim.org

[27] J. F. Ziegler, M. D. Ziegler, and J. P. Biersack, "SRIM – The stopping and range of ions in matter (2010)," *Nuclear Instruments and Methods in Physics Research Section B: Beam Interactions with Materials and Atoms*, vol. 268, pp. 1818–1823, 2010.

[28] K. F. Flynn, J. E. Gindler, and L. E. Glendenin, "The mass distribution for spontaneous fission of ^{252}Cf," *Journal of Inorganic and Nuclear Chemistry*, vol. 37, pp. 881–885, 1975.

[29] K. Flynn, J. Gindler, and L. Glendenin, "Mass distributions for the spontaneous fission of ^{248}Cm and ^{250}Cf," *Journal of Inorganic and Nuclear Chemistry*, vol. 39, pp. 759–762, 1977.

[30] A. Göök, F.-J. Hambsch, S. Oberstedt, and M. Vidali, "Prompt Fission Neutron Experiments on ^{235}U(n,f) and ^{252}Cf(SF)," *Physics Procedia*, vol. 64, pp. 190–196, 2015.

[31] J. W. Meadows, "Cf-252 Fission Neutron Spectrum from 0.003 to 15.0 MeV," *Physical Review*, vol. 157, pp. 1076–1082, 1967.

[32] Y. T. Oganessian and V. Utyonkov, "Superheavy nuclei from ^{48}Ca-induced reactions," *Nuclear Physics A*, vol. 944, pp. 62–98, 2015.

[33] A. Såmark-Roth, D. Cox, D. Rudolph, L. Sarmiento, B. Carlsson, J. Egido, P. Golubev, J. Heery, A. Yakushev, S. Åberg *et al.*, "Spectroscopy along flerovium decay chains: Discovery of Ds 280 and an excited state in Cn 282," *Physical review letters*, vol. 126, no. 3, p. 032503, 2021.

[34] H. Haba, F. Fan, D. Kaji, Y. Kasamatsu, H. Kikunaga, Y. Komori, N. Kondo, H. Kudo, K. Morimoto, K. Morita *et al.*, "Production of Bh 266 in the Cm 248 (Na 23, 5 n) Bh 266 reaction and its decay properties," *Physical Review C*, vol. 102, p. 024625, 2020.

[35] R. Venkataraman, F. Bronson, V. Atrashkevich, M. Field, and B. Young, "Improved detector response characterization method in ISOCS and LabSOCS," *Journal of Radioanalytical and Nuclear Chemistry*, vol. 264, pp. 213–219, 2005.

[36] S. H. Lee, J. H. Yoo, and J. H. Kim, "Ion exchange characteristics of rhodium and ruthenium from a simulated radioactive liquid waste," *Korean Journal of Chemical Engineering*, vol. 21, pp. 1038–1043, 2004.

[37] J. V. Kratz and Y. Nagame, "Liquid-Phase Chemistry of Superheavy Elements," in *The Chemistry of Superheavy Elements*, M. Schädel and D. Shaughnessy, Eds. Berlin, Heidelberg and s.l.: Springer Berlin Heidelberg, 2014, pp. 309–374.

[38] F. W. Strelow, R. Rethemeyer, and C. Bothma, "Ion Exchange Selectivity Scales for Cations in Nitric Acid and Sulfuric Acid Media with a Sulfonated Polystyrene Resin." *Analytical Chemistry*, vol. 37, pp. 106–111, 1965.

[39] D. Wittwer, F. S. Abdullin, N. Aksenov, Y. V. Albin, G. Bozhikov, S. Dmitriev, R. Dressler, R. Eichler, H. Gäggeler, R. Henderson *et al.*, "Gas phase chemical studies of superheavy elements using the dubna gas-filled recoil separator–stopping range determination," *Nuclear Instruments and Methods in Physics Research Section B: Beam Interactions with Materials and Atoms*, vol. 268, no. 1, pp. 28–35, 2010.

[40] M. J. Beauchamp, G. P. Nordin, and A. T. Woolley, "Moving from millifluidic to truly microfluidic sub-100-μm cross-section 3D printed devices," *Analytical and bioanalytical chemistry*, vol. 409, pp. 4311–4319, 2017.

[41] A. Yakushev, "Data to be published elsewhere," 2021.

[42] A. Yakushev, L. Lens, Ch. E. Düllmann, M. Block, H. Brand, T. Calverly, M. Dasgupta, A. Di Nitto, Götz, S. Götz, H. Haba, L. Harkness-Brennan, R.-D. Herzberg, F. Hessberger, D. Hinde, A. Hübner, E. Jäger, D. Judson, J. Khuyagbaatar, B. Kindler, Y. Komori, J. Konki, J. Kratz, J. Krier, N. Kurz, M. Laatiaoui, B. Lommel, C. Lorenz, M. Maiti, A. Mistry, C. Mokry, Y. Nagame, P. Papadakis, A. Roth, D. Rudolph, J. Runke, L. Samiento, T. Sato, M. Schädel, P. Scharrer, B. Schausten, J. Steiner, P. Thörle-Pospiech, N. Toyoshima, A Trautmann, J. Uusitalo, A. Ward, M. Wegrzecki, and V. Yakusheva, "First attempt to study nihonium (Nh, Z = 113) chemically at TASCA," *preparation for submission to Frontiers in Chemistry*, 2021.

Chapter 4

Development of a fast characterization setup for radionuclide generators demonstrated by a ^{227}Ac-based generator

D. Krupp [1], Ch. E. Düllmann[2,3,4], L. Lens[1] and U.W. Scherer[1]

[1] Institut für Physikalische Chemie und Radiochemie, Hochschule Mannheim - University of Applied Sciences, 68163 Mannheim, Germany
[2] Department of Chemistry - TRIGA site, Johannes Gutenberg University, Fritz-Strassmann-Weg 2, 55128 Mainz, Germany
[3] GSI Helmholtzzentrum für Schwerionenforschung mbH, Planckstr. 1, 64291 Darmstadt, Germany
[4] Helmholtz Institute Mainz, Staudingerweg 18, 55128 Mainz, Germany

Published in: Radiochimica Acta 109, 205-214 (2021)

DOI:https://doi.org/10.1515/ract-2020-0077

The following article was submitted as full article to Radiochimica Acta in 2020. It deals with the development of a continuous elution system for the short-lived alpha emitter ^{211}Bi ($t_{1/2}$ = 2.14 min ± 0.02 min) in dilute hydrochloric acid solution. In order to monitor the activity concentration in solution during continuous elution and to be able to quickly characterize such generator systems, the gamma radiation was additionally measured using a NaI(Tl) borehole detector. For this purpose, a data acquisition software based on Matlab was developed to record the analog signal of the NaI(Tl) detector with National Instruments hardware in energy and time resolution. The system will be used in the future for pre-experiments with functionalized alpha detectors.

Own contributions

The experimental design as well as the writing of the publication were self-directed with input from the co-authors. The software development as well as the generator design and the analysis of the data were also performed self-directed.

Abstract

The development of a setup for a fast online characterization of radionuclide generators is reported. A generator utilizing the mother nuclide ^{227}Ac sorbed on a cation exchange resin is continuously eluted by using a peristaltic pump. To allow continuous and pulse-free elution of a large volume over extended time periods a 3D-printed interface designed to remove pressure-oscillations induced by the pump was placed between pump and generator column to ensure undisturbed generator elution. The eluate of the generator is passed through a 3D printed flow cell placed inside a borehole Na(Tl)-scintillation detector for high counting efficiency. Alternatively, a HPGe detector suitable for nuclide identification was used to demonstrate the validity of the online method. The detection system combines conventional gamma-ray spectrometry with fast list mode data acquisition in the Matlab software package. Elution experiments were performed at different flow rates of hydrochloric acid, separating ^{211}Bi ($t_{1/2}$ = 2.14 min) free from its parent nuclides. In addition, to prove the versatility of the setup, experiments at different hydrochloric acid concentrations were performed resulting in the elution of pure ^{211}Pb ($t_{1/2}$ = 36.1 min) and ^{223}Ra ($t_{1/2}$ = 11.43 d), respectively.

4.1 Introduction

Radionuclide generators are able to provide a large variety of short- and intermediate-lived radionuclides without the need for large production facilities, such as accelerators or fission reactors. The most common field of applications is nuclear medicine, mainly using simple generators consisting of two radionuclide generations, only. Besides the longstanding use of ^{99}Mo/^{99m}Tc generators [1], which are the workhorse of diagnostic nuclear medicine, numerous new systems have been developed or are under development [2], ranging from light elements, e.g. ^{44}Ti/^{44}Sc [3], over ^{82}Sr/^{82}Rb [4] [5] up to heavier ones, e.g. ^{140}Nd/^{140}Pr [6]. Even elements with high atomic number up to the actinides are used [7] [8] e.g. ^{228}Ra/^{228}Ac [9]. Such actinide-based systems, which typically feed decay chains containing multiple radioisotopes, are able to establish multi-generation equilibria, e.g. ^{225}Ac/^{213}Bi [10] or ^{228}Th/^{212}Pb [11]. In contrast to medical applications utilizing reasonably long-lived radionuclides, the off-line production of short lived radionuclides is of special interest for fundamental nuclear chemistry research, e.g. providing homologs of superheavy elements (Z ≥ 104), like lead isotopes in case of flerovium (Fl, Z = 114), [12] and bismuth isotopes for moscovium (Mc, Z = 115) [13] [14]. A suitable system for homolog studies is the decay series of ^{227}Ac (see Figure 4.1) which feeds radionuclides with half-lives covering a substantial range.

Figure 4.1: *Main decay chain of ^{227}Ac with half-life and decay mode of each generation.*

In case of Mc, the generator set-up could be used to deliver short lived bismuth in aqueous solutions for offline studies with a fast liquid chemistry setup, like the SISAK extraction system [15] or a recently published system with functionalized silicon alpha detectors [16]. The state-of-the-art for the characterization

of radionuclide generators is based on the batch-wise measurement of fractions eluted under a variety of specific conditions. After an elution experiment, some time has to pass for reaching secular or transient equilibrium before the next elution experiment can be started [14]. This limits the frequency of utilisation or requires more than one generator system to quickly evaluate the performance of a generator system. To overcome these limitations, a novel system has been developed to allow flow-through type characterization of radionuclide generators.

4.2 Materials and Methods

4.2.1 Chemicals and devices

All reagents were used without further purification. Sodium hydroxide, acetonitrile, ethanol, DOWEX 50W X 8 ion exchange resin were obtained in p.a. and 35 wt% hydrochloric acid in supra pure quality from Roth, Germany. 1 MBq no-carrier-added [^{227}Ac]Ac(NO_3)$_3$ was procured from Eckert & Ziegler (reference date: 04.10.2017). Deionized (DI) water (G = 0.055 µS/cm) was prepared with a TKA Micro pure water purification device (Thermo Scientific). 3D-printed parts were constructed in Inventor 2018 (Autodesk), processed in Cura 4.5 (Ultimaker), and printed with a SLA-based 3D printer “Moai” (Peopoly) from methacrylate-based UV-Resin supplied by Peopoly.

4.2.2 Measurement setup

For nuclide identification, gamma-ray spectrometry was performed using an “GEM-38210” HPGe detector (38 % rel. efficiency) (Ortec), in combination with a “2022” type amplifier (Canberra). The amplified unipolar output signal was split and digitalized in a “Multiport II" MCA (Canberra) and a "NI 9239" (National Instruments) data acquisition device, mounted in a "NI cDAQ-9174" chassis. The MCA data were processed in “Genie 2000 version 3.2” (Canberra) to obtain energy-resolved spectra. The NI-DAQ data were recorded and processed in a Matlab (Version R2020a) based script, utilizing the signal processing- and data acquisition toolbox. Analog data were measured at a 50 kHz sampling rate at 24-bit resolution in a range from -10 V to +10 V. To calibrate the corresponding energy range in electron Volt, a “TC814” Pulser (Tennelec) was used. In flow-through experiments, a 3D printed flow cell was mounted in a 4 cm x 6 cm NaI(Tl) scintillation detector type “51BP51/2M” with a 3 cm x 1.8 cm borehole (13 % efficiency at 351 keV) (Scionix). The flow rate of the liquid phase was controlled by a "Reglo ICC" peristaltic pump (Ismatec). The spectrometry setup is shown in Figure 4.2.

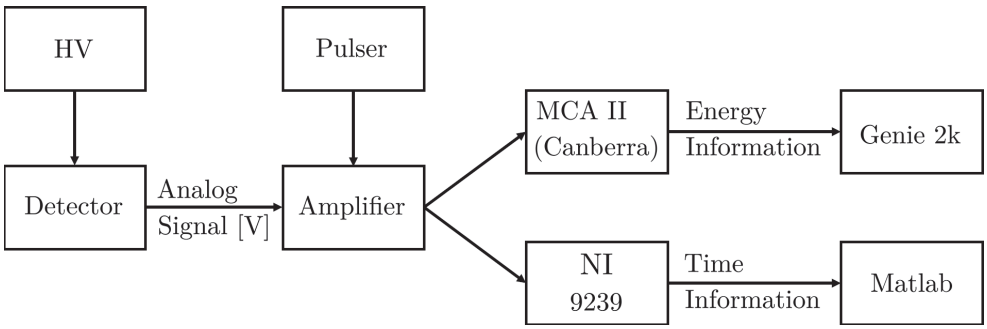

Figure 4.2: *General spectrometry setup with conventional data acquisition in Genie 2000 and additional data acquisition in Matlab with a NI 9239 DAQ device.*

4.2.3 Matlab based data processing

The Matlab script analyses the timestamp of each individual detected event in Volt. Raw data were saved in packages of one hundred thousand data points, each representing 2 seconds of the experiment (Figure 4.3, left). Subsequently, a peak search algorithm was used to list all pulses (with the corresponding timestamp), which were detected during a whole experiment. Afterwards, the listed pulse-heights [V] were converted into a histogram, resulting in a pulse height resolved spectrum (Figure 4.3, middle). Then, the peak region associated with the decay of radioisotopes of interest (see Table 4.1) is used to generate the time resolved elution profile (Figure 4.3, right).

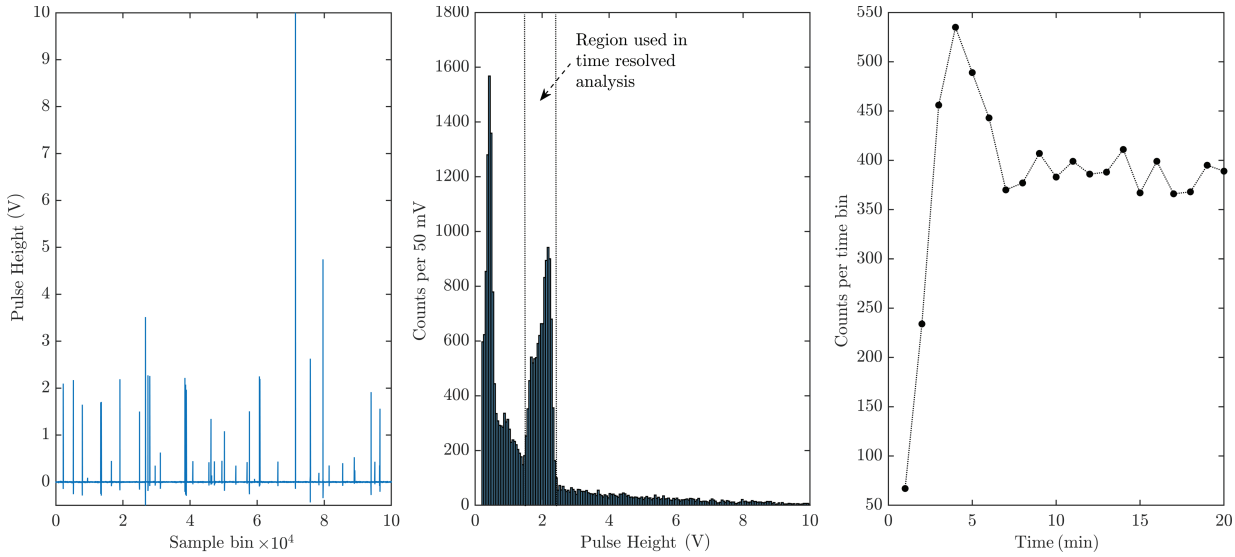

Figure 4.3: *Matlab Data Analysis: 2 second batch of raw data (left), pulse-height resolved histogram (middle) and time resolved elution profile (right).*

4.2.4 Generator setup

3 mL of DOWEX AG 50W X 8 ion exchange resin were dry packed in a 5 mL glass column. A peristaltic pump was attached to the column nozzle and adjusted to a flow rate of 1 mL/min. The resin was rinsed five times with 1 mL aliquots of the following solutions: 0.4 M HCl, 1 M NaOH, Ethanol, 0.4 M HCl, and finally 0.2 M HCl. Between each of these steps, the column was flushed with 5 mL DI water, to remove the

liquid remaining from the previous rinsing step. Subsequently, 1 kBq ^{227}Ac, in equilibrium with its decay products, was dissolved in 2 mL of a 0.2 M HCl and loaded onto the column. For the Ac loading, the flow rate was adjusted to 0.5 mL/min. Finally, the column was rinsed with 10 mL 0.2 M HCl. A 3D-printed interface was mounted on top of the glass column to connect the peristaltic pump to the column. The buffer volume allows to diminish the pressure pulsation induced by the peristaltic pump to a level that no longer affects column separation quality. Thus pulsation-free and continuous elution of the generator, irrespective of the selected flow rate, is ensured. The eluate was passed through a 3-way valve, with the options to perform either batch-wise measurements with a HPGe detector or continuous monitoring with a NaI(Tl)type scintillation detector equipped with a flow cell. The inner volume of the spiral-shaped flow cell was adjusted to 1 mL. A schematic overview of the generator setup is shown in Figure 4.4.

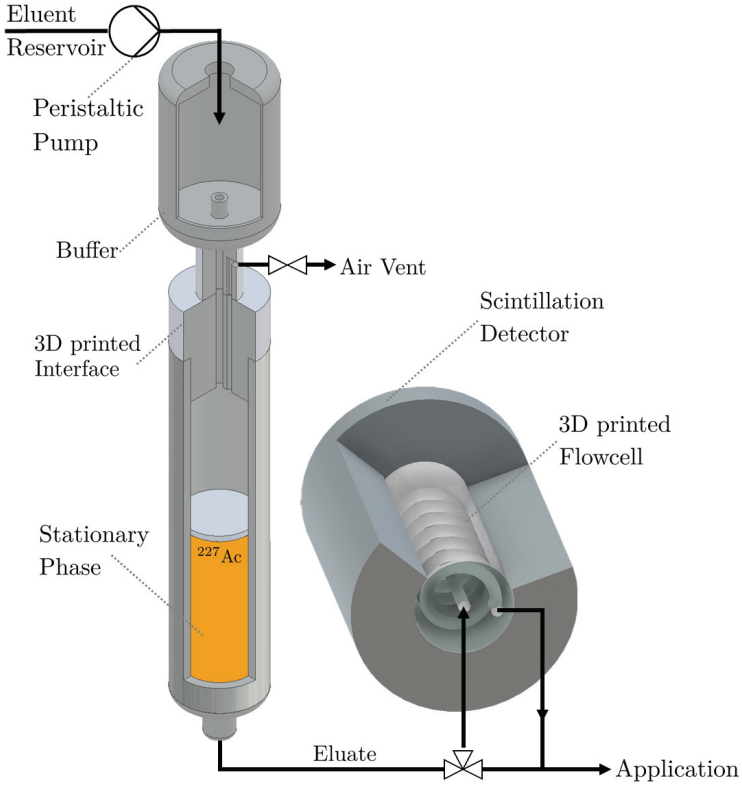

Figure 4.4: *Schematic overview of the ^{227}Ac generator system with online NaI(Tl) scintillation detector, which can be bypassed with a 3 way valve.*

4.2.5 Elution experiments

All batch-wise elution experiments were performed at a flow rate of 1.4 mL/min. Each batch consisted of 1 mL eluate, measured in a 20 mL glass vial (therefore, all samples were measured in the same geometry) on a HPGe detector, for 900 s. The nuclide identification and peak-area determination were performed using Genie2000. The threshold for a relevant full-energy peak was set to 3 times the surrounding background. Spectra for Matlab-based half-life analysis were measured for 2400 s. For continuous elution experiments, the eluate was passed through a scintillation detector equipped with a flow cell as described above. The borehole scintillation detector was chosen for its high intrinsic and geometric efficiencies. The flow cell was used to extend the residence time of the sample inside the borehole. Experiments of this type were

performed for 30 min at various flow rates and different concentrations of hydrochloric acid. 20 min after completion of an experiment, the collected eluate was measured for 900 s on a HPGe detector to verify that no column bleeding occurred. Corresponding background measurements were performed in all types of experiments, in the same setup, and over the same counting interval.

4.3 Results and discussion

4.3.1 Generator preparation

The original ^{227}Ac stock solution had been processed last time more than 210 days before use by us. Hence, equilibrium along the complete decay chain was established. A γ-ray spectrum of the ^{227}Ac stock solution, in equilibrium with its decay products, was acquired for 3600 seconds and is shown in Figure 4.5.

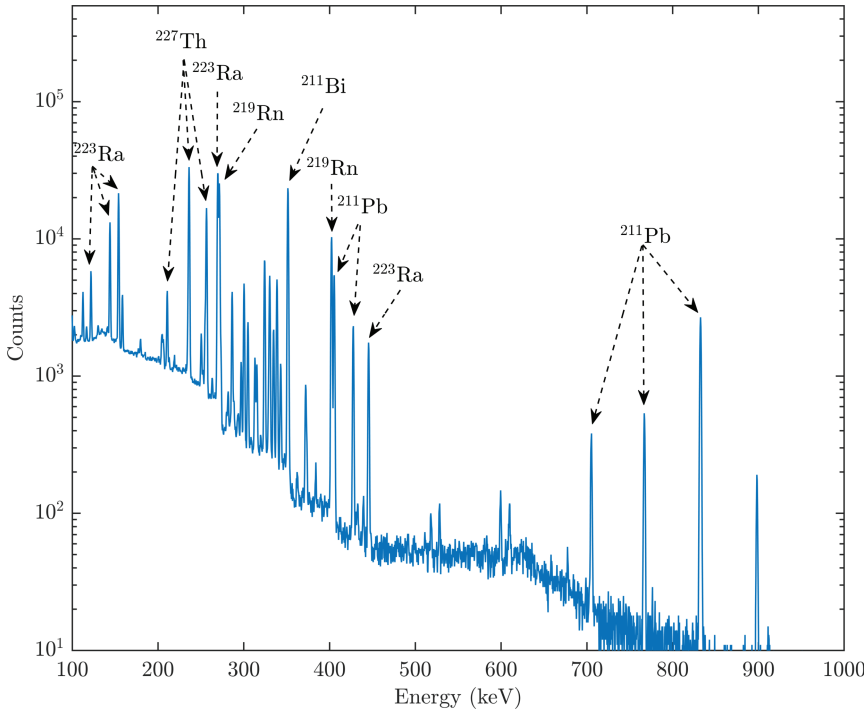

Figure 4.5: *Gamma spectrum of the ^{227}Ac stock solution. Not all γ-lines were labelled due to readability.*

For better readability, not all lines are labelled in Figure 4.5. The efficiency-corrected areas of all lines represent a typical relative abundance of ^{227}Ac and its daughters in full equilibrium and are in good agreement with those of literature spectra [17].

4.3.2 ^{211}Bi elution in batch experiments

Before batch elution experiments were performed, the radiochemical purity of the 0.4 M HCl eluate was determined by two methods. First, the 5 mL of the eluate were analyzed by γ-ray spectrometry using a HPGe detector. A representative spectrum is shown in Figure 4.6.

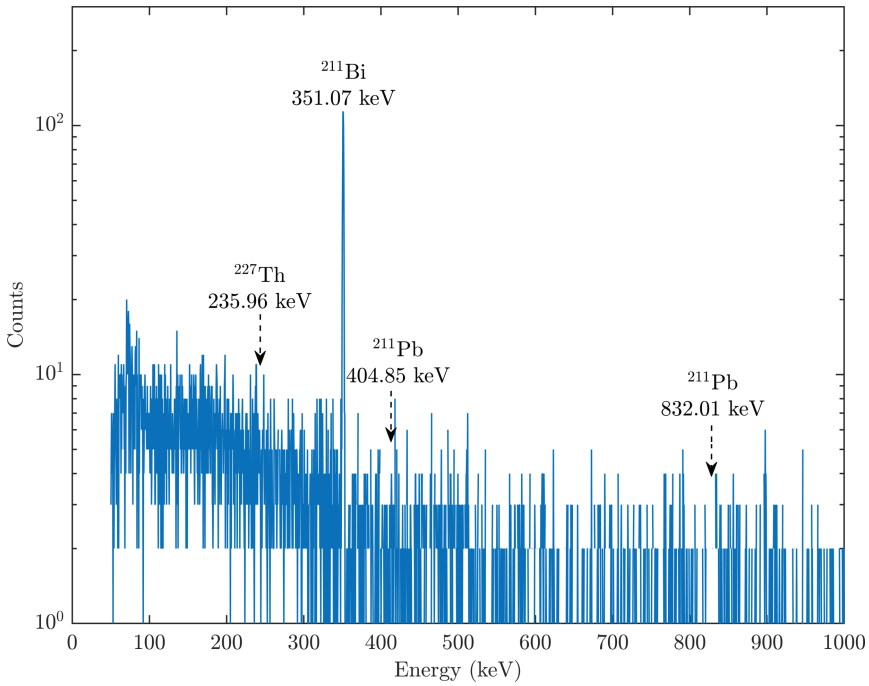

Figure 4.6: *Representative γ-lines of a generator sample in 0.4 M HCl.*

The only γ-line observed above background originates from the decay of ^{211}Bi (351.07 keV Iγ= 13.02 % [18]) from the ^{227}Ac decay series (see Table 4.1).

Table 4.1: *Most prominent γ-lines of the ^{227}Ac decay series [18].*

Nuclide	$t_{1/2}$	γ-ray energy [keV]	Intensity [%]
^{227}Ac	21.77 y	99.60	< 0.01
^{227}Th	18.70 d	235.96	12.9
^{223}Ra	11.43 d	269.46	13.9
^{219}Rn	3.96 s	271.23	10.8
^{215}Po	1.78 ms	No γ	-
^{211}Pb	36.1 min	404.85	3.78
		832.01	3.52
^{211}Bi	2.14 min	351.07	13.02
^{207}Tl	4.77 min	897.77	0.26

No significant decay (i.e., signal three times above background) of ^{211}Pb was detected in samples eluted with 0.4 M HCl. As ^{227}Ac has no prominent γ-line, its progeny ^{227}Th was used as an indicator for column bleeding. Thorium in diluted hydrochloric acid would strongly adsorb on the cation exchange resin. The minimum detectable thorium-227 activity (MDA) in measurements lasting 900 s was calculated with Genie 2000 [19] with uncertainty calculations according to DIN ISO 11929 [20]. No thorium-227 breakthrough above the MDA of 3.49 Bq was observed in any of the performed experiments. In addition, a 20 mL generator sample was eluted with 0.4 M HCl, placed directly on the HPGe detector and measured for 86400 s lifetime. The resulting γ-ray spectrum is shown in Figure 4.7.

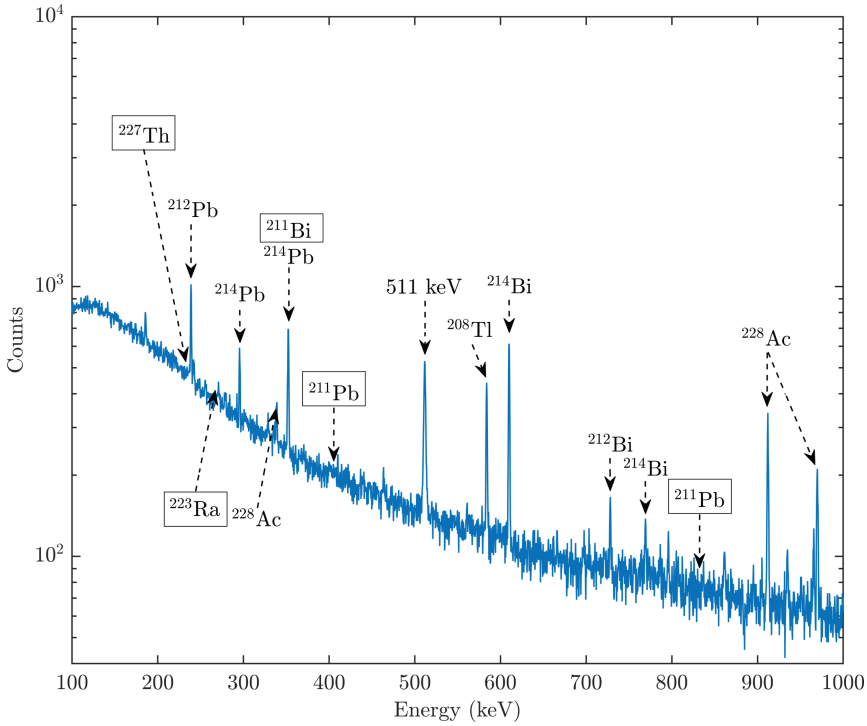

Figure 4.7: *Gamma spectrum of a 20 mL generator sample in 0.4 M HCl, measured for 86400 s. The progenies of the ^{227}Ac decay are given inside boxes. The other γ-line originate from the background.*

The MDA was 5.23 Bq ^{227}Th and 5.39 Bq for the ^{223}Ra in this long term measurement. The minimum detectable activity increased in this measurement relative to the short time measurements, because of the increased background level and the interference of the naturally occurring radionuclides in the surrounding, like ^{212}Pb. However, no ^{227}Th, ^{223}Ra or ^{211}Pb was detected in the long term measurement. In addition to conventional γ-ray spectrometry, a half-life analysis was performed by using measured data of samples recorded by the Matlab list mode system. Therefore, two measurements were performed: initially, the background count rate in an energy window around 351.07 keV was measured without sample solution. Subsequently, a sample eluted from the generator was collected in a 20 mL glass vial, placed on the HPGe detector, and measured for 2400 s. Background- and sample-data were analysed in the same energy window. The resulting decay curve is shown in Figure 4.8.

The measured decay curve was compared with a theoretical ^{211}Bi decay:

$$R(t) = R_0 \cdot e^{-\frac{ln(2)}{t_{1/2}}} + \bar{R_{BG}} \tag{4.1}$$

By using a nonlinear solver function with the initial count rate (R_0) and the average background count rate ($\bar{R_{BG}}$) as free parameters, the measured half-life of the decay curve ($t_{1/2}$) was determined. Convergence criterium was the minimal achievable difference between the summed square differences between theoretical and measured values. The solver calculation resulted in a half-life of 110.2 s ± 10.5 s, which is slightly shorter than the literature value of 128.4 s ± 1.2 s [18]. For the background region, the solver model calculated a mean background of 63.96 ± 8.00 counts per minute, which is in good agreement, with the measured 64.10 ± 8.01 counts per minute. Hence, no increased half-life or a background offset was

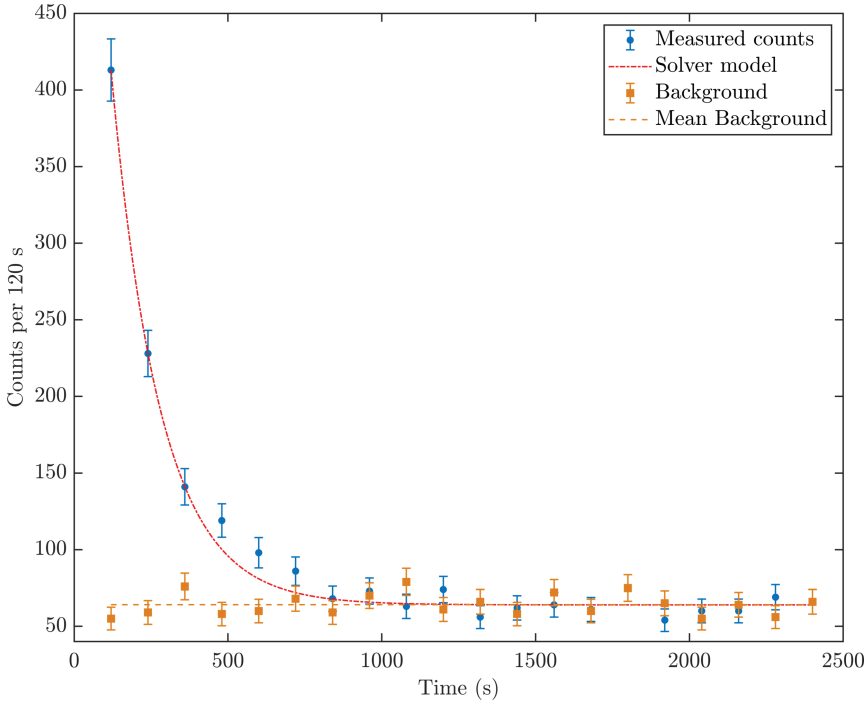

Figure 4.8: *Decay curve of a generator sample in 0.4 M HCl. The data were recorded with a NI-DAQ interface and processed in a Matlab-based script. The model of the decay curve was calculated by a solver analysis.*

measured, indicating that no relevant amounts of radionuclides with longer half-lives were eluted under the chosen conditions. After determining the radionuclidic purity of the eluate, the generator was characterized, according to one of the currently performed standard procedures: 1 mL batches were collected at a constant flow rate (here 1.4 mL/min) and measured in the same geometry using a HPGe detector. Between each batch, the generator system was allowed to re-establish equilibrium by waiting for at least 22 min (10 half-lives of ^{211}Bi). Acquired spectra were analyzed by Genie2000. The resulting peak areas of the 351.07 keV peak of each of the fractions are shown in Figure 4.9. The values are plotted relative to the largest peak area, which is referred to as the maximum eluted activity. The resulting curve has an untypical shape for elution profiles as known from literature. For comparison, the estimated profile of a typical elution curve is plotted in a dashed line.

The maximum activity per batch was observed at 3.5 mL. Afterwards, the measured activity drops to around 60 % of the maximum activity. Typical elution curves shown in the literature [14] are peaklike shaped. In our setup (see Figure 4.4), the ^{211}Bi grows in fast enough to allow for constant production of activity, resulting in the elution curve profile shown in Figure 4.9.

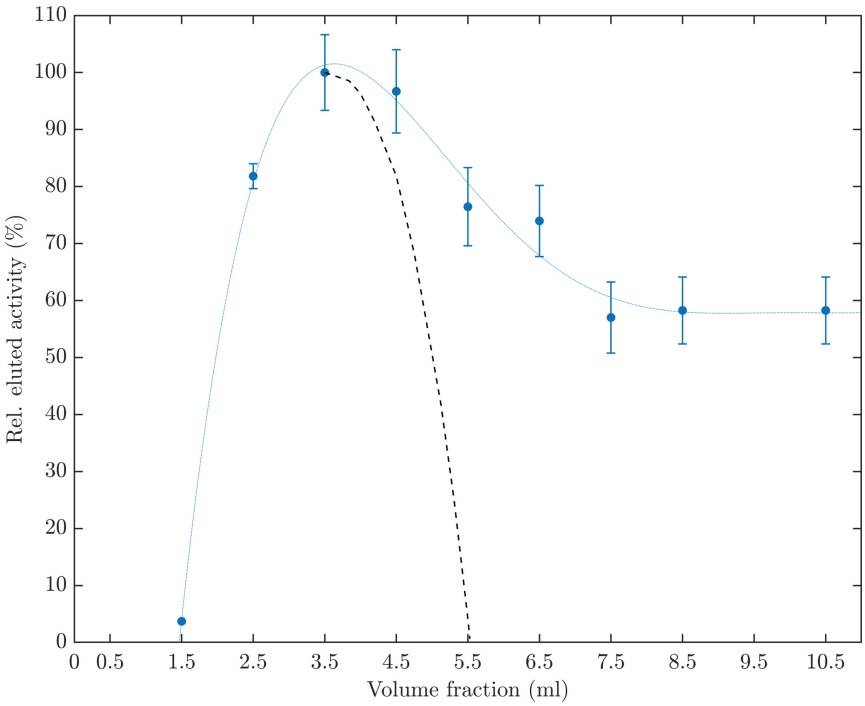

Figure 4.9: *Elution series based on batch-wise elution of ^{211}Bi and subsequent measurement on a HPGe detector. The line is intended to guide the eye.*

4.3.3 ^{211}Bi elution in continuous experiments

In contrast to the batch elution experiments, in a new set of experiments data were sampled with a NaI(Tl) detector in a single continuous run. This allows the quick characterization of a generator over an extended time period and, depending on the chosen flow rate, over a large volume (up to 60 mL). The batch experiments already showed only ^{211}Bi to be eluted in 0.4 M HCl. Hence, this concentration was used to investigate the temporal system stability at different flow rates. Figure 4.10 shows the experimental results of three elution experiments at 1 mL/min. The measured pulses (counts) are sorted in 60 s time bins.

The measured count rate was clearly distinguishable from a background measurement, which was performed over the same time period. In the following section, in addition to the measured count rates, the corresponding activities are mentioned in brackets. The highest ^{211}Bi count rate was obtained after 4 min, at 4 mL, with a range between 538 ± 23 cpm and 496 ± 22 cpm (490 ± 24 Bq - 448 ± 23 Bq). This is in good agreement with the batch experiment, where the maximum occurred between 3 mL and 4 mL. Further elution resulted in a lower count rate, which stabilizes at levels between 444 ± 21 cpm and 317 ± 18 cpm (396 ± 22 Bq - 272 ± 19 Bq). In agreement with the batch experiment (see Figure 4.9), the shape of the elution curve shown in Figure 4.10 differs from conventional elution curves with Gaussian-like profiles. The plateau section after the peak maximum is due to the short half-life of ^{211}Bi, which allows equilibrium to - at least partially - establish rapidly. For more clarity, Figure 4.11 shows the mean values of the elution experiment at 1 mL/min consisting of a peak maximum and a plateau. This sum function is decomposed in the elution peak with Gaussian-like shape with a tailing and the ingrowth function of ^{211}Bi reaching equilibrium with its longer-lived parent nuclides.

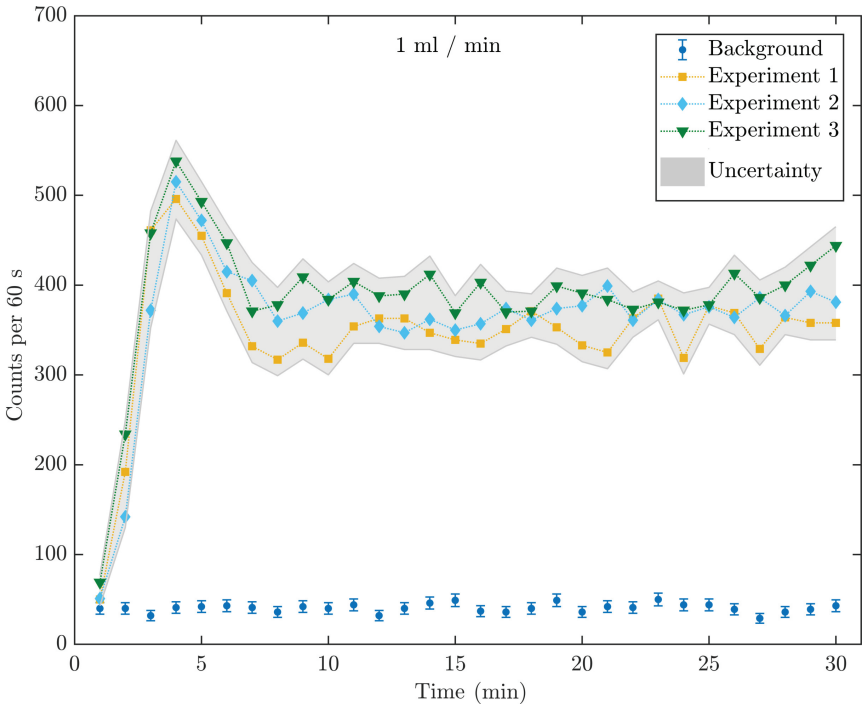

Figure 4.10: *Experimental results at a flow rate of 1.0 mL/min with 0.4 M HCl, including a background measurement over the same interval. The raw data were processed as described in section 2.3. The uncertainty limits represent the lowest and highest detected count rate ± 1 σ of all performed experiments. Lines between the individual data points are intended to guide the eye.*

In experiments with higher flow rates of 1.4 mL/min and 2 mL/min, the count rate maximum shifts towards earlier time bins, as it is expected for increased flow rates. Still, the maximum count rate is observed at an elution volume around 4 mL in each experiment. At 1.4 mL/min flow rate (total volume is 42 mL per experiment), the maximum count rate was between 628 ± 25 cpm and 516 ± 23 cpm (578 ± 26 Bq - 468 ± 24 Bq). The plateau region was between 402 ± 20 cpm and 313 ± 18 cpm (356 ± 21 Bq - 268 ± 19 Bq). At flow rates of 2 mL/min (total volume is 60 mL per experiment), the maximum count rate was between 664 ± 26 cpm and 535 ± 23 cpm (614 ± 27 Bq - 487 ± 24 Bq), with a plateau count rate between 384 ± 20 cpm and 291 ± 17 cpm (338 ± 21 Bq - 247 ± 18 Bq). The collected eluates of the different flow rate experiments were measured 15 min after completion of a single experiment with a HPGe detector to detect longer-lived components. Again, no significant γ-lines above background level could be detected. The general tendency over the performed flow rate experiments showed a higher count rate at the peak maximum as the ^{211}Bi activity in equilibrium is transported faster to the detection system. However, the residence time of the eluent in the generator and the flow cell is decreased, resulting in a decreased count rate in the plateau region at higher flow rates. Nevertheless, no count rate drop was observed even at higher flow rates, indicating that this generator system could be used as a constant injection system for short-lived ^{211}Bi.

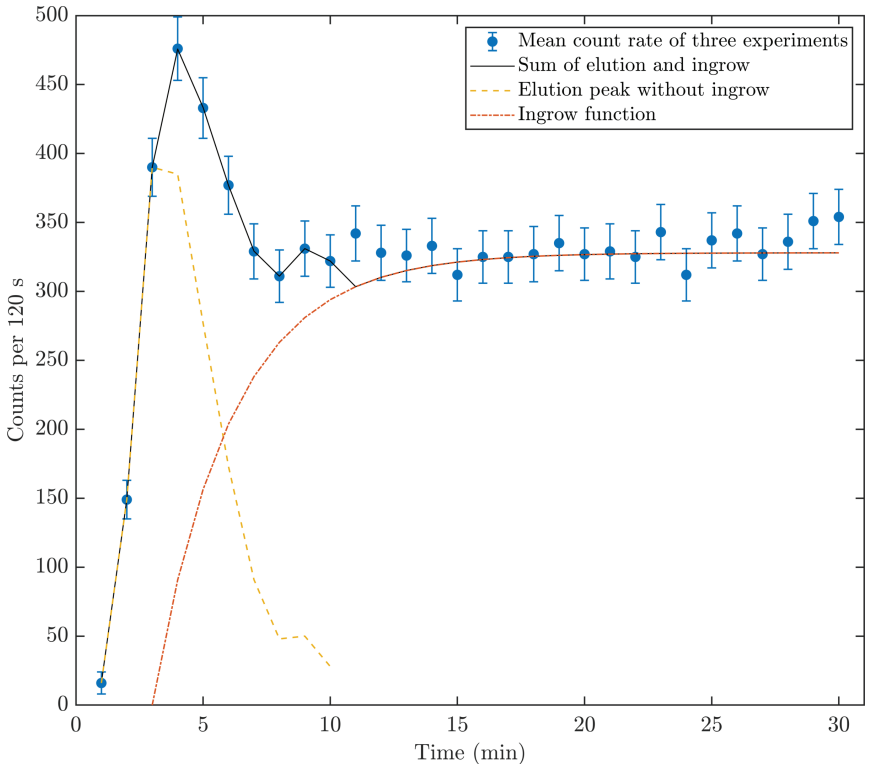

Figure 4.11: *Decomposition of the elution curve at 1 mL/min. The mean value was calculated for the three experiments, with its standard deviation. The elution peak without ingrowth is presented in dashed lines. The ingrowth is presented in a dash-dotted curve. The sum of the theoretical ingrow and the elution peak is shown in a solid line.*

4.3.4 HCl concentration-dependent elution experiments

Consequently, the generator system was further tested at different hydrochloric acid concentrations. Based on studies of distribution coefficients of actinides and their decay products on Dowex 50W X 8 ion exchange material by Strelow [21] and Alhassanieh et al. [22], lower HCl concentrations (0.1 M and 0.2 M) should result in the elution of bismuth without eluting its parent nuclides (see Table 4.2).

Table 4.2: *Distribution coefficients of relevant cations of the actinium-227 series according to Strelow [21] and Alhassanieh et al. [22].*

Cation	HCl(aq) concentration [mol/L]					
	0.1	0.2	0.5	1.0	2.0	3.0
Th^{4+}	> 10^5	> 10^5	10^5	2049	239	114
Ra^{2+}	> 10^5	> 10^5	4748	779.7	No Data	60.9
Pb^{2+}	> 10^4	1420	183	35.66	9.8	6.8
Bi^{3+}	« 1	« 1	< 1	1	1	1
Tl^{+}	173	91	41	22.32	9.9	5.8

However, no elution of any radionuclide including ^{211}Bi was observed in a set of three experiments with 0.1 M HCl and 0.2 M HCl at a flow rate of 1 mL/min. This observation is in agreement with experiments of Despotopulos et al. [14], who used a ^{228}Th based generator to produce ^{212}Bi / ^{212}Pb. This system also required concentrations of at least 0.4 M HCl to elute ^{212}Bi. One explanation for the difference in

these observations could originate from the different experimental setup used in the work of Strelow [21] in 1960 and the one in the more recent experiments [13] [14]. Nonetheless, elution experiments at HCl concentrations of 0.4 M (see Figure 4.10) showed results, which are in agreement with the older [21] and newer [14] literature. Here, the Pb is strongly adsorbed on the ion exchange material and only Bi is eluted. Contrary to the already performed studies with longer-lived Bi isotopes, e.g. ^{212}Bi (60.55 min) [14] and ^{213}Bi (45.59 min) [10], the ^{211}Bi (2.14 min) produced in our work is so short-lived that it regenerates fast enough during elution to reach a steady state between the secular equilibrium with the long-lived parent nuclides and the elution in 0.4 M HCl. At higher HCl concentration of 2 mol/L, in addition to the ^{211}Bi, also ^{211}Pb (36.1 min) is desorbed and mobilized. The observed elution curve has the typical shape.

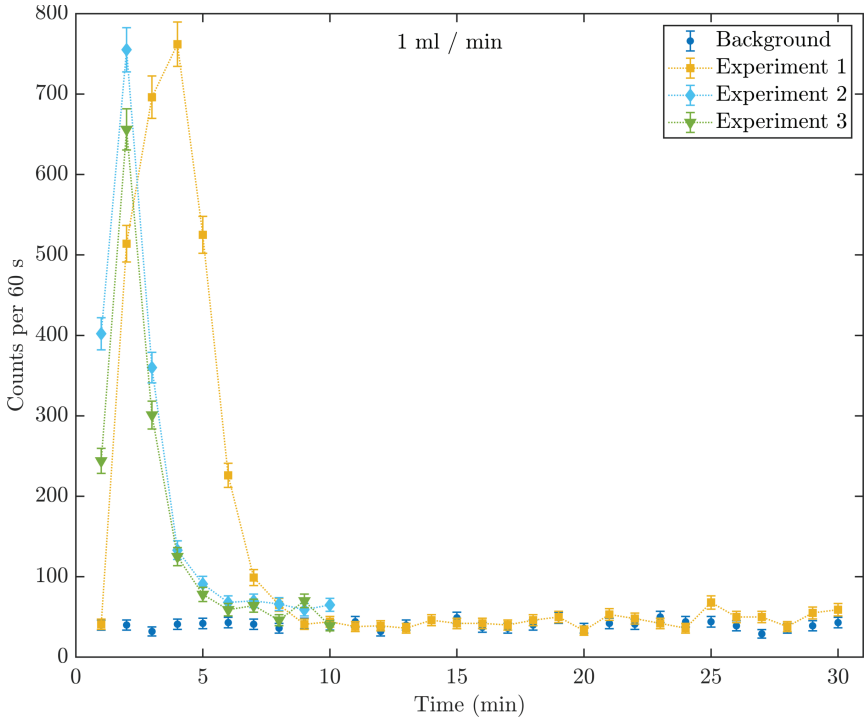

Figure 4.12: *Experimental results at a flow rate of 1.0 mL/min with 2 M HCl, including a background measurement over the same period. The uncertainty limits represent the detected count rate ± 1 σ in all performed experiments. Lines intend to guide the eyes.*

Due to the additional ^{211}Pb elution, the peak maximum is even higher than in experiments performed at 0.4 M HCl. However, reaching equilibrium between the strongly adsorbed long-lived parent nuclides like (^{227}Ac – ^{223}Ra) and ^{211}Pb would take 18 times longer than for ^{211}Bi, resulting in a steep drop of the count rate, down to the background region. The HPGe γ-spectrum of the collected eluate is shown in Figure 4.13.

The only γ-lines detectable in a 30 mL fraction eluted with 2 M HCl originate from ^{211}Pb and its progenies ^{211}Bi and ^{207}Tl. This observation is in agreement with measurements published in literature, e.g. Despotopulos et al. [14], who performed elutions of ^{212}Pb with 2 M HCl in over 5 mL total elution volume with an interval of 4 days between each elution. They also did not observe any breakthrough of parent nuclides in their system. The ion exchange column reported in our work was eluted a second time after 5 h. As the count rates observed after 10 min (the duration of the first experiment) had decreased to background, a measurement time of 10 min was chosen for the second and third elution experiments.

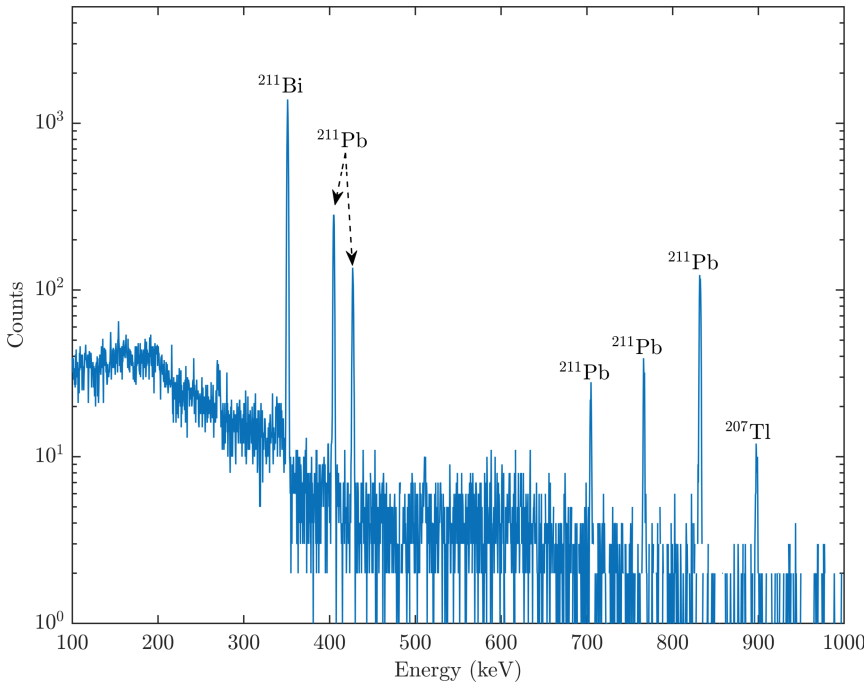

Figure 4.13: *Generator eluate γ-ray spectrum of the first experiment with 2 M HCl*

Here, one can observe a steeper increase in the count rate as compared with the first experiment (see Figure 4.12). The explanation for this peak shift towards earlier times, is given by the γ-ray spectrum of the eluate of the third experiment (see Figure 4.14):

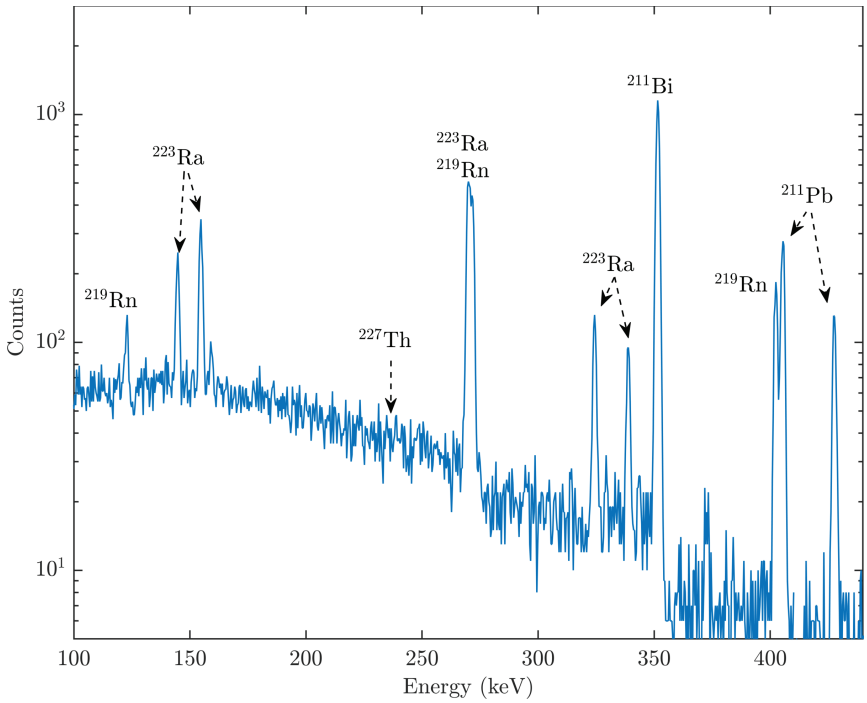

Figure 4.14: *γ-ray spectrum of a 10 mL fraction eluted with 2 M HCl after repeated elution. The scale was set to the interval of 100 – 500 keV for better visibility of the individual relevant γ-lines.*

After eluting with larger volumes of 2 M HCl, also radium is mobilized, resulting in a broader ^{223}Ra distribution over the column and transport of some free radium through the system. The ^{223}Ra has a

relatively long half-life of 11.43 d. Therefore, the largest fraction remains on the column without significant loss of activity between the experiments. As ^{211}Pb and ^{211}Bi quickly establish secular equilibrium with the ^{223}Ra parent present in the system, the maximum count rate occurs at earlier eluted volumes. This radium co-elution after longer continuous generator elutions or in high-frequency elutions should also be taken into account for other generator systems based on DOWEX 50W X 8 as it limits the maximum available activity per elution in case of routine use at high frequencies.

4.4 Conclusion

A fast characterization tool for radionuclide generator systems is presented. By combining conventional γ-ray spectrometry on borehole scintillation detectors with fast event-based sampling, it is possible to investigate the properties of a radionuclide generator with good statistics and high reproducibility without the need to re-establish equilibrium between subsequent applications. The system was tested with ^{227}Ac, loaded on DOWEX 50W X 8, a strong cation exchange resin which is widely used for generator applications. For constant elution from this ^{227}Ac loaded column, a 3D-printed interface was mounted on top of the generator column to ensure a pulse-free elution from the column, without risking the column running dry. Similar to the interface, a flow cell with an inner spiral-shaped transport line of 1 mL volume was 3D-printed, to define the volume passing the borehole scintillation detector. Our data are in good agreement with recent literature on similar-type generators. In addition to what was previously reported, we also demonstrate the behaviour of this well-known ion exchange resin in long-term continuous elution over periods up to 30 min and 60 mL. Elution rates of ^{211}Bi ($t_{1/2}$ = 2.14 min) with 0.4 M HCl were constant over long times, without co-eluting ^{211}Pb or ^{223}Ra. This could be used, e.g., as a pulse-free constant injection system for the short-lived, alpha- and gamma-emitter ^{211}Bi in homolog element experiments of element 115, moscovium. Another application could be the constant elution of ^{213}Bi from a ^{225}Ac generator system. The principle can also be applied to other complex generators system if an appropriate separation scheme can be established. At HCl concentrations of 2 mol/L, the co-elution of ^{211}Pb ($t_{1/2}$ = 36.1 min) and subsequently of ^{223}Ra ($t_{1/2}$ = 11.43 d) were observed with this fast characterization tool, too. Consequently, this setup will be tested for the ^{228}Th ($t_{1/2}$ = 1.91 a) decay chain [14], yielding the longer lived isotopes ^{212}Pb ($t_{1/2}$ = 10.64 h) and ^{212}Bi ($t_{1/2}$ = 60.55 min), as the elements involved in this generator system would be the same, except for actinium.

4.5 References

[1] S. Banerjee, M. R. A. Pillai, and N. Ramamoorthy, "Evolution of Tc-99m in diagnostic radiopharmaceuticals," in *Seminars in nuclear medicine*, vol. 31, no. 4. Elsevier, 2001, pp. 260–277.

[2] F. Rösch and F. Knapp, "Radionuclide generators," *Handbook of nuclear chemistry*, 2011.

[3] D. Filosofov, N. Loktionova, and F. Rösch, "A ^{44}Ti/^{44}Sc radionuclide generator for potential application of ^{44}Sc-based PET-radiopharmaceuticals," *Radiochimica Acta*, vol. 98, no. 3, pp. 149–156, 2010.

[4] M. Kensett, P. Horlock, S. Waters, and D. Bateman, "Experience with a ^{82}Sr/^{82}Rb generator for clinical use," *International Journal of Radiation Applications and Instrumentation. Part A. Applied Radiation and Isotopes*, vol. 38, no. 3, pp. 227–231, 1987.

[5] V. Dhawan, "Model for ^{82}Sr/^{82}Rb generator elution profiles: A secondary approach to radioassay/-dosimetry," *International Journal of Radiation Applications and Instrumentation. Part A. Applied Radiation and Isotopes*, vol. 38, no. 3, pp. 233–239, 1987.

[6] K. Zhernosekov, D. Filosofov, S. M. Qaim, and F. Rösch, "A ^{140}Nd/^{140}Pr radionuclide generator based on physico-chemical transitions in ^{140}Pr complexes after electron capture decay of ^{140}Nd-DOTA," *Radiochimica Acta*, vol. 95, no. 6, pp. 319–327, 2007.

[7] S. Mirzadeh, "Generator-produced alpha-emitters," *Applied radiation and isotopes*, vol. 49, no. 4, pp. 345–349, 1998.

[8] C. Müller, N. P. van der Meulen, M. Benešová, and R. Schibli, "Therapeutic radiometals beyond ^{177}Lu and ^{90}y: production and application of promising α-particle, β–particle, and auger Electron emitters," *Journal of Nuclear Medicine*, vol. 58, no. Supplement 2, pp. 91S–96S, 2017.

[9] K. E. Aldrich, M. N. Lam, C. Eiroa-Lledo, S. A. Kozimor, L. M. Lilley, V. Mocko, and B. W. Stein, "Preparation of an Actinium-228 Generator," *Inorganic chemistry*, vol. 59, no. 5, pp. 3200–3206, 2020.

[10] M. R. McDevitt, R. D. Finn, G. Sgouros, D. Ma, and D. A. Scheinberg, "An ^{225}Ac/^{213}Bi generator system for therapeutic clinical applications: construction and operation," *Applied Radiation and Isotopes*, vol. 50, no. 5, pp. 895–904, 1999.

[11] S. P. Hassfjell and P. Hoff, "A generator for production of ^{212}Pb and ^{212}Bi," *Applied radiation and isotopes*, vol. 45, no. 10, pp. 1021–1025, 1994.

[12] L. Guseva, G. Tikhomirova, and N. Dogadkin, "An ^{227}Ac- ^{211}Pb generator for test experiments of solution chemistry of element 114," *Journal of radioanalytical and nuclear chemistry*, vol. 260, no. 1, pp. 167–172, 2004.

[13] K. N. Kmak, J. D. Despotopulos, and D. A. Shaughnessy, "Separation of Pb, Bi and Po by cation exchange resin," *Journal of Radioanalytical and Nuclear Chemistry*, vol. 314, no. 2, pp. 985–989, 2017.

[14] J. D. Despotopulos, K. N. Kmak, K. J. Moody, and D. A. Shaughnessy, "Development of a ^{212}Pb and ^{212}Bi generator for homolog studies of flerovium and moscovium," *Journal of Radioanalytical and Nuclear Chemistry*, vol. 317, no. 1, pp. 473–477, 2018.

[15] J. P. Omtvedt, J. Alstad, T. Bjørnstad, Ch. E. Düllmann, K. Gregorich, D. Hoffman, H. Nitsche, K. Opel, D. Polakova, F. Samadani *et al.*, "Chemical properties of the transactinide elements studied in liquid phase with SISAK," *The European Physical Journal D*, vol. 45, no. 1, pp. 91–97, 2007.

[16] D. Krupp and U. W. Scherer, "Prototype development of ion exchanging alpha detectors," *Nuclear Instruments and Methods in Physics Research Section A: Accelerators, Spectrometers, Detectors and Associated Equipment*, vol. 897, pp. 120–128, 2018.

[17] A. Fazio and P. Carconi, "Measurement of absolute γ-ray emission probabilities in the decay of ^{227}Ac in equilibrium with its progeny," 2019.

[18] International Nuclear Structure and Decay Data Network, "Nuclear data services: evaluated nuclear structure and decay data," 29.05.2020. [Online]. Available: https://www.nndc.bnl.gov/ensdf/

[19] L. Done and M. Ioan, "Minimum detectable activity in gamma spectrometry and its use in low level activity measurements," *Applied Radiation and Isotopes*, vol. 114, pp. 28–32, 2016.

[20] International Organization for Standardization, *ISO 11929: Determination of the Characteristic Limits (decision Threshold, Detection Limit and Limits of the Confidence Interval) for Measurements of Ionizing Radiation: Fundamentals and Application*. ISO, 2010.

[21] F. Strelow, "An ion exchange selectivity scale of cations based on equilibrium distribution coefficients," *Analytical Chemistry*, vol. 32, no. 9, pp. 1185–1188, 1960.

[22] O. Alhassanieh, A. Abdul-Hadi, M. Ghafar, and A. Aba, "Separation of Th, U, Pa, Ra and Ac from natural uranium and thorium series," *Applied radiation and isotopes*, vol. 51, no. 5, pp. 493–498, 1999.

Chapter 5

Conclusion and Outlook

In this work, new technologies were developed and investigated that will make possible future liquid phase experiments SHE that are with shorter-lived than currently accessible ones. For this purpose, all aspects of an accelerator-based experiment were considered and made more efficient by means of new technological approaches.

By using the vacuum to liquid transfer chamber (VLTC), many individual steps of the SHE transport to a chemical experiment can be bypassed, which increases both the speed and the yield of the transport process. By combining a physical preseparator with the VLTC, the by-products of the fusion reaction are first separated from the SHE to be investigated. Instead of subsequently thermalizing the SHE in gas, adsorbing them on aerosol particles, transporting them via gas jet to an experiment and transferring them into the liquid phase, the SHE are implanted directly from the low-pressure side of the preseparator into the liquid phase of the chemical experiment with the aid of the VLTC. For this study, experiments were carried out with $^{250/252}$Cf fission products. The fission products were directly implanted into a diluted nitric acid solution from a low pressure region through a 6.0 µm thin Mylar foil. Subsequently, the fission products were identified and quantified by γ-spectrometry measurement of the solution. In addition, simulations were performed with the well esteblished simulation program SRIM (Stopping and Range of Ions in Matter) in combination with a Matlab program developed for this purpose. The residence time of radionuclides in the VLTC was determined with ^{68}Ga and a self-designed listmode program. In addition, a generalized calculation showed that each element of the SHE series has at least one radionuclide that could be rapidly transported to a liquid phase chemistry experiment using the VLTC system.

Further, instead of considering the chemical experiments, sample preparation and measurement as three individual points, the functionalization of α-detectors with chemically selective functional groups was used to combine the above-mentioned individual steps and thus also to increase the speed of the actual chemical experiment. In a proof of concept experiment, commercial α-detectors were coated with organosilanes, which were further functionalized to form sulfonic acid groups as a group of strong cation exchangers. [$^{234/238}$U]UO_2^{2+}-cations could be selectively adsorbed on the modified detector surfaces from aqueous solution. Due to the thin organosilane layers, the resulting alpha particles could be measured with high energy resolution. In addition, the long-term stability of the silane surfaces over one week could be demonstrated. By regenerating the modified surfaces with hydrochloric acid, the uranium could be selectively desorbed. This measurement system was also tested for concept viability using the simulation programs SRIM and AASIFIT (Advanced Alpha-Spectrometric Simulation and Fitting).

In order to further test the developed list-mode program and to have an accelerator facility independent source for continuous short-lived α-emitters in aqueous solution, a ^{227}Ac based ^{211}Bi ($t_{1/2}$ = 2.14 min) generator was developed. Using the list-mode program, it was shown that this system can be used to continuously and selectively separate α-emitting ^{211}Bi in dilute hydrochloric acid from the remaining ^{227}Ac progeny. The presence of other ^{227}Ac progeny above the detection limit could be excluded by γ-spectrometry. By providing a constant stream of short lived α-emitting ^{211}Bi in aqueous solution, many preliminary experiments with the VLTC chamber in combination with functionalization α-detectors can be performed even without access to an accelerator facility in the future.

Future Studies

In this thesis, new approaches were developed for the rapid and efficient investigation of the heaviest elements, the superheavy elements, in the aqueous phase. In a next step, experiments with the VLTC behind an advanced physical preseparator such as TASCA have to be carried out. In experiments with the SISAK system in combination with the Berkeley Gas-filled Separator (BGS), Omtvedt et al. have reported successful experiments with ^{257}Rf ($t_{1/2}$ = 4.4 s). The conventional aerosol gas-jet / dissolution apperatus technique was still used. With the new VLTC system, such experiments could be repeated to assess the relative increase in transport efficiency. Instead of the existing systems such as SISAK or ARCA II, flow cells can be equipped with chemically functionalized α-detectors behind the VLTC. In addition to the existing possibility of performing ion exchange experiments with the functionalized α-detectors, the range of possible functional groups should be expanded. This would allow a larger variety of experiments to be carried out regarding different questions of the aqueous phase chemistry of the SHE. Since the detector surface is coated with organic functional groups after silanization, a large number of chemically selective groups, such as further ion exchanger groups or complexing agents, can be introduced by well-known organic chemistry reactions. By using chemically selective alpha detectors in combination with the VLTC system, the efficiency of a liquid phase chemistry experiment can be further increased in the future, so that investigations of elements beyond seaborgium directly in the liquid phase are also possible.

Chapter 6

Appendix

6.1 Programms for Data Acquisition

6.1.1 Listmode in combination with Genie 2K (C++)

Communication between the program and Genie 2K takes place via the S560 programming module. The individual events are written out channel by channel in an ASCII file when the live time is updated. The fundamental structure of the program is based on the "S560 Genie 2000 Programming Library User's Manual V3.2".

```
// D.Krupp: Listmode in Genie 2K based on S560 Module
#include <iostream>
// Windows includes
#include <windows.h>
#include <crackers.h>
// C run time library includes
#include <tchar.h>
#include <stdio.h>
#include<fstream>
#include<string>

// GENIE 2000 User Library includes

#pragma pack(show) // C4810
#pragma pack(2) // n = 2
#pragma pack(show) // C4810
#include <citypes.h>
#include <Spasst.h>
#include <sad.h>
#include <get_put.h>
#include <driver.h>
#include <ci_files.h>
```

```
#include <campdef.h>
#include <cam_n.h>
#include <CAMDEF.H>
#include <DRVERR.H>

#pragma pack(show) // C4810
#pragma pack(8) // n = 8
#pragma pack(show) // C4810

// GENIE 2000 Utility Library includes

#include <utility.h>

int main()
{
std::cout << "D.Krupp: Alpha-Listmode\n";

HMEM hDSC;
INT iRC;
SHORT sRC, sRet, sDum1;
SHORT sReturn;
ULONG ulRC;
USHORT usDum2;

vG2KEnv();

// Establish a connection to the local VDM iut
iRC = iUtlCreateFileDSC(&hDSC, 0, 0);
if (iRC) {
printf("Error creating a VDM connection: %u", iRC);
return((int)1);
}

// Local Detector Names
DetectorOf_T stDet;
sRC = SadFirstInputEx(hDSC, &stDet);

while (sRC == CSI_Okay) {
printf("Detector Name = %s\n", stDet.szDetectorName);
printf("MID File Name = %s\n", stDet.szFileNameMID);
switch (stDet.usTypeMCA)
{
case MCA_I2kSim:
```

```
printf("MCA Type = InSpector-2000 Simulator\n");
break;
case MCA_InSpectDSP:
printf("MCA Type = InSpector-2000\n");
break;
case MCA_Lynx:
printf("MCA Type = Lynx\n");
break;
case MCA_Falcon5000:
printf("MCA Type = Falcon\n");
break;
case MCA_uniSpec:
printf("MCA Type = UniSpec\n");
break;
case MCA_PORTABLE:
printf("MCA Type = InSpector\n");
break;
default:
printf("MCA Type = Unknown\n");
}
sRC = SadNextInputEx(hDSC, &stDet);
}

// Open the detector DET01 datasource

sRC = SadOpenDataSource(hDSC, (char*)"DET01", CIF_Detector,
ACC_Exclusive | ACC_SysWrite | ACC_ReadWrite, TRUE, (char*)"");

if (sRC == CSI_Verify) {
printf("Error failed to verofy DET01 parameter settings.");
return((int)1);
}
else if (sRC) {
sRet = SadGetStatus(hDSC, &ulRC, &sDum1, &usDum2);
printf("Error opening DET01: %x", ulRC);
return((int)1);
}

ULONG aulSpc[2048];
sRC = SadGetSpectrum(hDSC, 1, 2048, 0, &aulSpc);
if (sRC) {
printf("Error failed to get the spectra channel.");
return((int)1);
```

```
}

//Set acquisition preset to 30 seconds livetime
{
Preset_T stPSet;
FillMemory(&stPSet, sizeof(Preset_T), '\0');
stPSet.flPsetMode = CAM_M_PMOD_LIVE;

stPSet.unTime.dPsetTime = 10; // Live-Time Einstellung

sRC = SadPutStruct(hDSC, WST_SetPreset, 1, 1, &stPSet,
sizeof(Preset_T));
if (sRC) {
printf("Error failed to set livetime preset.");
return((int)1);
}

}

// Clear the aquisition memory
sRC = SadControlDSC(hDSC, MCA, CTL_ClearData);
if (sRC) {
printf("Error failed to clear aquisition memory");
return((int)1);
}

// Start the aquisition
sRC = SadControlDSC(hDSC, MCA, CTL_StartAcq);
if (sRC) {
printf("Error failed to start aquisition");
return((int)1);
}

// wait for acquisitoin to complete
{
DSQuery_T stQData;
double dLive;
sRC = SadQueryDataSource(hDSC, DSQ_Status, &stQData);
if (sRC) {
printf("Error hardware query failed");
return((int)1);
}
/*REAL dOldIntegral = 0.0;
```

```
REAL dDiffCps = 0.0; */
ULONG ulRecord = 1;
USHORT Start = 1;
USHORT Stop = 2048;

while (stQData.stDS.fsStatus & DSS_Busy) {
Sleep(1000); // Sleep for 1 second
sRC = SadGetParam(hDSC, CAM_X_ELIVE, 0, 0, &dLive, sizeof(double));
if (!sRC) {
printf("\rLivetime seconds: %f \t Diff. cps: %f \t
Start %i ch \t Stop %i ch", dLive, Start, Stop);
}
sRC = SadQueryDataSource(hDSC, DSQ_Status, &stQData);
if (sRC) {
printf("Error hardware query failed");
return((int)1);
}

// Ch abfragen
CalcParam_T stCalc;

stCalc.usStart = 1;
stCalc.usStop = 2048;

Start = stCalc.usStart;
Stop = stCalc.usStop;

// ------------------------------------

sRC = SadGetSpectrum(hDSC, 1, 2047, 0, &aulSpc);
if (sRC) {
printf("Error failed to get the spectra channel.");
return((int)1);
}

//sRC = SadPutSpectrum(hDSC, 5, 500, &aulSpc);

std::ofstream file;
file.open("C:/test/speichern.txt", std::ios_base::app);

file << dLive << ";";
for (int i = 0; i < 2047; ++i) {
```

```
file << std::to_string(aulSpc[i]) << " ";

// std::cout << "Channel " << i << " " << aulSpc[168] << std::endl;
}
file << "\n";
file.close();

// ------------------------------------

ulRecord = ulRecord + 1;

}

}

// save to file, should have the spectrum
HMEM hDSC2;
iRC = iUtlCreateFileDSC(&hDSC2, 0, 0);
if (iRC != 0) {
printf("Error creating a VDM connection: %u", iRC);
return((int)1);
}

sRC = SadCreateFile(hDSC2, (char*)"C:\\genie2k\\camfiles\\Mein.cnf",
        true, CAM_CTYP_ACQD, CAM_CAP_GSPEC, 2048); //4096
sRC = SadFlush(hDSC2);
sRC = SadCloseDataSource(hDSC2);
sRC = SadOpenDataSource(hDSC2, (char*)"C:\\genie2k\\camfiles\\Mein.cnf",
        CIF_NativeSpect, ACC_ReadWrite, false, (char*)"");
sRC = SadSaveAs(hDSC, hDSC2);
sRC = SadFlush(hDSC2);
sRC = SadCloseDataSource(hDSC2);
sRC = SadDeleteDSC(hDSC2);

// Cleanup and exit
sRC = SadCloseDataSource(hDSC);
sRC = SadDeleteDSC(hDSC);

std::cout << std::endl;
std::cout << "Programm ist fehlerfrei durchgelaufen!\n";
return ((int)0);
}
```

6.1.2 Listmode in combination with National Instruments Hardware (Matlab)

Analog signals are recorded with NI hardware and digitized in matlab. The data are then available as continuous individual .mat packets. With the sample rate, a time stamp can be assigned to each signal.

```
% D. Krupp DAQ in Matlab

close all;
clear global all;
clc;

global buffer;
buffer = [];
i = 1;
devices = daq.getDevices; % Searches connected DAQ hardware
% Defines "s" as a reference to the current measurement
s = daq.createSession('ni');

% Defines the input in DAQ hardware and the measured quantity
s.addAnalogInputChannel('cDAQ1Mod1',3,'Voltage');
s.Rate = 50000; % Defines a sample rate [1/s]

% Bypasses the automatic determination of the buffer size
s.IsNotifyWhenDataAvailableExceedsAuto = false;

s.DurationInSeconds = 28800; % defines the sample time

% Manual definition of the buffer size
s.NotifyWhenDataAvailableExceeds = 1000000;
% Query the current array length in the buffer
lis = addlistener(s,'DataAvailable',@Funkt1);

prepare(s);
% Synchronize DAQ parameters with hardware
Info_screen = ['DAQ software 1.1' "D.Krupp";... % Create an info file
'DAQ device' string(devices.Description);...
'Rate [1/s]' string(s.Rate);...
'Messzeit [s]' string(s.DurationInSeconds);...
'Puffersize [/]' string(s.NotifyWhenDataAvailableExceeds);...
'Beginn der Messung' string(datetime('now'))];

for i = 1
```

```
disp('Schach...');

startBackground(s); % Start DAQ
wait(s);
i = i +1;

end

wait(s); % Waiting for measurement to finish
delete(lis);

disp('Matt!');

% Writing additional data to the info file
% and saving it date-specifically
Info_screen = [Info_screen;...
'Ende der Messung' string(datetime('now'))];
save(string(datetime('now','Format','dd_MM_yy''-''HH_mm_ss''INFO')),...
'Info_screen');

function Funkt1(~,event) % Function to save and empty the buffer

global buffer;

buffer = [event.Data];
save(string(datetime('now','Format','dd_MM_yy''-''HH_mm_ss')),...
'buffer');

buffer = [];

end
```

6.1.3 Analysis of raw data in Matlab

The .mat data are loaded into the program one after the other. For each .mat file a minimum peak height of a voltage peak is searched for as a fast filter. If the minimum peak height is found, all signal peaks are analyzed including their time stamps and are written into a result file. From this a histogram (number of events against signal intensity) can be constructed. The histogram also contains the time information of all peaks and can be output as a graph by specifying the peak boundaries.

```
% Rawdata Analysis
clear all
close all

run_status = 0;
threshold = 0.3;
Dis = 0.3;
DT = 20;
Ergebnis = [];
sample_rate = 50000;
t_mess = 1200;
Area = [];
loks = [];

%Thold = 0.2;

% Analysis of rawdata
Inventar = dir('*mat');
Inventar = rmfield(Inventar, {'folder', 'date', 'bytes', 'isdir',...
        'datenum'});
dir_size = length(Inventar) -1;

% Evaluation I: Creation of a histogram (Counts / Volt)

for a = 1:dir_size

load(Inventar(a).name);
run_status = run_status + 1;
progress = run_status/dir_size*100

if max(buffer) >= threshold % Skip spectra without event

peak_shape = abs(buffer(:,1));

% pks = Signal height [V] loks = Peakposition [Ch]
```

```
[pks,loks] = findpeaks(peak_shape(:,1),'MinPeakHeight',Dis,...
'MinpeakDistance',DT);

Area = loks - loks; % Creation of a N x 1 Matrix;

figure(1)
plot(buffer(:,1))
hold on
plot(peak_shape(:,1))
% pks = Signal height [V] loks = Position of the maximum [Ch]
findpeaks(peak_shape(:,1),'MinPeakHeight',Dis,...
'MinpeakDistance',DT);
hold off

for b = 1:length(loks) % Einzelanalyse jedes gefundenen Peaks

U_lim = loks(b)-5;
O_lim = loks(b)+5;
end

% Integration per peak "i" over each channel "Ch"
% within the specified integration limits
for c = U_lim:O_lim
Area(b) = Area(b) + buffer(c,1);
end

end

peak_info = [Area Area];

for d = 1:length(loks)

peak_info(d,2) = (loks(d)+(a-1)*length(buffer))/sample_rate;

end

Ergebnis = [Ergebnis; peak_info];

end

%Cleanup
clear run_status
clear threshold
```

```
clear dis
clear DT
clear a
clear b
clear c
clear d

%%
% First energy spectrum after raw data analysis

[Ergebnis_per_ch,edges] = histcounts(Ergebnis(:,1),...
'BinWidth',0.014,'BinLimits', [0.1 2]);
Ergebnis_per_ch = transpose(Ergebnis_per_ch);
edges = transpose(edges);

figure(3)
histogram(Ergebnis(:,1),'BinWidth',0.015,'BinLimits', [0.1 2])

%%
p = 3;

Frequenz = [];

% Evaluation II: Time information per channel

Ergebnis_per_ch = [Ergebnis_per_ch;0]; % Adjust matrix size
Frequenz = edges;       % Channelsize
% Line Two: Total Number of Events in the Channel
Frequenz(:,2) = Ergebnis_per_ch;

for k = 1:length(edges)             % Sorting the individual events

for m = 1:length(Ergebnis)

if Ergebnis(m,1) >= edges(k) && Ergebnis(m,1) < edges(k+1)
Frequenz(k,p)=Ergebnis(m,2);
p=p+1;

end

end

p=3;
```

```
end

%% Evaluation IV: Half-life

decay = [];
lt_decay = [];

t_ch = 60;  % Size per timebin

t_hist = 0:t_ch:t_mess;
t_hist(1) = 0.01;
t_hist = transpose(t_hist);

% if t_hist(end) < t_mess
%     t_hist = [t_hist; t_mess];
% end

ch_low = 1;
ch_high = 100;

chart = Frequenz(ch_low:ch_high,3:end);

decay = transpose(histcounts(chart,t_hist));

lt_chart = [];

lt_chart = chart(:);
lt_chart = sort(lt_chart);
lt_chart(lt_chart ==0) = [];

lt_decay = mean(lt_chart)*log(2)/3600

lt_chart = [];

figure

plot(decay,'Marker','o','LineStyle','none');
xlabel('Time Bin [/]');
ylabel('Counts per time bin [/]');
title({'Decay of Peak Nr.' i});

%%
```

```
for i = 1:t_peak_nr

k = i*2;
ch_low = round(t_peak_lim(k-1));
ch_high = round(t_peak_lim(k));

chart = Frequenz(ch_low:ch_high,3:end);

decay(:,i) = transpose(histcounts(chart,t_hist));

lt_chart = [];

lt_chart = chart(:);
lt_chart = sort(lt_chart);
lt_chart(lt_chart ==0) = [];

lt_decay(i) = mean(lt_chart)*log(2)/3600

lt_chart = [];


figure(i+1)


plot(decay(:,i),'Marker','o','LineStyle','none');
xlim([0 length(decay(:,i))]);
ylim([0 max(decay(:,i))]);
xlabel('Time Bin [/]');
ylabel('Counts per time bin [/]');
title({'Decay of Peak Nr.' i});

end

%% Evaluation III: Energy Calibration

answer = questdlg('Should an energy calibration be performed?',...
'Energiekalibration','Ja','Nein','Ja');

switch answer

case 'Ja'
```

```
% figure(1)

e_peak_nr = inputdlg('How many peaks are used?',...
'Peakanzahl',[1 50],{'1'});
e_peak_nr = str2double(e_peak_nr);

[ch_peak] = ginput(e_peak_nr);

for i = 1:e_peak_nr
e_peak=inputdlg('Energie?',...
'Energiezuordnung',[1 50],{'Energie in keV'});
ch_peak(i,2) = str2double(e_peak);
end

fitResults = polyfit(ch_peak(:,1),ch_peak(:,2),1);

figure(2)
plot(ch_peak(:,1),ch_peak(:,2))

Ergebnis_per_ch = [Ergebnis_per_ch Ergebnis_per_ch];

for i = 1:length(Ergebnis_per_ch)
Ergebnis_per_ch(i,2) = fitResults(1,1)*i + fitResults(1,2);
end

Frequenz(:,1) = Ergebnis_per_ch(:,2);

figure(1)
plot(Ergebnis_per_ch(:,2),Ergebnis_per_ch(:,1))
xlim([Ergebnis_per_ch(1,2) Ergebnis_per_ch(end,2)]);
xlabel('Energie [keV]');
ylabel('Counts [/]');
title({'Alpha-Spektrum'});

case 'Nein'

end
```

6.2 SRIM in Matlab

The Matlab program loads a single energy *E0* or an array of energies *E_ Array* into an SRIM input file *.IN* and calculates the loss of kinetic energy for an element *Z* when passing through a range *R*.

```
% Dominik Krupp: SRIM in Matlab

global E_Array;
E_Array = [];

%%
%-----------------------------------
% Einlesen des Input-file
%   Z X --> 92

i = 1;              % Iteration
SRIM_Input = {};    % Rawdata - Result of SRIM
Z = 19;             % Proton
Z0 = Z;

n = [];             % Variable for unit conversion
pxy = [];           % Factors for Polyfitfunction
p =[];              % Result of the Polyfitfunktion
Ergebnis = [];

global E0;          % Energy in MeV
%E0 = X;            % Fixed value for the starting energy
global Range;       % Range in a Material in um
Range = 6.2;
Element = 114;

E_line = '---Ion Energy : E-Min(keV), E-Max(keV)'; % Beginn Table
Start = ' Energy    Elec.    Nuclear    Range  Straggling   Straggling';
Stop = '-------------------------------------------------------------';

while Z < 92
Z = Z +1;

fid = fopen('3.IN','r');
tline = fgetl(fid);
i=1;
while tline ~= -1 % If tline is empty -1 is returned
SRIM_Input{i,1} = tline;
```

```
tline = fgetl(fid);
i = i+1;
end

fclose('all');

SRIM_Input{5,1} = [num2str(Z), ' 289'];

iE = 1;
while strcmp(SRIM_Input{iE,1},E_line)==0
iE = iE+1;
end
iE = iE+1;

E0 = E_Array(Z-Z0);

SRIM_Input{iE,1} = ['100 ',num2str(E0*1000)];

fid = fopen('SR.IN','w+');

for k = 1:length(SRIM_Input)
fprintf(fid,'%s\r\n', SRIM_Input{k,1});
end
save = SRIM_Input;
SRIM_Input = {};

fclose('all');
system('SRModule.exe');

%------------------ Processing of the raw results
i = 1;
tline_result = [];
fid_result = fopen('result','r');
tline_result = fgetl(fid_result);
Rawdata_s = [];

while strcmp(Start,tline_result)==0
tline_result = fgetl(fid_result);
end

tline_result = fgetl(fid_result);

while strcmp(Stop,tline_result)==0
```

```
tline_result = fgetl(fid_result);

if strcmp(Stop,tline_result)==1

else
Rawdata_s{i,1} = tline_result;
i = i+1;
end

end

Rawdata_s = strrep(Rawdata_s,',','.');

Rawdata_s_c = [];
i = 1;

for i = 1:length(Rawdata_s)
Buffer = [strsplit(Rawdata_s{i,1},' ')];
Buffer = Buffer(2:length(Buffer));
Rawdata_s_c = [Rawdata_s_c; Buffer];
i = i+1;
end
Buffer = [];

Data = [];
i = 1;
n = [];
Data(:,1) = str2double(Rawdata_s_c(:,1));

for i = 1:length(Rawdata_s_c) %Alle Energien auf MeV bringen

n = Rawdata_s_c(i,2);

if strcmp(n,'MeV')

elseif strcmp(n,'eV')
Data(i,1) = Data(i,1)/1000000;
elseif strcmp(n,'keV')
Data(i,1) = Data(i,1)/1000;
else
disp('Fehler: Unbekannte Energieeinheit')
end
```

```
i=i+1;

end

i = 1;
n = [];
Data(:,2) = str2double(Rawdata_s_c(:,5));

for i = 1:length(Rawdata_s_c) %Alle Reichweiten auf um bringen

n = Rawdata_s_c(i,6);

if strcmp(n,'m')
Data(i,2) = Data(i,2)*1000000;
elseif strcmp(n,'mm')
Data(i,2) = Data(i,2)*1000;
elseif strcmp(n,'um')

elseif strcmp(n,'A')
Data(i,2) = Data(i,2)/10000;

else
disp('Fehler: Unbekannte Reichweiteeinheit')
end

i=i+1;

end

fclose('all');

%---------------------------------
% Lookup for Range calculation

i = 1;
pxy = [];
p = [];
n =[];
range_input = Data(length(Data),2) - Range;
E1_MeV = [];
E1_keV = [];
```

```
for i = 1:length(Data)
if Data(i,2) < range_input %
n = i;
end

i = i+1;

end

pxy(2,2) = Data(n,1);
pxy(1,2) = Data(n+1,1);
pxy(2,1) = Data(n,2);
pxy(1,1) = Data(n+1,2);
p = polyfit(pxy(:,1),pxy(:,2),1);
E1_MeV = p(1) * range_input + p(2); %
E1_keV = E1_MeV*1000;

Ergebnis(Z-Z0,1) = Z;
Ergebnis(Z-Z0,2) = E1_MeV;

end

%---------- Daten fit

[q,s] = polyfit(Ergebnis(:,1),Ergebnis(:,2),1);
[y_fit,delta] = polyval(q,Ergebnis(:,1),s);

plot(Ergebnis(:,1),Ergebnis(:,2),'bo')

Ex_u_delta = [];
Ex_u_delta(:,1) = Ergebnis(:,1);
Ex_u_delta(:,2) = y_fit(:,1);
Ex_u_delta(:,3) = delta(:,1);
Ex_u_delta(:,4)= Ex_u_delta(:,2) + 2*Ex_u_delta(:,3);
Ex_u_delta(:,5)= Ex_u_delta(:,2) - 2*Ex_u_delta(:,3);

fit(1,1) = Element;
fit(1,2) = q(1)*Element+q(2);

hold on
plot(fit(1),fit(2),'ro')

q_err = polyfit(Ex_u_delta(:,1),Ex_u_delta(:,4),1);
```

```
fit(1,3)=0;

fit(1,4) = q_err(1)*Element+q_err(2);

q_err = polyfit(Ex_u_delta(:,1),Ex_u_delta(:,5),1);
fit(1,5) = q_err(1)*Element+q_err(2);

Ex_u_delta = [Ex_u_delta; fit];

plot(Ex_u_delta(:,1),Ex_u_delta(:,2),'r-');

errorbar(fit(1),fit(2),(fit(2)-fit(5))/2,(fit(4)-fit(2))/2,'ro');
set(gca,'TickLabelInterpreter','latex');
%plotregression
hold off
disp('Done!')
```

List of Figures

List of Tables